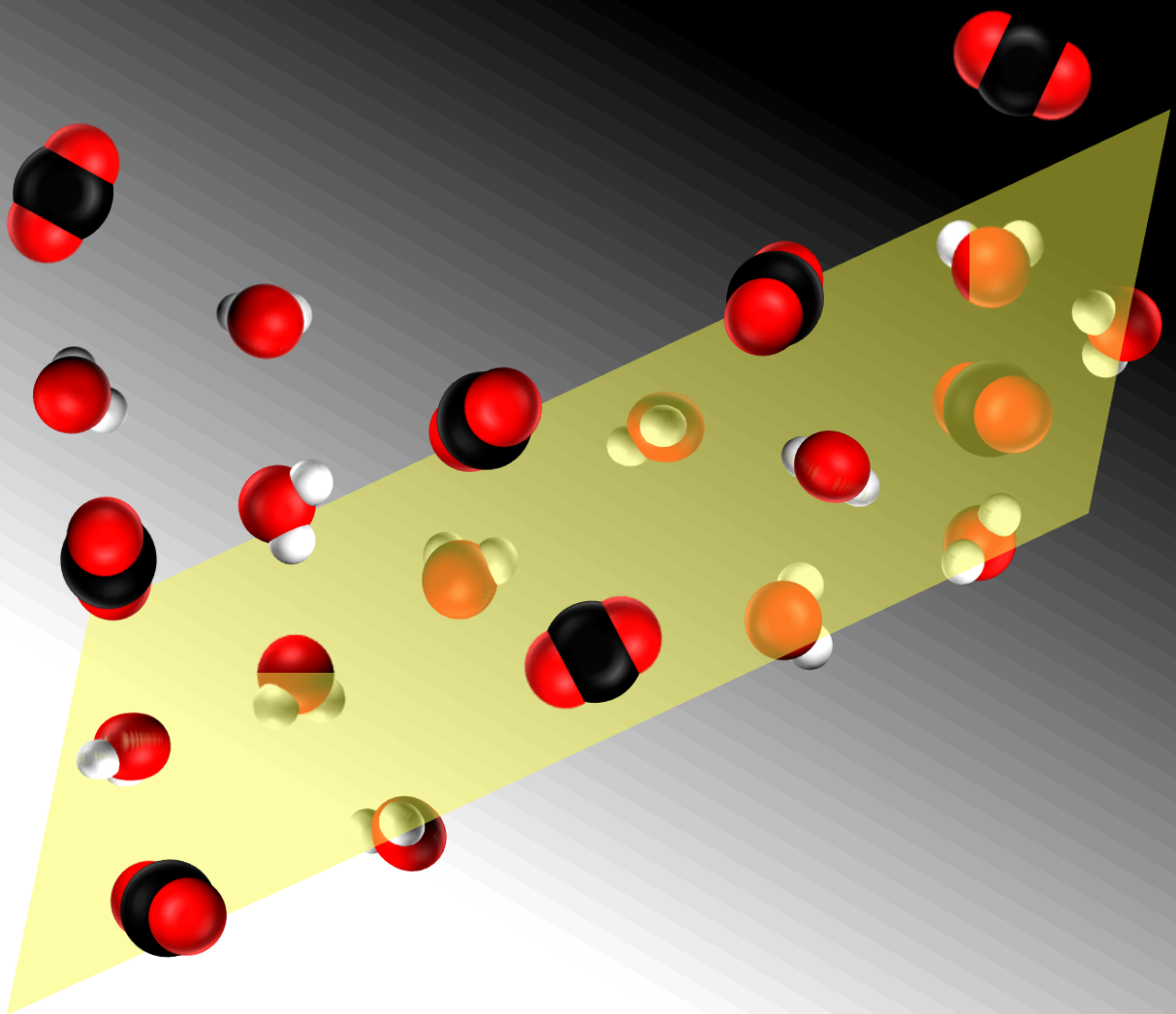


Beata T. Koziara

Thin sulfonated poly(ether ether ketone)  
films for the dehydration  
of compressed carbon dioxide



*Thin sulfonated poly(ether ether ketone)  
films for the dehydration  
of compressed carbon dioxide*

This research was performed in the cooperation framework of Wetsus, centre of excellence for sustainable water technology ([www.wetusus.nl](http://www.wetusus.nl)). Wetusus is co-funded by the Dutch Ministry of Economic Affairs and Ministry of Infrastructure and Environment, the European Union Regional Development Fund, the Province of Fryslân, and the Northern Netherlands Provinces. The authors would like to thank the participants of the research theme “Dehydration” for the fruitful discussions and their financial support.



### **Promotion committee**

*Chairman:*

prof. dr. J.W.M. Hilgenkamp

University of Twente

*Promotor:*

prof. dr. ir. D.C. Nijmeijer

University of Twente

prof. dr. ir. N.E. Benes

University of Twente

*Members:*

prof. dr. ir. I.F.J. Vankelecom

Catholic University of Leuven

prof. dr. A.A. van Steenhoven

Eindhoven University of Technology

dr. S. Metz

Wetusus

prof. dr. S.R.A. Kersten

University of Twente

dr. M.A. Hempenius

University of Twente

dr. ir. H. Wormeester

University of Twente

*Cover design*

Beata T. Koziara

Thin sulfonated poly(ether ether ketone) films for the dehydration of compressed carbon dioxide  
ISBN: 978-94-6259-806-5

Printed by Ipskamp Drukkers B.V., Enschede

© 2015 Beata Teresa Koziara, Enschede, The Netherlands

**THIN SULFONATED POLY(ETHER ETHER KETONE)  
FILMS FOR THE DEHYDRATION  
OF COMPRESSED CARBON DIOXIDE**

**DISSERTATION**

to obtain  
the degree of doctor at the University of Twente,  
on the authority of the rector magnificus,  
Prof. Dr. H. Brinksma  
on account of the decision of the graduation committee,  
to be publicly defended  
on Friday 9<sup>th</sup> of October 2015 at 12:45

by

**Beata Teresa Koziara**

born on 20<sup>th</sup> of November 1983  
in Cracow, Poland

This dissertation has been approved by:

prof. dr. ir. D.C. Nijmeijer (promotor)

prof. dr. ir. N.E. Benes (promotor)

## Table of Contents

|  |     |
|--|-----|
| <b>Chapter 1</b>   | 1   |
| Introduction   |     |
| <b>Chapter 2</b>   | 13  |
| Optical anisotropy, molecular orientations, and internal stresses in thin sulfonated poly(ether ether ketone) films          |     |
| <b>Chapter 3</b>   | 37  |
| The effects of water on the molecular structure and the swelling behavior of sulfonated poly(ether ether ketone) films       |     |
| <b>Chapter 4</b>   | 55  |
| Thermal stability of sulfonated poly(ether ether ketone) films: on the role of protodesulfonation                            |     |
| <b>Chapter 5</b>   | 89  |
| Modification of thin sulfonated poly(ether ether ketone) films using ethylene glycol and glycerol                            |     |
| <b>Chapter 6</b>   | 111 |
| Dehydration of supercritical carbon dioxide using hollow fiber membranes: simulations in Aspen Plus® and economic evaluation |     |
| <b>Chapter 7</b>   | 149 |
| Conclusions and Outlook  |     |
| <b>Summary</b>   | 159 |
| <b>Samenvatting</b>  | 165 |
| <b>Acknowledgements</b>  | 171 |



# Chapter 1

## Introduction



## 1.1 Dehydration of compressed carbon dioxide

Dehydration of compressed carbon dioxide is performed to recover the carbon dioxide after its use in the extraction of water from solid materials, such as food products. The removal of water from foods can, for instance, aid to extend the foods shelf life. Dehydration using near critical, or supercritical carbon dioxide provides several benefits over other drying methods that are used in the food industry, such as hot air and freeze-drying. At temperatures and pressures close to their critical point, fluids combine gas-like and liquid-like properties which facilitates effective extractions [1]. The relatively high density of these fluids, similar to that of liquids, provides a high solvation power [2]. On the other hand, their low viscosities and high diffusivities, similar to those of gases, allow for their easy penetration of food matrices and fast solute transport [2]. In addition, around the critical point the strong effects of temperature and pressure on the physico-chemical properties of a fluid provide a means to tune the fluid density and viscosity for specific products or processes [3]. Because there is no vapor-liquid interface in a supercritical phase, no capillary stresses are induced in a solid matrix, enabling products to retain their shape without damage. For comparison, drying of solid materials with hot air is often accompanied with heat-induced damage, material shrinkage, and loss of nutrients. In freeze drying, the food microstructure is generally preserved, but this technique is energy intensive and time consuming, because of the enthalpy required for freezing the water for the slow sublimation of water in vacuum [4, 5].

Compared to other fluids, carbon dioxide has numerous advantages. The critical point is readily accessible (31.1 °C and 73.8 bar) and carbon dioxide is non-toxic [6]. By operating at low temperatures, the oxidation of sensitive products is avoided [7]. Residual non-toxic carbon dioxide can be easily removed from the food matrix by simple depressurization. Additionally, carbon dioxide is inexpensive and produced on a large scale [8].

Currently, the dehydration of compressed carbon dioxide is performed via adsorption of the water on zeolite adsorbents. In the continuous drying process, shown in Figure 1.1a, the compressed fluid recirculates between the drying chambers, in which the water is extracted from the food products, and between the zeolite beds, in which the dissolved water is adsorbed on the zeolites. The process is operated in a semi-continuous manner: several zeolite beds are used in parallel, some of which are in a sorption mode, while others are being regenerated after they became saturated. Typically, the recovery of the adsorption capacity of zeolites requires

heating to high temperatures (up to 600 °C for full regeneration), which corresponds to high operating costs [9, 10]. Therefore, a replacement of the zeolite beds with a membrane unit can be a promising alternative (Figure 1.1b). Membrane technology is known to be energy efficient [11] and the dehydration can be performed in a continuous fashion. The high water activity in the compressed carbon dioxide (~1 in a completely saturated fluid), combined with the slightly elevated temperatures used in food drying processes (40 – 60 °C), create a high driving force for water permeation.

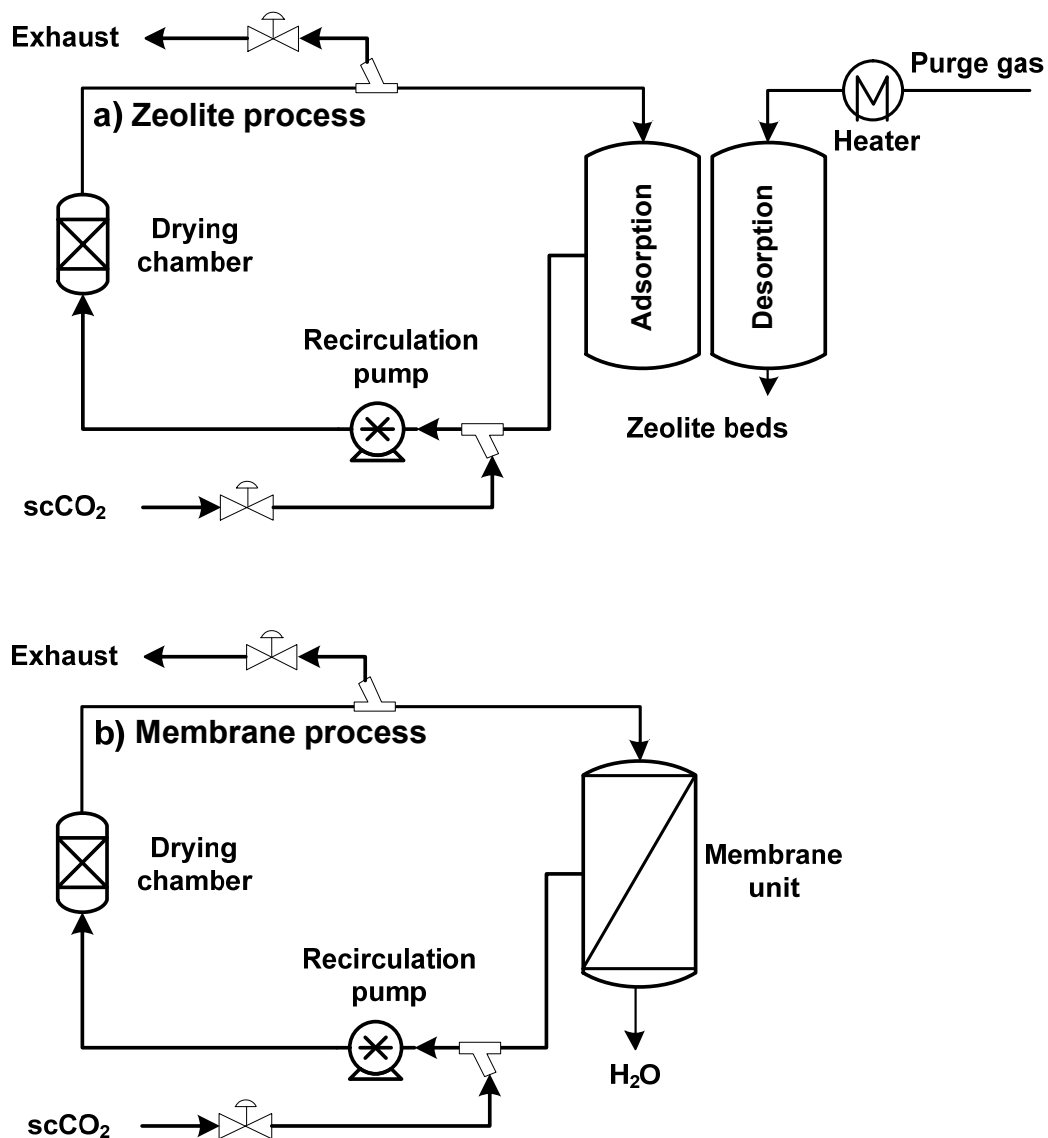


**Figure 1.1** Scheme of a continuous food drying process using scCO<sub>2</sub> with (a) zeolite beds [2] and (b) a membrane unit for scCO<sub>2</sub> dehydration.

Nevertheless, membrane technology for the dehydration of compressed carbon dioxide is challenging and several aspects have to be considered. The main ones are: (1) a suitable membrane material is required that is stable during operation; (2) a method is required to remove water from the permeate side such that the high driving force over the membrane is maintained for water permeation. The sections below will shortly elucidate these challenges, followed by a concise description of the content of this thesis.

## 1.2 Challenges in the process

### 1.2.1 Membrane material

Among the suitable materials for dehydration of compressed carbon dioxide is sulfonated poly(ether ether ketone) (SPEEK), shown in Figure 1.2. SPEEK is the sulfonated form of the high-performance, mechanically strong and glassy polymer, poly(ether ether ketone) PEEK [12]. The degree of sulfonation,  $DS$  (%), is defined as the percentage of repeating units of PEEK that contains an  $-SO_3^-$  group. In contrary to pure PEEK, SPEEK possesses high affinity for water, due to the presence of the hydrophilic sulfonic acid groups. The hydrophilic properties, coupled with low permeability of gases, make SPEEK a suitable membrane material for the dehydration process. Previous studies on SPEEK composite hollow fiber membranes showed high water permeances and high selectivities of water over nitrogen and carbon dioxide [13, 14].

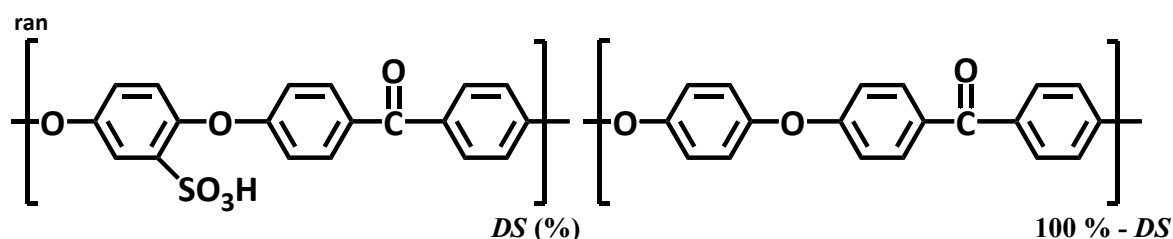


**Figure 1.2** Structure of sulfonated poly(ether ether ketone) (SPEEK) with a given  $DS$  (%), randomly sulfonated. In this thesis, highly sulfonated SPEEK with a  $DS$  of 68 and 84 % is used.

Despite the good performance of SPEEK membranes in molecular separations, the membrane stability in specific process conditions remains a challenge. Increasing the materials affinity for water can be achieved by more extensive sulfonation (higher *DS*), but this is at the cost of the reduced mechanical stability of the material, because the facilitated uptake of water can lead to excessive swelling, in particular at elevated temperatures. Moreover, in processes that involve fluctuations in temperature and humidity, the dynamic changes in water sorption and desorption can progressively increase stresses and defects in the material [15]. Generally, the *DS* is a compromise between water affinity and membrane stability. To facilitate higher *DS* values, extensive research is devoted to reinforcement of SPEEK, in order to strengthen the material while maintaining the hydrophilic properties [16-27].

In the context of membrane stability and swelling, two membrane types can be considered. The first configuration is an asymmetric integrally skinned membrane that consists of a dense selective layer atop of a porous support, both of the same material. Such membranes possess good structural stability, because the swelling behavior of the two layers is compatible. The second configuration is a composite membrane that consists of a porous support with atop a coated dense selective layer of a different material. Composite membranes are more susceptible to interfacial stresses, as the swelling of the support and selective layer can be distinct. A hydrophobic support that delivers mechanical stability swells usually much less than a hydrophilic layer on top of it. This can lead to deteriorated membrane integrity. However, some difficulties have been reported with the formation of the porous substrate in integrally skinned SPEEK membranes for dehydration applications [25]. The conditions required to obtain a dense selective layer can lead to the formation of a support with insufficient porosity. This hinders the water permeation through such integrally skinned SPEEK hollow fibers [25]. Composite membranes have advantageous of rather facile preparation of defect free, thin selective layers with tunable thickness, by using commercially available porous supports. With (ultra-)thin films higher permeances can be obtained [28-30]. In previous research on SPEEK and other highly hydrophilic polymeric hollow fiber membranes, in general, a maximum water permeance in the order of ~5000 GPU is reported. The typical thicknesses of the selective layers used in those studies is in the order of a few micrometers [31]. The maximum water permeance has been attributed to limitations induced by concentration polarization, rather than by the membrane thickness [31]. Nevertheless, in a study on ultra-thin polydopamine films (thickness <100 nm), a higher water permeance is reported: 9000 GPU [32]. For an effective

and efficient dehydration process thus the aim would be to prepare films that are sufficiently thin and stay defect free under the application conditions.

### 1.2.2 Process design

Another challenge is the design of a process that allows the removal of water from the permeate side. For dehydration processes with low feed pressure, such as harvesting of water from air (ambient pressure) or flue gas dehydration (2.5 bar), a vacuum can be applied at the permeate side to collect water [13, 33]. In the process of dehydration with compressed carbon dioxide, the feed pressure is relatively high. In this thesis, the feed pressure is considered to be  $\sim 100$  bar, but in practice it can be even up to 200 bar, depending on the food product to be dried. The high pressure of the feed corresponds to a high driving force for the carbon dioxide. Despite the low carbon dioxide permeability of SPEEK reported in literature (20 Barrer in a highly swollen state [14]), the high driving force for transport of carbon dioxide can still result in high fluxes of this component. Hence, the use of a vacuum at the permeate side does not appear to be beneficial. Instead, a sweep gas to collect permeating water can be a more feasible option. As sweep gas, carbon dioxide could be used. The disadvantage is that in that case, the permeate stream has to be recirculated and regenerated to avoid high gas emissions. In addition, carbon dioxide losses from the retentate have to be compensated for. These steps create additional process costs. A representative process is shown in Figure 1.3.

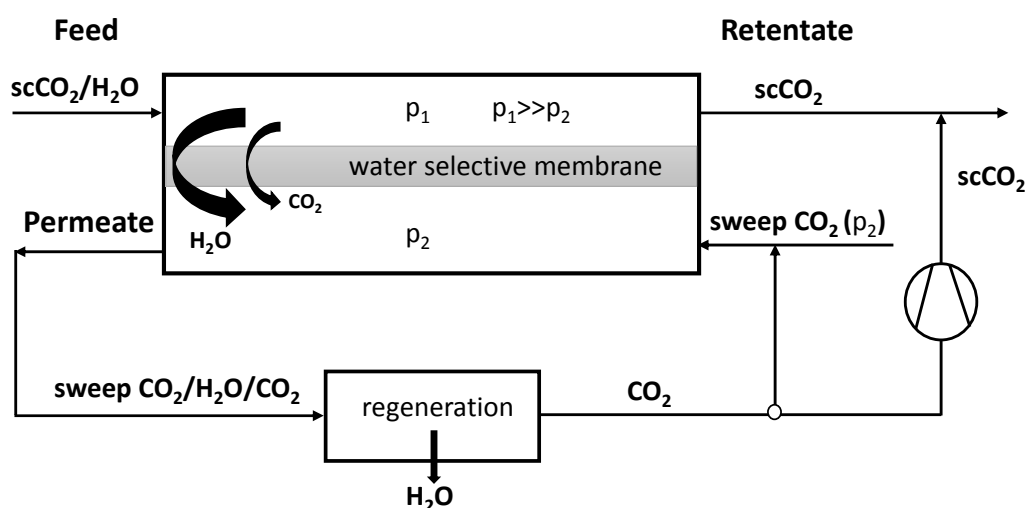


**Figure 1.3** Scheme of a dehydration process of  $\text{scCO}_2$  using a hollow fiber membrane module. To avoid high  $\text{CO}_2$  emissions, permeate has to be recirculated and regenerated.

### 1.3 Scope of the thesis

This thesis aims to investigate and elaborate on the above-described aspects, starting from the fundamentals, and to give directions for further technology development. Within this context, the thesis covers studies on the intrinsic properties of thin SPEEK films that can potentially be used in composite follow fiber membranes, to assess their applicability (in terms of stability) in high water activity systems. In addition, the designs of processes for dehydration of compressed carbon dioxide are evaluated and the added value of a membrane unit in such processes is assessed.

**Chapter 2** is focused on the intrinsic properties of thin film SPEEK membranes that are coated on a substrate, using spectroscopic ellipsometry as one of the main characterization techniques. In particular, the extent of optical anisotropy in the SPEEK films is investigated. Optical anisotropy can arise from molecular orientations and internal stresses in a material. The effects of various formation procedures, solvents with distinct properties, and conditioning temperatures, on the extent of optical anisotropy are investigated. It is shown under which conditions thin SPEEK films tend to be isotropic.

The impact of above investigated anisotropy on swelling behavior is the focus of **Chapter 3**. Two distinct phenomena determine the behavior of thin SPEEK films upon exposure to liquid water. Particularly interesting is the effect of humidity during and after film formation on the internal molecular arrangements in the SPEEK membranes, causing distinct swelling of films with an equal  $DS$ . The hydration state of the polymer backbone during film formation is shown to have a crucial effect on the internal structure of the SPEEK films.

**Chapter 4** is focused on SPEEK thermal stability that is considerably reduced compared to pure PEEK. This study involves various measurement techniques to determine the onset temperatures of degradation of the highly sulfonated SPEEK membranes, for short and long term exposure to elevated temperature. The effects on thermal stability of thin SPEEK films when the protons in the sulfonic acid groups are exchanged with sodium ions are investigated as well.

**Chapter 5** investigates a possible reinforcement method of sulfonated polymers by chemical modification: formation of interpenetrating networks using polyols (ethylene glycol and glycerol). Various concentrations of the polyols are used and the effect on water-induced

swelling of thin SPEEK films is investigated. The results indicate that various materials properties and the internal structure (swelling, thermal decomposition, anisotropy) are affected by the chemical modification.

**Chapter 6** presents Aspen Plus<sup>®</sup> simulations of the dehydration of carbon dioxide using a hollow fiber membrane module. Two process designs are evaluated on the basis of practical and economic considerations. In one system the permeate is recirculated and regenerated, in the other system it is not. It is discussed how the two systems respond (in terms of performance and costs) to changing membrane properties, in low and high feed stream processes. The factors contributing to the process costs are elaborated on.

In **Chapter 7** all results and findings are summarized and discussed, and conclusions are drawn. A vision on further process development is presented.

## References

1. Nalawade, S.P., F. Picchioni, and L.P.B.M. Janssen, *Supercritical carbon dioxide as a green solvent for processing polymer melts: Processing aspects and applications*. Progress in Polymer Science (Oxford), 2006. **31**(1): p. 19-43.
2. Almeida-Rivera, C.P., S. Khalloufi, and P. Bongers, *Prediction of supercritical carbon dioxide drying of food products in packed beds*. Drying Technology, 2010. **28**(10): p. 1157-1163.
3. Patil, V.E., et al., *Permeation of supercritical fluids across polymeric and inorganic membranes*. Journal of Supercritical Fluids, 2006. **37**(3): p. 367-374.
4. Aguilera, J.M., A. Chiralt, and P. Fito, *Food dehydration and product structure*. Trends in Food Science and Technology, 2003. **14**(10): p. 432-437.
5. Ratti, C., *Hot air and freeze-drying of high-value foods: A review*. Journal of Food Engineering, 2001. **49**(4): p. 311-319.
6. Kemmere, M.F. and T. Meyer, *Supercritical Carbon Dioxide: in Polymer Reaction Engineering*. 2006: Wiley-VCH Verlag GmbH & Co. KGaA. 1-339.
7. Almeida-Rivera, C., et al., *Mathematical description of mass transfer in supercritical-carbon-dioxide-drying processes*, in *Computer Aided Chemical Engineering*, M.C.G. E.N. Pistikopoulos and A.C. Kokossis, Editors. 2011, Elsevier. p. 36-40.
8. Metz, B. and I.P.o.C.C.W.G. III., *Carbon Dioxide Capture and Storage: Special Report of the Intergovernmental Panel on Climate Change*. 2005: Cambridge University Press.
9. Nikolaev, V.V., A.N. Vshivtsev, and A.D. Shakhov, *Regeneration of zeolitic adsorbents by organic solvents*. Chemistry and Technology of Fuels and Oils, 1997. **33**(6): p. 344-346.
10. Jacobs, P.A. and R.A. van Santen, *Zeolites: Facts, Figures, Future*. 1989: Elsevier Science.
11. Baker, R.W., *Membrane Technology and Applications*. 2nd ed. 2004, California: John Wiley & Sons, Ltd.
12. *Victrix®PEEK polymers*. [cited 2015 04 March]; Available from: <http://www.victrix.com/en/victrix-peek>.
13. Sijbesma, H., et al., *Flue gas dehydration using polymer membranes*. Journal of Membrane Science, 2008. **313**(1-2): p. 263-276.
14. Potreck, J., *Membranes for flue gas treatment. Transport behavior of water and gas in hydrophilic polymer membranes*. PhD Thesis 2009, University of Twente.
15. Oh, K.-H., et al., *Enhanced Durability of Polymer Electrolyte Membrane Fuel Cells by Functionalized 2D Boron Nitride Nanoflakes*. ACS Applied Materials & Interfaces, 2014. **6**(10): p. 7751-7758.
16. Di Vona, M.L., et al., *SPEEK-TiO<sub>2</sub> nanocomposite hybrid proton conductive membranes via in situ mixed sol-gel process*. Journal of Membrane Science, 2007. **296**(1-2): p. 156-161.
17. Kaliaguine, S., et al., *Properties of SPEEK based PEMs for fuel cell application*. Catalysis Today, 2003. **82**(1-4): p. 213-222.
18. Fontananova, E., et al., *Stabilization of sulfonated aromatic polymer (SAP) membranes based on SPEEK-WC for PEMFCs*. Fuel Cells, 2013. **13**(1): p. 86-97.
19. Colicchio, I., et al., *Development of hybrid polymer electrolyte membranes based on the semi-interpenetrating network concept*. Fuel Cells, 2006. **6**(3-4): p. 225-236.
20. Xing, D.M., et al., *Characterization of sulfonated poly(ether ether ketone)/polytetrafluoroethylene composite membranes for fuel cell applications*. Fuel Cells, 2005. **5**(3): p. 406-411.



21. Han, M., et al., *Considerations of the morphology in the design of proton exchange membranes: Cross-linked sulfonated poly(ether ether ketone)s using a new carboxyl-terminated benzimidazole as the cross-linker for PEMFCs*. International Journal of Hydrogen Energy, 2011. **36**(3): p. 2197-2206.
22. Song, J.-M., et al., *The effects of EB-irradiation doses on the properties of crosslinked SPEEK membranes*. Journal of Membrane Science, 2013. **430**: p. 87-95.
23. Celso, F., et al., *SPEEK based composite PEMs containing tungstophosphoric acid and modified with benzimidazole derivatives*. Journal of Membrane Science, 2009. **336**(1-2): p. 118-127.
24. Cai, H., et al., *Properties of composite membranes based on sulfonated poly(ether ether ketone)s (SPEEK)/phenoxy resin (PHR) for direct methanol fuel cells usages*. Journal of Membrane Science, 2007. **297**(1-2): p. 162-173.
25. Shao, P., et al., *Composite membranes with an integrated skin layer: preparation, structural characteristics and pervaporation performance*. Journal of Membrane Science, 2005. **254**(1-2): p. 1-11.
26. Wang, J., et al., *Novel covalent-ionically cross-linked membranes with extremely low water swelling and methanol crossover for direct methanol fuel cell applications*. Journal of Membrane Science, 2010. **363**(1-2): p. 112-119.
27. Yang, T., *Composite membrane of sulfonated poly(ether ether ketone) and sulfated poly(vinyl alcohol) for use in direct methanol fuel cells*. Journal of Membrane Science, 2009. **342**(1-2): p. 221-226.
28. Ogieglo, W., et al., *Probing the surface swelling in ultra-thin supported polystyrene films during case II diffusion of n-hexane*. Macromolecular Chemistry and Physics, 2013. **214**(21): p. 2480-2488.
29. Salih, A.A.M., et al., *Interfacially polymerized polyetheramine thin film composite membranes with PDMS inter-layer for CO<sub>2</sub> separation*. Journal of Membrane Science, 2014. **472**: p. 110-118.
30. Gorgojo, P., et al., *Ultrathin polymer films with intrinsic microporosity: Anomalous solvent permeation and high flux membranes*. Advanced Functional Materials, 2014. **24**(30): p. 4729-4737.
31. Metz, S.J., *Water vapour and gas transport through polymeric membranes*. PhD Thesis 2003, University of Twente.
32. Pan, F., et al., *Bioinspired fabrication of high performance composite membranes with ultrathin defect-free skin layer*. Journal of Membrane Science, 2009. **341**(1-2): p. 279-285.
33. Bergmair, D., et al., *System analysis of membrane facilitated water generation from air humidity*. Desalination, 2014. **339**(1): p. 26-33.





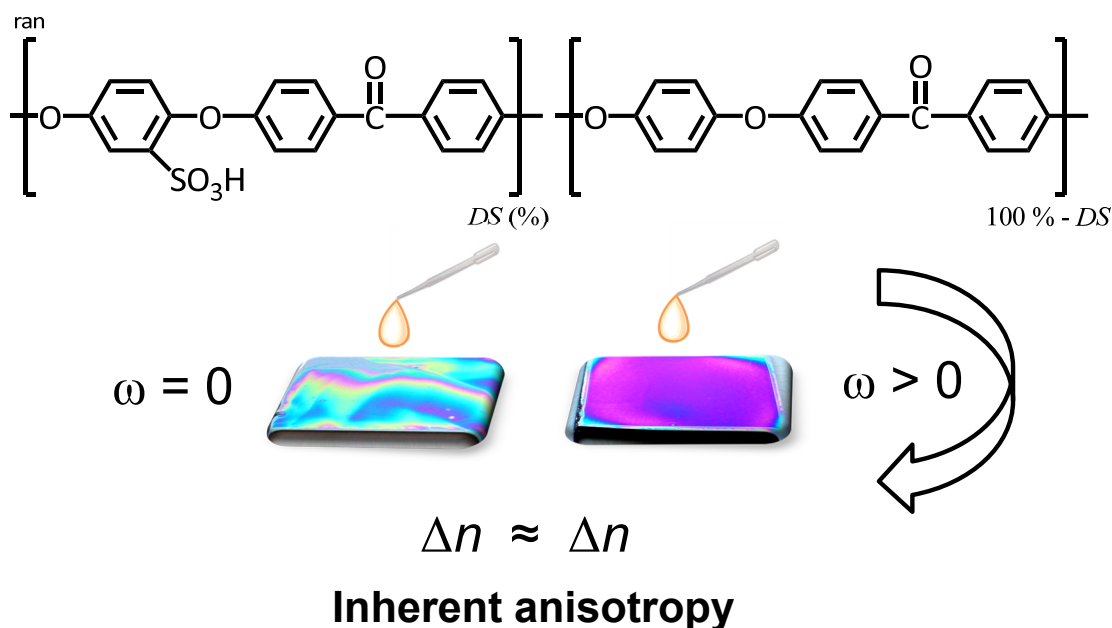
# Chapter 2

## Optical anisotropy, molecular orientations, and internal stresses in thin sulfonated poly(ether ether ketone) films

This chapter has been published as:

Koziara, B.T.; Nijmeijer, K.; Benes, N.E., *Optical anisotropy, molecular orientations, and internal stresses in thin sulfonated poly(ether ether ketone) films*. *Journal of Materials Science* **2015**, 50 (8), 3031-3040.

## Abstract



The thickness, the refractive index, and the optical anisotropy of thin sulfonated poly(ether ether ketone) films, prepared by spin-coating or solvent deposition, have been investigated with spectroscopic ellipsometry. For not too high polymer concentrations ( $\leq 5$  wt%) and not too low spin speeds ( $\geq 2000$  rpm), the thicknesses of the films agree well with the scaling predicted by the model of Meyerhofer, when methanol or ethanol are used as solvent. The films exhibit uniaxial optical anisotropy with a higher in-plane refractive index, indicating a preferred orientation of the polymer chains in this in-plane direction. The radial shear forces that occur during the spin-coating process do not affect the refractive index and the extent of anisotropy. The anisotropy is due to internal stresses within the thin confined polymer film that are associated with the preferred orientations of the polymer chains. The internal stresses are reduced in the presence of a plasticizer, such as water or an organic solvent, and increase to their original value upon removal of such a plasticizer.

## 2.1 Introduction

The properties of membranes derived from sulfonated poly(ether ether ketone) (SPEEK) have been investigated for many years. SPEEK films have a distinct thermo-chemical-mechanical stability. In addition, the degree of sulfonation (*DS*) of SPEEK can be changed, which can be beneficial for many applications. In the vanadium redox flow battery and fuel-cell applications, the sulfonic acid groups in SPEEK enable conductivity of protons [1-8]. In biorefinery applications and reverse electrodialysis, the sulfonic groups provide the possibility to exchange cations [9, 10]. The high affinity for water of the negatively charged groups empowers application of SPEEK membranes in dehydration processes [11-15]. Additionally, due to the amorphous structure and high glass-transition temperature, SPEEK membranes have been considered good candidates for high-pressure gas separation [16-18].

Despite the merits, the high concentration of sulfonic acid groups also has drawbacks. In comparison to pure poly(ether ether ketone) (PEEK), the sulfonation of this material to SPEEK causes a significant reduction in thermal stability [19]. This reduction in stability becomes larger for a higher degree of sulfonation [20]. Generally, above 200 °C, chemical decomposition of SPEEK starts to occur, which is initiated from the sulfonated domains [21, 22]. Therefore, the thermal treatments that are frequently performed after formation of membranes to relieve stresses and remove solvents, are challenging in the case of SPEEK. The effective removal of non-volatile, high boiling point casting solvents, such as *N*-methylpyrrolidone (NMP) and dimethyl sulfoxide (DMSO), is hindered [22], and alternative removal methods have been reported, such as rinsing-out of DMSO in boiling water [23].

In addition, the highly non-equilibrium glassy state of polymeric films can be affected by high spin speeds or rapid solvent evaporation [24, 25]. These may cause polymer chains to orient in preferential directions. The preferred orientations of polymer chains induce internal stresses in the material that in turn can affect the permeability and the selectivity [26]. For many polymers, the heating above the glass transition temperature and subsequent thermal quenching remove the non-equilibrium characteristics. Concerning SPEEK, the study of Reyna-Valencia et al. has shown that membranes with a degree of sulfonation of 63 and 83 %, formed from solvent casting using *N,N*-dimethylacetamide (DMAc) and dimethylformamide (DMF), exhibited polymer chain orientations [27]. Notably, their study shows that repeated heating to temperatures close to the glass transition temperature causes reorganization of the material,

with more pronounced preferential orientations of the polymer chains in the plane parallel to the surface of the film [27]. As such, SPEEK membranes are affected by their processing history and the thermal cycling results in relaxations that cause the material to become anisotropic, instead of isotropic.

In this paper, we focus on the relations between SPEEK film formation procedures and the molecular orientations in the obtained SPEEK films. Two techniques have been used for film preparation; spin-coating and solution deposition. For spin-coating, methanol and ethanol have been used as volatile organic solvents with distinct physical properties. For solution deposition, the volatile methanol and non-volatile NMP have been selected. Motivated by the study of Reyna-Valencia et al. [27], we conduct a systematic study on the effects of induced polymer relaxations on the internal stresses in SPEEK films, by changing the ambient relative humidity and the conditioning temperatures. The extent of polymer chain orientation is related to the optical anisotropy of the films [28], which in this study is determined with spectroscopic ellipsometry.

## 2.2 Theory

### Spectroscopic ellipsometry

Spectroscopic ellipsometry is an optical method that is used to determine thickness and wavelength-dependent refractive indices (optical dispersion) of films atop a substrate. For a detailed explanation, the interested reader is referred to the book of Fujiwara [29]. In short, the method is based on measuring the change in the polarization state of p- and s-polarized light upon reflection at a surface. In practice, linearly polarized light is used as incident beam and after reflection the light has become, to a certain extent, elliptically polarized. The ellipticity is quantified by two angles: the amplitude component *Psi* ( $\Psi$ ) [ $^{\circ}$ ] and phase difference *Delta* ( $\Delta$ ) [ $^{\circ}$ ]. Combined, these can be expressed as the complex reflectance ratio,  $\rho$  [-]:

$$\rho = \frac{r_p}{r_s} = \tan(\Psi) \cdot e^{i\Delta} \quad \text{Eq. 2.1}$$

where  $r_p$  and  $r_s$  is the reflectivity of the p- and s-polarized light [-], respectively.

The dispersion and thickness of a film are obtained by fitting an optical model to the experimentally obtained spectra. This is expedited by using a simple expression for the

dispersion. Various empirical expressions are available. For transparent isotropic materials, the Cauchy relation is generally considered appropriate [29]:

$$n(\lambda) = A + \frac{B}{\lambda^2} + \frac{C}{\lambda^4} \quad \text{Eq. 2.2}$$

where  $n(\lambda)$  is the wavelength dependent refractive index [-],  $\lambda$  is the wavelength of the light [nm], and  $A$ ,  $B$  and  $C$  are coefficients that describes the dependency of the refractive index on the wavelength.

The quality of the fit of the optical model to the experimental data is given as the Mean Square Error (*MSE*). There is no fixed *MSE* value that resolves if a model can be considered correct or not. For thicker films and *in-situ* measurements, a maximum value of 20 is considered to be reasonable [30].

For anisotropic materials, the refractive index is dependent on the propagation direction of the light in the material. When the refractive index is different in all directions,  $n_x \neq n_y \neq n_z$ , the material is referred to as biaxial anisotropic. Thin polymer films often exhibit uniaxial anisotropy, with a different refractive index in the direction perpendicular to the surface of the film,  $n_x = n_y \neq n_z$ . The  $z$ -direction corresponds with the so-called optical axis, i.e., the axis of symmetry with all perpendicular directions optically equivalent. The difference between two refractive indices is called optical anisotropy,  $\Delta n$ , also termed birefringence. In this paper, we refer to  $\Delta n$  as to optical anisotropy. In the case of a uniaxial anisotropic material, the single optical anisotropy value is given by:

$$\Delta n = n_{xy} - n_z \quad \text{Eq. 2.3}$$

Here,  $n_{xy}$  is referred to as the in-plane refractive index (also termed ordinary) and  $n_z$  is referred to as the out-of-plane refractive index (also termed extraordinary). The optical anisotropy is correlated with internal stresses in a material by the empirical equation [31]:

$$\Delta n = C \cdot (\sigma_1 - \sigma_2) \quad \text{Eq. 2.4}$$

where  $\sigma_1$  and  $\sigma_2$  are principal in-plane and out-of-plane stresses [Pa] and  $C$  is the stress-optical coefficient [ $\text{Pa}^{-1}$ ].



## 2.3 Experimental

### 2.3.1 Materials

SPEEK was obtained by sulfonation of PEEK (Viktrex, United Kingdom) using sulfuric acid according to the method reported by Shibuya et al. [32]. The degree of sulfonation ( $DS\%$ ) determined by  $^1\text{H-NMR}$  in  $\text{DMSO-d}_6$  using a AscendTM 400 (Bruker) at a resonance frequency of 400 MHz, according to the method described by Zaidi et al. [33], was 84 %. Methanol and ethanol (Emsure® grade of purity) were obtained from Merck (The Netherlands), NMP 99 % extra pure was obtained from Acros Organics (The Netherlands).  $\text{DMSO-d}_6$  (99.5 atom % D) was obtained from Sigma-Aldrich (The Netherlands). Nylon membrane 25 mm syringe filters (pore size 0.45  $\mu\text{m}$ ) were obtained from VWR International. Polished,  $\langle 100 \rangle$ -oriented silicon wafers were obtained from Okmetic (Finland). Nitrogen gas (4.5) was supplied by Praxair (The Netherlands).

### 2.3.2 Film preparation

Films were coated on pre-cut pieces of a silicon wafer. Prior to coating, the solutions were filtered using syringe filters to remove solid contaminations. The two following methods were used for SPEEK film formation.

#### Spin-coating

Films were formed by spin-coating of SPEEK dissolved in either methanol or ethanol (3, 5 and 7 wt%). The spinning time was always 50 s. The spin speed was set at 1000, 2000, 3000 or 4000 rpm. All samples were prepared in duplicate; one part was treated under vacuum at 30 °C for 48 h, and the second part under vacuum at 140 °C for 48 h.

#### Solution deposition

Films were formed by deposition of SPEEK dissolved in methanol or *N*-methylpyrrolidone (NMP) on the substrate and subsequent solvent evaporation. Thus, the spin speed was equal to zero. Prior to deposition from the SPEEK/NMP solution, the silicon wafers were pre-treated 20 minutes in oxygen plasma, in order to ensure NMP wettability of silicon wafer. Without plasma treatment, the NMP solutions did not wet the wafers. All samples were prepared in duplicate; one part was treated under vacuum at 30 °C for 48 h, and the second part under vacuum at 140 °C for 48 h.

### 2.3.3 Ellipsometry measurements

An M-2000 spectroscopic ellipsometer (J.A. Woollam Co., Inc., USA) was used. The size of the light spot for the standard configuration was 2 mm. For the films obtained with the solution deposition technique, focusing probes were used with a light spot size of 150  $\mu\text{m}$ . This was necessary to cope with the very extensive thickness variations within each of these films. *Ex-situ* experiments were conducted at three angles of incidence ( $55^\circ$ ,  $65^\circ$ , and  $70^\circ$ ) for the initial investigations of the optical anisotropy of the SPEEK films (section 2.4.1). Further systematic studies were conducted at an angle of incidence of  $70^\circ$ . *In-situ* drying measurements under nitrogen were conducted for 15 minutes using a custom-made temperature-controlled glass flow cell [34]. Prior to entering the flow cell, the nitrogen was dried with a water absorbent and was led through an oxygen trap.

The CompleteEase 4.64 software (J.A. Woollam Co., Inc.) was used for spectroscopic data modeling. The optical properties of the silicon wafer, and the native oxide silica layer on top of it, were taken from the software database. The thickness of the native silicon oxide was measured with spectroscopic ellipsometry and the obtained value of  $\sim 2$  nm was fixed in further modeling. The wavelength range included in the fitting was 450 – 900 nm; in this range SPEEK is transparent and the Cauchy relation (Eq. 2.2) can be applied. All values reported for  $n$  and  $\Delta n$  correspond to the value at the wavelength of a helium–neon laser (632.8 nm). Depolarization that occurs due to thickness inhomogeneity was always carefully checked and fitted. In uniaxial modeling, the  $B$  parameters of the Cauchy equation for  $n_{xy}$  and  $n_z$  were coupled to ensure a physical realistic optical dispersion for SPEEK films. By coupling  $B_{xy}$  and  $B_z$ , a parallel trend of  $n_{xy}$  and  $n_z$  with wavelength is imposed and it is prevented that they cross.

### 2.3.4 Analysis of variance

Analysis of variance (ANOVA) with a confidence interval of 95 % was used to substantiate the significant differences in optical properties of SPEEK films formed under various conditions in spin-coating.

## 2.4 Results and Discussion

### 2.4.1 Optical anisotropy

Figure 2.1 shows the ellipsometry spectra of a representative SPEEK film coated on a silicon substrate. Both the  $\Psi$  and  $\Delta$  spectra show a single oscillation with a position and amplitude that depends on the angle of incidence. These raw spectra are typical for SPEEK films of several hundred nanometers.

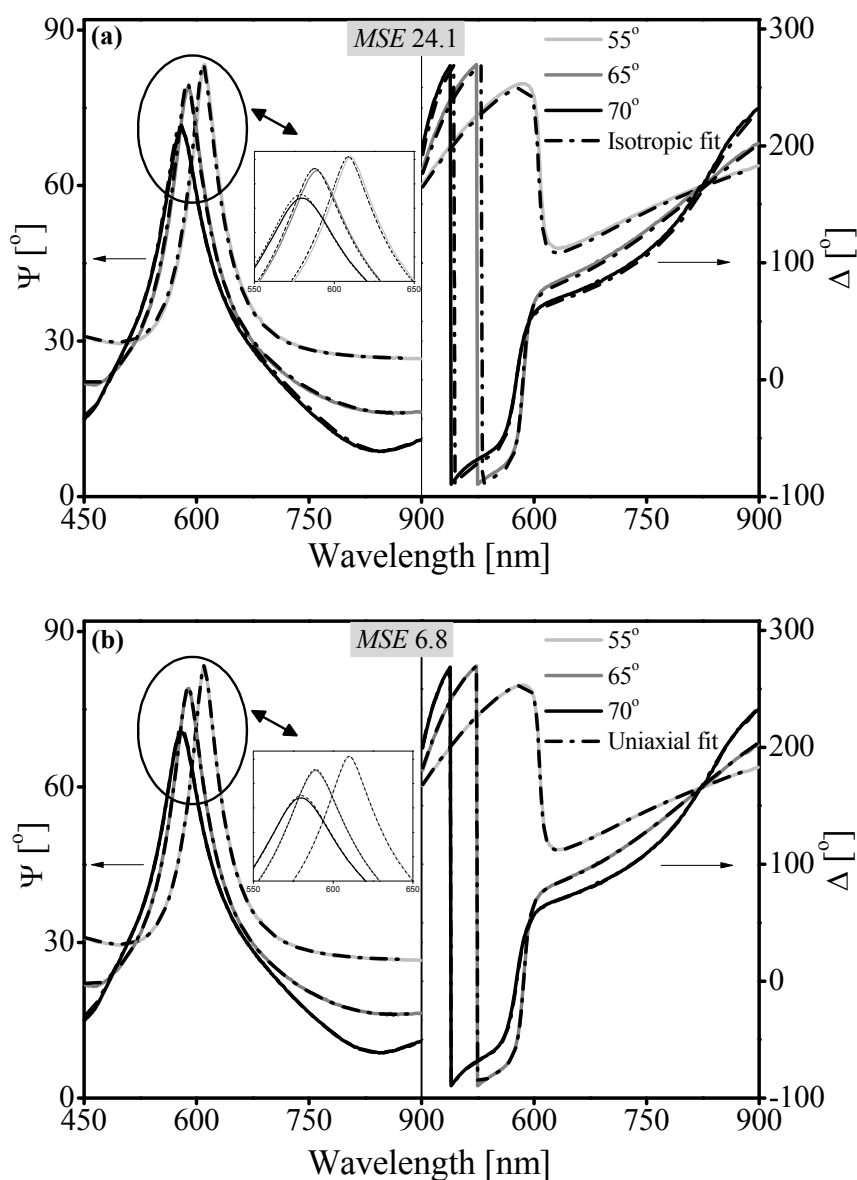


**Figure 2.1** Isotropic (a) and uniaxial (b) fit for  $\Psi$  and  $\Delta$  of a representative SPEEK film with a thickness of 324 nm, coated on a silicon wafer.

Fitting simultaneously the data obtained at the three angles, with an optical model that considers the material to be isotropic, yields a thickness of 324.4 nm (Figure 2.1a). However, the  $MSE=24.1$ , corresponding to this optical fit, is relatively high and not acceptable for a single film of low thickness. The high  $MSE$  value is mainly due to the skewness of the spectra that cannot be captured by the isotropic optical model. Fitting the data with a model that considers the material as uniaxial anisotropic results in an essentially unchanged thickness of 324.8 nm, but also in a significant reduction in  $MSE$  to a value of 6.8 (Figure 2.1b). This significant decrease in  $MSE$  is considered to indicate that SPEEK films are anisotropic and  $\Delta n$  should be taken into account. Spectra obtained at different spots and after different sample rotations within the  $xy$  plane show no differences in  $\Delta n$ , implying that the SPEEK films exhibit no biaxial anisotropy and that the uniaxial  $\Delta n$  does not depend on the radial position on the wafer. The observed optical uniaxial anisotropy coincides with the observations of Reyna-Valencia et al. [27], who also determined  $\Delta n$  using an optical method and correlated the value of  $\Delta n$  to in-plane polymer chain orientations.

Here, we study several factors that may affect  $\Delta n$  and that are discussed in more detail below. The factors are the ambient relative humidity, the drying process, film formation via spin-coating and solution deposition, the use of volatile and non-volatile solvents, and the film conditioning under vacuum at 30 and 140 °C.

## 2.4.2 The effect of ambient relative humidity and subsequent drying

The dynamics of the changes in thickness and refractive indices of a representative SPEEK film, upon drying under nitrogen, are presented in Figure 2.2a. In Figure 2.2b, the black solid lines in the  $Psi$  and  $Delta$  spectra correspond to spectra obtained under ambient conditions (relative humidity  $RH=50\%$ ), prior to drying.

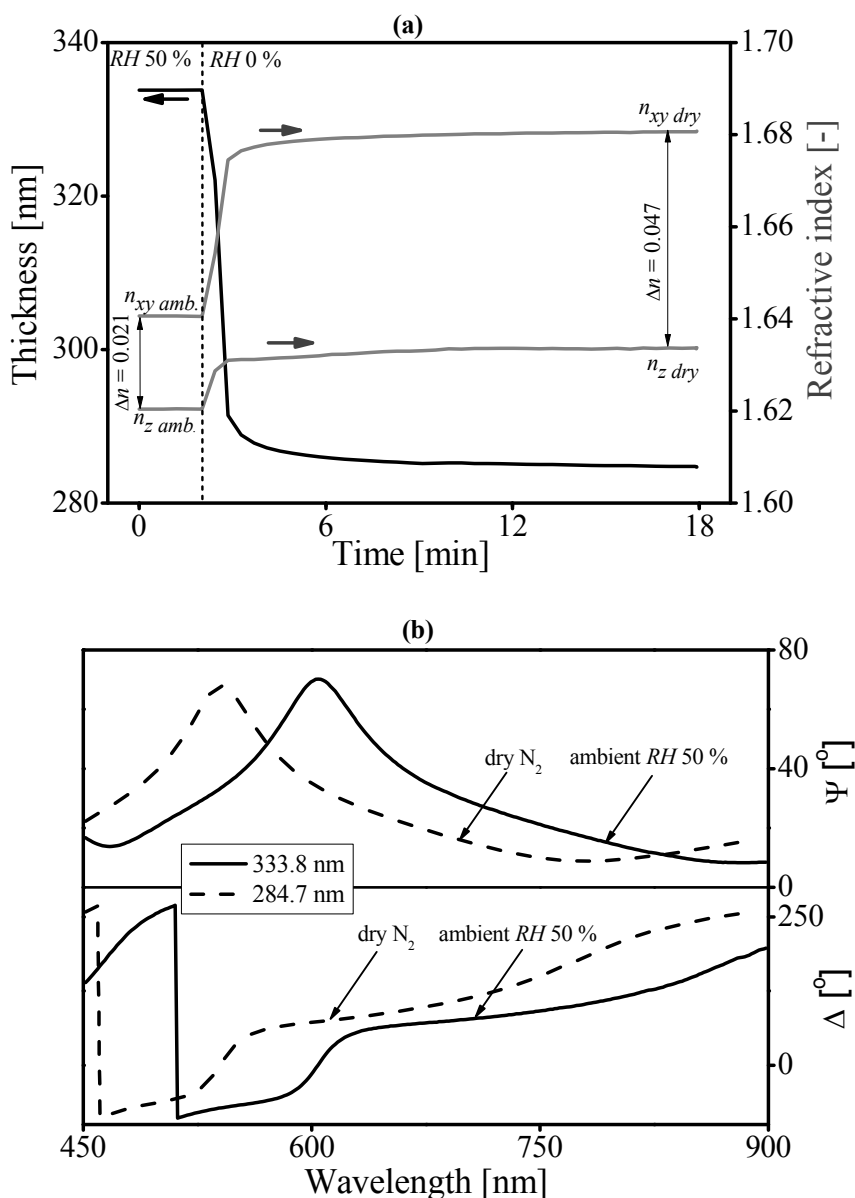


**Figure 2.2** Thickness, refractive indices and optical anisotropy of a SPEEK film (a) in the ambient and in dry  $N_2$ , and (b) corresponding  $Psi$  ( $\Psi$ ) and  $Delta$  ( $\Delta$ ) data in the ambient (solid line) and at the end of the drying in  $N_2$  (dashed line). The film was spin-coated from a 5 wt% methanol solution at 2000 rpm and conditioned under vacuum at 30 °C for 48 h.

The dashed lines correspond to the spectra obtained at the end of the drying process. The shift of oscillations towards lower wavelengths indicates a decrease in film thickness. The dynamics of the changes in thickness are representative for a desorption process involving both water diffusion and polymer relaxation. Initially, a sharp decrease in thickness is observed, due to diffusion limited removal of water. The subsequent slower reduction in thickness is related to polymer relaxation, which is a process with a much larger time constant. These observations are consistent with those of Potreck et al., who studied vapor sorption in SPEEK by mass uptake [35]. During desorption, the sample thickness decreased from an initial thickness of 333.8 nm to 284.7 nm at the end of the desorption process. Concurrently, the refractive indices of the film increased, indicating the removal of water and the densification of the polymer. Thus, the refractive index of the films is lower under ambient conditions as compared to under dry nitrogen. The presence of the sulfonic acid groups in SPEEK makes the material highly hydrophilic and causes the polymer films to swell and plasticize in the presence of water vapor [36, 37]. Because the refractive index of liquid water, 1.33, is lower than that of the polymer, the swollen films have a lower overall refractive index.

The removal of water also causes a significant increase in optical anisotropy, from 0.021 to the value of 0.047. This increase indicates that the stresses in the material become higher upon removal of water. The increase of optical anisotropy upon desorption of water coincides with the observations of Reyna-Valencia et al. [27], who have shown that upon repeated thermal cycling, SPEEK films undergo orientations that result in increased and constant optical anisotropy. Moreover, they reported that the direction of the orientations was in-plane to the surface of the film. SPEEK films studied in our paper also exhibit orientations in the same direction. This is evidenced by the in-plane refractive  $n_{xy}$ , which is always higher than the out-of-plane refractive index  $n_z$ .

Thus, the results show that the ambient relative humidity has a direct impact on the thickness and optical anisotropy of SPEEK films. High affinity for the moisture results in swelling that in turn reduces the internal stresses. The effect becomes stronger with increasing relative humidity, as the sorption of water for SPEEK increases sharply above  $RH=50\%$ . These observations imply that correct reporting of properties of SPEEK films requires specification of the relative humidity.

Additionally, the usage of SPEEK in processes, in which SPEEK films are alternately exposed to high humidity and dry conditions, results in repeated changes in material dimensions. Such behavior damages the membrane integrity, and reinforcement procedures are necessary [38].

### 2.4.3 Spin-coating with volatile solvents

#### Effect on thickness

Figure 2.3 shows the thicknesses as a function of the spin speed for several SPEEK films, prepared by using either methanol or ethanol as a solvent. The measurements were performed in a humid ambient ( $RH=50\%$ ). At a spin speed of 1000 rpm, no layers could be obtained from 5 and 7 wt% solutions, due to poor substrate wettability at those conditions. The two distinct conditioning temperatures of 30 and 140 °C did not result in a difference in thickness.

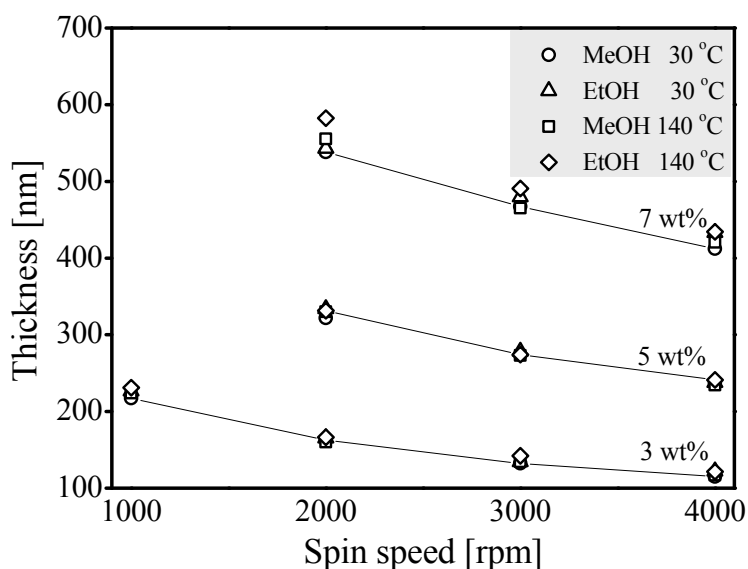


**Figure 2.3** The thicknesses of SPEEK films formed via spin-coating from methanol (○ and □) and ethanol (△ and ◇) solutions of concentrations 3, 5 and 7 wt%, and conditioned under vacuum at 30 °C (○ and △) or 140 °C (□ and ◇). Thickness values have been obtained from the center of the sample. Lines are to guide the eye.

Methanol and ethanol are highly volatile solvents, commonly used for the fabrication of SPEEK membranes with a high *DS* [39]. The viscosity of methanol (0.00059 Pa·s) is approximately half of that of ethanol (0.0012 Pa·s), and the vapor pressure of methanol (13.02 kPa) is almost twice as high as that of ethanol (5.95 kPa) [40, 41]. However, the data show no significant differences in the thickness of the films for the two solvents, despite the different solvent properties. This is in agreement with the scaling predicted by the model of Meyerhofer [42]. In this model, the film thinning process is considered to comprise two distinct and subsequent stages. In the first stage, the film thinning is only due to centrifugal induced radial flow. In the second stage, the film thinning is only due to solvent evaporation. The resulting expression for the film thickness,  $h$  [nm], predicts the following scaling:

$$h \sim (\eta_0 \cdot \rho_{vap})^{\frac{1}{3}} \omega^{-\frac{1}{2}} \quad \text{Eq. 2.5}$$

This expression contains the initial solution viscosity  $\eta_0$  [Pa·s], the solvent vapor pressure  $\rho_{vap}$  [kPa], and the spin speed  $\omega$  [rpm]. Based on this model, the expected difference in layer thickness for the two solvents is ~3 %. For the films obtained from the solutions with the low concentrations (3 and 5 wt%) and high spin speeds (2000 – 4000 rpm), the thickness scales with  $\omega^m$ , where  $m$  is an empirical scaling parameter. For both solvents and concentrations, the value of  $m$  varied between -0.44 and -0.5. This is again in good agreement with the scaling predicted by the expression of Meyerhofer [42, 43]. Also, the  $R$ -squared of the linear fits for calculation of the  $m$  is >0.998. For the higher concentration of 7 wt%, the scaling  $m$  is between -0.32 and -0.42 indicating that the simple model starts to fail for higher concentrations. The linear fits are also less appropriate, as is evidenced from the  $R$ -squared values (~0.98).

The presented thickness values are obtained from the centers of the samples. The thickness at the outer sides of the samples is typically a few percent less. This is due to the shear thinning viscosity of the polymer solutions, and the radial dependence of the shear forces. The effect is more pronounced for more concentrated polymeric solutions. The results are in concurrence with the research of Manish Gupta et al., who also reported shear thinning behavior for SPEEK solutions [44].



### Effect on optical anisotropy and refractive index

Figure 2.4a and b depict  $\Delta n$  and  $n_{xy}$  of the films corresponding to Figure 2.3 as a function of the spin speed, respectively. Only the data for the 3 and 5 wt% solutions are presented. For the 7 wt% solution, inhomogeneous films ( $MSE > 20$ ) were obtained, resulting in a pronounced scattering of the  $\Delta n$  and  $n_{xy}$  values. The films were measured under humid ambient ( $RH=50\%$ ) and dry nitrogen atmosphere ( $RH=0\%$ ). The spin speed was varied in the range 1000–4000 rpm to investigate if shear forces during the spinning process affect the orientation of the polymer chains. In addition to the variable spin speed, the difference in viscosity of methanol and ethanol also implies distinct shear forces.

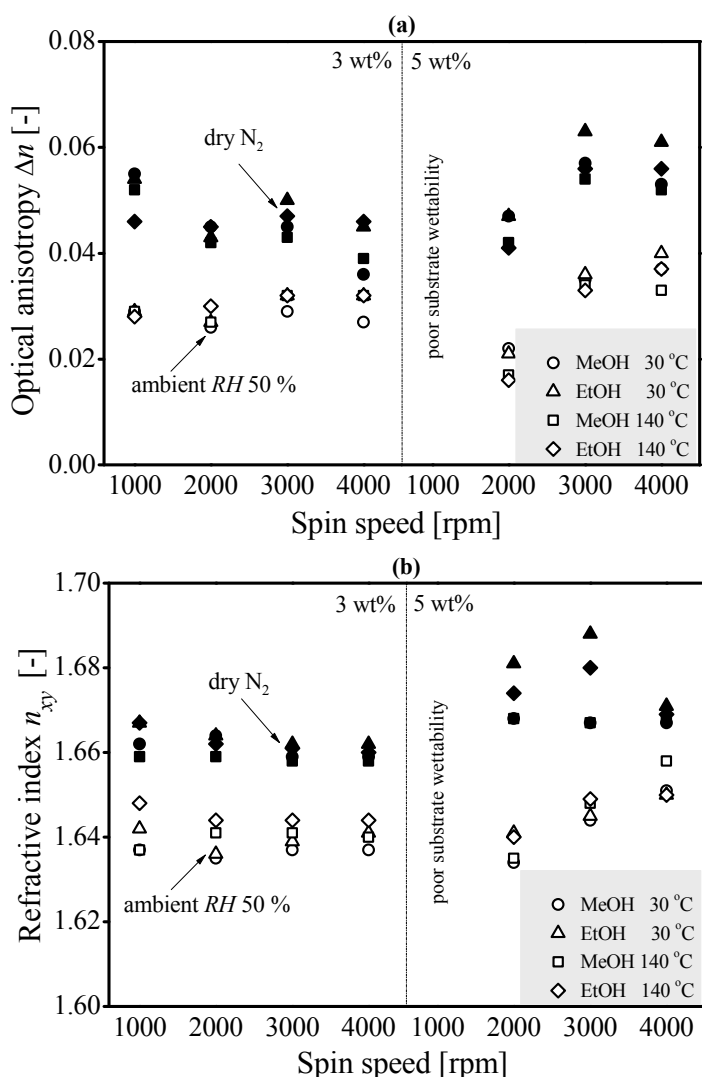


**Figure 2.4** Optical anisotropy,  $\Delta n$  (a) and in-plane refractive index,  $n_{xy}$  (b) of SPEEK films formed via spin-coating from methanol ( $\circ$  and  $\square$ ) or ethanol ( $\Delta$  and  $\diamond$ ) of concentrations 3 and 5 wt%, and conditioned under vacuum at 30 °C ( $\circ$  and  $\Delta$ ) or 140 °C ( $\square$  and  $\diamond$ ). Open symbols indicate the ambient humid atmosphere ( $RH=50\%$ ) and closed symbols indicate the end of the drying process. The films obtained from 7 wt% are omitted due to high film inhomogeneity.

For the data obtained at high spin speed ( $\geq 2000$  rpm) for 3 wt% solutions, no significant systematic dependence of  $\Delta n$  and  $n_{xy}$  on the spin speed or solvent properties is observed. The analysis of variance confirms that no statistically relevant differences exist for those films. This indicates that the shear forces during the spinning process have no direct apparent effect on the stresses inside the final films, which is consistent with the absence of variations in  $\Delta n$  and  $n_{xy}$  as a function of the position on the sample. For the lower spin speed of 1000 rpm, some changes, which are supported by ANOVA, in  $\Delta n$  and  $n_{xy}$  can be observed. These can be possibly caused by factors associated when applying very low spin speeds, such as poor surface wettability, increased film inhomogeneity, or changed drying rates [45, 46].

For the 5 wt%, there are statistical significant changes in the values of  $\Delta n$  and  $n_{xy}$ . In particular, for 2000 rpm, the analysis of variance indicates that the values of  $\Delta n$  and  $n_{xy}$  are significantly lower as compared to 3000–4000 rpm. The differences are possibly related to the decreased homogeneity of the films obtained at low spin speeds from more concentrated solutions. A lower homogeneity corresponds to more spatial randomness, and hence, would be manifested by a lower  $\Delta n$ . To support this conclusion, films from 7 wt% solution were so inhomogeneous that their *MSE* exceed the value of 20.

The refractive index is strongly correlated with the density of the film, and the uniaxial anisotropy is related to internal stresses in the film originating from polymer chain orientations. For films from a 3 wt% solution, the refractive index and uniaxial anisotropy are not affected by the spinning conditions; the film thickness can be adjusted by the spin speed without affecting the other film properties. For a higher concentration, 5 wt%, films with lower and higher anisotropy and higher and lower density can be produced. For all SPEEK films,  $n_{xy}$  is higher than  $n_z$ . This signifies that the SPEEK polymer chains are preferentially oriented in-plane to the surface of the film. These orientations are not caused by the radial flow and forces pertaining to the spin-coating process, and are not affected by the physical properties of the solvent used. Furthermore, the preferred chain orientations persist when thermal conditioning is performed at 140 °C instead of 30 °C. 140 °C is apparently too far from the glass transition ( $\sim 200$  °C) [47] to induce structural changes in the polymer films. Both temperatures are sufficient to ensure removal of any residual methanol and ethanol. The internal stresses in the films are affected by the presence of water. Water has high affinity for the charged sulfonic groups and will readily sorb into the material. The presence of water results in plasticization: the polymer chains become more mobile due to the presence of the water. The enhanced

mobility, combined with the dilation of the film in the  $z$ -direction to accommodate the water sorption, causes relaxations of the polymer chains with less preferred in-plane orientations.

#### 2.4.4 Solution deposition with a volatile and a non-volatile solvent

In the previous section, the plasticizing effect of water vapor has been discussed. Water sorption reduces the internal stresses in SPEEK membranes, and therefore, it also reduces the optical anisotropy. A similar effect can be expected to occur for other penetrants, especially for those that are able to dissolve SPEEK. Hence, here we study the optical properties of films that have been made using *N*-methylpyrrolidone (NMP) as a solvent. NMP dissolves SPEEK with a low  $DS$  [7], whereas methanol and ethanol are typically used to dissolve SPEEK with a high  $DS$ . The poor wettability of wafers by NMP complicates controlled spin-coating, which can be circumvented by using the solution deposition method, i.e., spin-coating at zero spin speed.

In Table 2.1 the representative data are presented for SPEEK films formed via solution deposition technique, using NMP or the more volatile methanol as solvent, and measured at  $RH=20\text{--}30\%$ . The film thicknesses could not be easily controlled but they are in the range of the thicknesses from Figure 2.3. The focus is put on optical properties.

Visual observations indicate that film formation occurs in approximately one minute in the case of methanol, and in several hours in the case of NMP. Before conditioning under vacuum at  $30\text{ }^\circ\text{C}$ , methanol-derived films were characterized 30 minutes after formation, and NMP-derived films 3 days after formation. The refractive index values  $n_{xy}$  of the NMP- and methanol-derived films are much lower than those of films corresponding to Figure 2.4b ( $>1.63$ ), indicating that the solvents are still present in the films. The refractive indices of methanol ( $n = 1.32$ ) and NMP ( $n = 1.47$ ) are much lower than that of the polymer, causing the effective refractive index to be reduced when the solvents are present in the films. For the methanol-derived films,  $n_{xy} = 1.58$  is higher as compared to  $n_{xy} = 1.51$  for the NMP-derived films. This result is consistent with the much faster evaporation of methanol as compared to NMP. The low refractive index in the case of the NMP-derived films is actually very close to the value of pure NMP. This indicates that a large concentration of NMP is still present in the film, even at three days after film formation. This is substantiated by the absence of anisotropy in the NMP swollen films;  $\Delta n = 0$  and the isotropic and anisotropic optical models give similar  $MSE$  values. In contrast, significant anisotropy is observed for films derived from the methanol solution;  $\Delta n > 0.01$  and lower  $MSE$  for the anisotropic optical model.

**Table 2.1** Thickness ( $d$ ), refractive index ( $n_{xy}$ ), optical anisotropy ( $\Delta n$ ) and  $MSE$  values for SPEEK films formed via a solution deposition technique using methanol and NMP, measured at  $RH=20-30\%$  after various film conditionings.

| Methanol                                    |                      |                         |                      |                    | NMP   |                      |                         |                      |                    |
|---|----------------------|-------------------------|----------------------|--------------------|---|----------------------|-------------------------|----------------------|--------------------|
| $d_{amb}$<br>[nm]                           | $n_{xy\ amb}$<br>[-] | $\Delta n_{amb}$<br>[-] | $MSE$<br>anisotropic | $MSE$<br>isotropic | $d_{amb}$<br>[nm]                           | $n_{xy\ amb}$<br>[-] | $\Delta n_{amb}$<br>[-] | $MSE$<br>anisotropic | $MSE$<br>isotropic |
| No heating, measured 30 min after formation |                      |                         |                      |                    | No heating, measured 3 days after formation |                      |                         |                      |                    |
| 402.5                                       | 1.585                | 0.014                   | 6.9                  | 15.1               | 236.6                                       | 1.518                | 0                       | 7.2                  | 7.3                |
| 402.7                                       | 1.583                | 0.013                   | 6.4                  | 14.3               | 234.7                                       | 1.513                | 0                       | 7.3                  | 7.4                |
| After 48 h under vacuum at 30 °C            |                      |                         |                      |                    |   |                      |                         |                      |                    |
| 343.1                                       | 1.652                | 0.037                   | 4.5                  | 27.5               | 388.5 <sup>1</sup>                          | 1.581                | 0.009                   | 9.5                  | 13.0               |
| 358.2                                       | 1.652                | 0.034                   | 4.5                  | 25.7               | 395.1 <sup>2</sup>                          | 1.568                | 0.009                   | 9.3                  | 13.1               |
| 487.5                                       | 1.643                | 0.039                   | 14.6                 | 42.4               | 420.7 <sup>3</sup>                          | 1.562                | 0.008                   | 10.0                 | 12.5               |
| 533.0                                       | 1.642                | 0.037                   | 12.3                 | 42.7               | 483.5 <sup>4</sup>                          | 1.579                | 0.006                   | 15.6                 | 17.0               |
| After 48 h under vacuum at 140 °C           |                      |                         |                      |                    |   |                      |                         |                      |                    |
| 312.1                                       | 1.648                | 0.035                   | 11.3                 | 26.0               | 238.9 <sup>1</sup>                          | 1.635                | 0.042                   | 7.7                  | 20.1               |
| 354.4                                       | 1.644                | 0.031                   | 8.7                  | 25.6               | 246.3 <sup>2</sup>                          | 1.632                | 0.042                   | 8.8                  | 21.0               |
| 487.6                                       | 1.648                | 0.035                   | 15.1                 | 38.9               | 307.4 <sup>3</sup>                          | 1.617                | 0.015                   | 12.9                 | 15.9               |
| 543.0                                       | 1.645                | 0.030                   | 13.7                 | 36.7               | 316.3 <sup>4</sup>                          | 1.616                | 0.012                   | 12.4                 | 15.0               |

<sup>1,2,3,4</sup> Indication of measurements with a particular number means that these are the measurements of the same sample spots of the NMP-derived films, which were conditioned firstly at 30 °C and subsequently at 140 °C.

Subsequently, the optical properties have been analyzed after the films have been conditioned under vacuum at 30 °C. The values for  $n_{xy}$  and  $\Delta n$  of methanol-derived films are comparable with those of films formed via spin-coating (Figure 2.4). During conditioning, the methanol is completely removed, causing an increase in density ( $n_{xy}$ ) and internal stresses ( $\Delta n$ ). Fitting with the anisotropic, instead of the isotropic optical model, results in a significant reduction of the *MSE*. NMP-derived films show a small positive value for  $\Delta n$  and a strongly increased  $n_{xy}$ . This indicates significant, but not complete removal of the NMP.

Finally, the films have been characterized after conditioning under vacuum at 140 °C. For methanol-derived films, the solvent is completely removed, similar to the conditioning at 30 °C. Because the temperature of 140 °C is too far from the glass transition temperature, no structural rearrangements of the polymer occur. Consequently, the temperature of the conditioning step does not significantly affect the optical properties of the methanol-derived films, and the corresponding *MSE*.

For the NMP-derived films, the removal of NMP at 140 °C is far more effective than at 30 °C. This is manifested by an increase in  $n_{xy}$  as well as in  $\Delta n$ . Still, for various spots on the sample, a lower anisotropy is observed, indicating that NMP is not removed completely at 140 °C. The difficult removal of NMP is due to its high boiling point, but also due to its favorable interactions with sulfonic acid groups [22, 48].

Overall, the results indicate that sorption of organic solvents can reduce the internal stresses in thin SPEEK films. Notably, the density of, and internal stresses in, thin SPEEK films are similar when comparing films prepared by spin-coating and solvent deposition. This further substantiates that stresses in the material are not affected by the shear forces induced during spin-coating, but are inherent to thin films of this sulfonated polymer. This conclusion is in agreement with literature. It is known that molecular orientations can originate from the self-alignment of polymeric chains, due to specific chemical properties (e.g. polarity) that cause interactions between molecules [28, 49]. These interactions drive polymeric chains to align in a specific manner. For SPEEK, the specific orientations are due to polar sulfonic acid groups. This is in line with the recent research of Krishnan et al., who found sulfonated polyimide thin films to be inherently anisotropic with the orientation along the in-plane direction [50].

Analysis of the anisotropy of the SPEEK samples that have been aged for one year shows that slow polymer relaxations do not lead to disappearance of the anisotropy in the thin

films. The slow relaxations do affect the homogeneity of the films. Fresh films derived from a 7 wt% solution cannot be accurately modeled ( $MSE > 20$ ), but after 372 days of aging, the  $MSE$  is significantly decreased ( $< 10$ ). The aged 7 wt% films have values for  $\Delta n$  that are of the same order as these of films derived from 5 wt% solutions. The inherent self-alignment orientations can only be irreversibly affected by chemical modifications [51], and, as we have shown, reversibly by plasticizing agents.

## 2.5 Conclusions

Molecular orientations in thin SPEEK films have been investigated using spectroscopic ellipsometry. The thin films exhibit a uniaxial optical anisotropy that implies preferred orientations of the polymer chains, which are for SPEEK in the in-plane direction. In turn, the preferred molecular orientations lead to internal stresses in the films. The molecular orientations do not originate from film formation conditions: different solvents, different film formation methods, and different hydrodynamic forces acting on the polymer chains during film formation, essentially, do not change the extent of anisotropy. The internal stresses, coupled with the density, can be varied to some extent when solutions with higher polymer concentrations are used for the spin-coating synthesis. The presence of molecular orientations in thin SPEEK films are inherent to this polymer, and are not removed by elevated temperatures. The associated internal stresses can be released by the presence of water or organic solvents. Subsequent removal of such penetrants is accompanied by a full reestablishment of the internal stresses.

## Acknowledgements

This work was performed in the cooperation framework of Wetsus, centre of excellence for sustainable water technology ([www.wetsus.nl](http://www.wetsus.nl)). Wetsus is co-funded by the Dutch Ministry of Economic Affairs and Ministry of Infrastructure and Environment, the European Union Regional Development Fund, the Province of Fryslân, and the Northern Netherlands Provinces. The authors would like to thank the participants of the research theme “Dehydration” for the fruitful discussions and their financial support.

## References

1. Winardi, S., et al., *Sulfonated poly (ether ether ketone)-based proton exchange membranes for vanadium redox battery applications*. Journal of Membrane Science, 2014. **450**: p. 313-322.
2. Li, Z., et al., *Properties Investigation of Sulfonated Poly(ether ether ketone)/Polyacrylonitrile Acid–Base Blend Membrane for Vanadium Redox Flow Battery Application*. ACS Applied Materials & Interfaces, 2014.
3. Hande, V.R., et al., *Cross-linked sulfonated poly (ether ether ketone) (SPEEK)/reactive organoclay nanocomposite proton exchange membranes (PEM)*. Journal of Membrane Science, 2011. **372**(1–2): p. 40-48.
4. Xue, S. and G. Yin, *Methanol permeability in sulfonated poly(etheretherketone) membranes: A comparison with Nafion membranes*. European Polymer Journal, 2006. **42**(4): p. 776-785.
5. Basile, A., et al., *Sulfonated PEEK-WC membranes for proton-exchange membrane fuel cell: Effect of the increasing level of sulfonation on electrochemical performances*. Journal of Membrane Science, 2006. **281**(1-2): p. 377-385.
6. Gil, M., et al., *Direct synthesis of sulfonated aromatic poly(ether ether ketone) proton exchange membranes for fuel cell applications*. Journal of Membrane Science, 2004. **234**(1-2): p. 75-81.
7. Li, L., J. Zhang, and Y. Wang, *Sulfonated poly(ether ether ketone) membranes for direct methanol fuel cell*. Journal of Membrane Science, 2003. **226**(1-2): p. 159-167.
8. Kreuer, K.D., *On the development of proton conducting materials for technological applications*. Solid State Ionics, 1997. **97**(1-4): p. 1-15.
9. Kattan Readi, O.M., M. Gironès, and K. Nijmeijer, *Separation of complex mixtures of amino acids for biorefinery applications using electro dialysis*. Journal of Membrane Science, 2013. **429**: p. 338-348.
10. Güler, E., et al., *Performance-determining membrane properties in reverse electro dialysis*. Journal of Membrane Science, 2013. **446**: p. 266-276.
11. Giuseppin, M.L.F., P.J. Smits, and G.W. Hofland, *Subcritical gas assisted drying of biopolymer material*. 2012, US 20120316331 A1.
12. Dalwani, M., et al., *Sulfonated poly(ether ether ketone) based composite membranes for nanofiltration of acidic and alkaline media*. Journal of Membrane Science, 2011. **381**(1-2): p. 81-89.
13. Sijbesma, H., et al., *Flue gas dehydration using polymer membranes*. Journal of Membrane Science, 2008. **313**(1-2): p. 263-276.
14. Huang, R.Y.M., et al., *Pervaporation separation of water/isopropanol mixture using sulfonated poly(ether ether ketone) (SPEEK) membranes: transport mechanism and separation performance*. Journal of Membrane Science, 2001. **192**(1–2): p. 115-127.
15. Jia, L., et al., *Sulfonation of polyetheretherketone and its effects on permeation behavior to nitrogen and water vapor*. Journal of Applied Polymer Science, 1996. **60**(8): p. 1231-1237.
16. Khan, A.L., et al., *SPEEK and functionalized mesoporous MCM-41 mixed matrix membranes for CO<sub>2</sub> separations*. Journal of Materials Chemistry, 2012. **22**(37): p. 20057-20064.
17. Khan, A.L., X. Li, and I.F.J. Vankelecom, *Mixed-gas CO<sub>2</sub>/CH<sub>4</sub> and CO<sub>2</sub>/N<sub>2</sub> separation with sulfonated PEEK membranes*. Journal of Membrane Science, 2011. **372**(1–2): p. 87-96.



18. Khan, A.L., X. Li, and I.F.J. Vankelecom, *SPEEK/Matrimid blend membranes for CO<sub>2</sub> separation*. Journal of Membrane Science, 2011. **380**(1-2): p. 55-62.
19. Luo, Y., et al., *Thermal degradation of sulfonated poly(aryl ether ether ketone)*. Journal of Analytical and Applied Pyrolysis, 1995. **34**(2): p. 229-242.
20. Knauth, P., et al., *Thermogravimetric analysis of SPEEK membranes: Thermal stability, degree of sulfonation and cross-linking reaction*. Journal of Analytical and Applied Pyrolysis, 2011. **92**(2): p. 361-365.
21. Jin, X., et al., *Sulfonated poly(aryl ether ketone)*. British Polymer Journal, 1985. **17**(1): p. 4-10.
22. Mikhailenko, S.D., et al., *Proton conducting membranes based on cross-linked sulfonated poly(ether ether ketone) (SPEEK)*. Journal of Membrane Science, 2004. **233**(1-2): p. 93-99.
23. Hou, H., et al., *Crosslinked SPEEK membranes: Mechanical, thermal, and hydrothermal properties*. Journal of Materials Research, 2012. **27**(15): p. 1950-1957.
24. Reiter, G., *Probing Properties of Polymers in Thin Films Via Dewetting*, in *Glass Transition, Dynamics and Heterogeneity of Polymer Thin Films*. 2013, Springer Berlin Heidelberg. p. 29-63.
25. Tsui, O.K.C., et al., *Equilibrium pathway of spin-coated polymer films*. Macromolecules, 2008. **41**(4): p. 1465-1468.
26. Huang, Y. and D.R. Paul, *Physical aging of thin glassy polymer films monitored by gas permeability*. Polymer, 2004. **45**(25): p. 8377-8393.
27. Reyna-Valencia, A., S. Kaliaguine, and M. Bousmina, *Structural and mechanical characterization of poly(ether ether ketone) (PEEK) and sulfonated PEEK films: Effects of thermal history, sulfonation, and preparation conditions*. Journal of Applied Polymer Science, 2006. **99**(3): p. 756-774.
28. I.M. Ward, *Structure and Properties of Oriented Polymers*. 2nd ed. 1997: Springer, The Netherlands
29. Fujiwara, H., *Principles of Spectroscopic Ellipsometry*, in *Spectroscopic Ellipsometry*. 2007, John Wiley & Sons, Ltd. p. 81-146.
30. J. A. Woollam, B.J., C. Herzinger, J. Hilfiker, R. Synowicki, and C. Bungay, *Overview of Variable Angle Spectroscopic Ellipsometry (VASE), Part I: Basic Theory and Typical Applications*. SPIE Proceedings, CR 72, (1999) 3 - 28, 1999.
31. Askadski, A.A., *Physical Properties of Polymers*. 1996: CRC Press, United States
32. Shibuya, N. and R.S. Porter, *Kinetics of PEEK sulfonation in concentrated sulfuric acid*. Macromolecules, 1992. **25**(24): p. 6495-6499.
33. Zaidi, S.M.J., et al., *Proton conducting composite membranes from polyether ether ketone and heteropolyacids for fuel cell applications*. Journal of Membrane Science, 2000. **173**(1): p. 17-34.
34. Ogieglo, W., et al., *Temperature-induced transition of the diffusion mechanism of n-hexane in ultra-thin polystyrene films, resolved by in-situ Spectroscopic Ellipsometry*. Polymer (United Kingdom), 2013. **54**(1): p. 341-348.
35. Potreck, J., et al., *Sorption induced relaxations during water diffusion in S-PEEK*. Physical Chemistry Chemical Physics, 2009. **11**(2): p. 298-308.
36. Hara, M. and J.A. Sauer, *Mechanical properties of ionomers*. Journal of Macromolecular Science - Reviews in Macromolecular Chemistry and Physics, 1994. **C34**(3): p. 325-373.
37. Reyna-Valencia, A., S. Kaliaguine, and M. Bousmina, *Tensile mechanical properties of sulfonated poly(Ether Ether Ketone) (SPEEK) and BPO<sub>4</sub>/SPEEK membranes*. Journal of Applied Polymer Science, 2005. **98**(6): p. 2380-2393.

38. Oh, K.-H., et al., *Enhanced Durability of Polymer Electrolyte Membrane Fuel Cells by Functionalized 2D Boron Nitride Nanoflakes*. ACS Applied Materials & Interfaces, 2014. **6**(10): p. 7751-7758.
39. Yen, S.-P.S., Narayanan Sekharipuram R., Halpert Gerald, Graham Eva, Yavrouian, Andre, *Polymer material for electrolytic membranes in fuel cells*. 1998.
40. Smallwood, I.M., *Ethanol*, in *Handbook of Organic Solvent Properties*. 1996, Butterworth-Heinemann: Oxford. p. 65-67.
41. Smallwood, I.M., *Methanol*, in *Handbook of Organic Solvent Properties*. 1996, Butterworth-Heinemann: Oxford. p. 61-63.
42. Meyerhofer, D., *Characteristics of resist films produced by spinning*. Journal of Applied Physics, 1978. **49**(7): p. 3993-3997.
43. Hall, D.B., P. Underhill, and J.M. Torkelson, *Spin coating of thin and ultrathin polymer films*. Polymer Engineering and Science, 1998. **38**(12): p. 2039-2045.
44. Gupta, M., A.P. Deshpande, and P.B.S. Kumar, *Rheology of concentrated sulfonated poly(ether ether ketone) solutions*. Journal of Applied Polymer Science, 2014. **131**(7): p. n/a-n/a.
45. Bornside, D.E., C.W. Macosko, and L.E. Scriven, *Modeling of spin coating*. Journal of imaging technology, 1987. **13**(4): p. 122-130.
46. Zhu, Z., et al. *Spin-coating defect theory and experiments*. in *ECS Transactions*. 2014. Electrochemical Society Inc.
47. Carbone, A., et al., *Sulphonated poly(ether ether ketone) membranes for fuel cell application: Thermal and structural characterisation*. Journal of Power Sources, 2006. **163**(1): p. 18-26.
48. Jun, M.-S., Y.-W. Choi, and J.-D. Kim, *Solvent casting effects of sulfonated poly(ether ether ketone) for Polymer electrolyte membrane fuel cell*. Journal of Membrane Science, 2012. **396**(0): p. 32-37.
49. Shimo, T. and M. Nagasawa, *Stress and birefringence relaxations of noncrystalline linear polymer*. Macromolecules, 1992. **25**(19): p. 5026-5029.
50. Krishnan, K., et al., *Proton conductivity enhancement in oriented, sulfonated polyimide thin films*. Journal of Materials Chemistry A, 2014. **2**(19): p. 6895-6903.
51. Zhang, Z., et al., *Novel approach to reducing stress-caused birefringence in polymers*. Journal of Materials Science, 2004. **39**(4): p. 1415-1417.



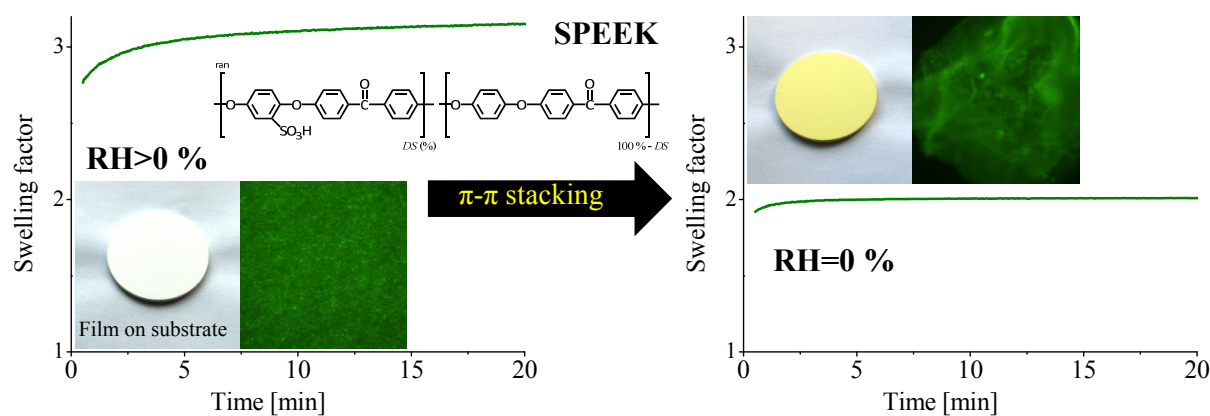
# Chapter 3

## The effects of water on the molecular structure and the swelling behavior of sulfonated poly(ether ether ketone) films

This chapter has been submitted to the Journal of Materials Science (in adapted form) as:

Koziara, B.T.; Akkilic, N.; Nijmeijer, K.; Benes, N.E., *The effects of water on the morphology and the swelling behavior of sulfonated poly(ether ether ketone) films.*

## Abstract



Thin sulfonated poly(ether ether ketone) films swell excessively in water. The extent of water-induced swelling is shown to be correlated with the optical anisotropy of the films, due to two distinct phenomena. Firstly, the optical anisotropy is directly related to the amount of water taken up from the ambient, and thus to amount of water present in the material just prior to swelling. Secondly, the optical anisotropy corresponds to internal stresses in the film that affect the free energy of the film, and thus the potential of the film to swell. The anisotropy vanishes upon sorption of liquid water and returns when the water is desorbed. When the water is completely removed, the film changes from more or less colorless to an intense yellow color that can be attributed to molecular assembly of the aromatic rings in the polymer backbone. The color change is reversible and occurs immediately upon exposure to low humidity. For films prepared in the absence of water, the lack of hydration of the sulfonic acid groups affects the packing of the polymer chains. This is manifested by a lower extent of water-induced swelling. The possibility to affect the polymer behavior by varying the hydration state during preparation can have important implications for applications of sulfonated polymer films.

### 3.1 Introduction

Membranes from highly sulfonated poly(ether ether ketone) (SPEEK) excessively swell upon contact with water. This is due to the high affinity that water has for the sulfonic acid groups in SPEEK. For some applications, a high concentration of water in the polymer can be beneficial, for instance, to facilitate proton transport in fuel cells [1] or for the dehydration performance [2-4]. However, too high concentration of water in membranes causes excessive swelling. A drawback of excessive swelling is the reduced mechanical strength that may lead to ruptures, in particular in the case of thin films that are constrained on a substrate. Constrained films can only swell in a single direction, and at a similar degree of swelling the elastic deformation of their network is thus more pronounced as compared to free-standing films [5]. Excessive swelling is also known to have an impact on the performance of membranes in molecular separation. In general, swelling leads to larger fluxes of all species present, and causes drastic reductions in selectivity. Much effort has been devoted to the reinforcement of SPEEK films. Approaches include chemical modifications, such as covalent and ionic cross-linking [6], doping with inorganic particles [7, 8] and creating structures with integrated skin layers [9].

The relations between swelling, proton transport and the chemical and intermolecular structure of SPEEK and other sulfonated polyelectrolyte films have been studied extensively [10-12]. The performance of membranes made from these polymers is reported to be affected by molecular orientations and chain assembly. Zhang et al. reported that SPEEK films with the same chemical structure, with a degree of sulfonation of 40 %, but formed at various relative humidity degrees, exhibit distinct molecular arrangement and orientation of the sulfonic acid groups [13]. The proton conductivity performance of those membranes is dissimilar. This implies that the proton transport characteristics of SPEEK are not only dictated by the amount of sulfonic acid groups, but also by their molecular arrangement. It can be anticipated that the molecular structural arrangements of SPEEK will also affect the swelling behavior upon contact with water.

In a previous study, we reported that thin SPEEK films exhibit certain structural arrangements, in particular, inherent orientations in the in-plane direction [14]. In short, SPEEK films, independently on the preparation route and formation procedure, are preferentially oriented in the  $xy$  direction as compared to the  $z$  direction [14]. This is manifested

by optical anisotropy,  $\Delta n$ , i.e.,  $\Delta n = n_{xy} - n_z > 0$ . In this expression,  $n_{xy}$  is the in-plane refractive index and  $n_z$  is the out-of plane refractive index. In the present paper, we study the relations between those structural arrangements of supported thin SPEEK films and (the dynamics of) their water-induced swelling, to assess if swelling can be significantly affected without chemical modification of the polymer. The paper comprises two parts. In the first part, the focus is on the correlation between optical anisotropy and swelling. In the second part, the focus is on the molecular assembly of the aromatic rings in the polymer backbone due to the absence of water during film formation, and on the consequences of such assembly for water-induced swelling.

## 3.2 Experimental

### 3.2.1 Materials

Two batches of SPEEK polymer were used: SPEEK with a degree of sulfonation (*DS*) 84 % – home-made, obtained by sulfonation of PEEK (Victrex) using sulfuric acid according to the procedure described in [15], and SPEEK *DS* 68 % – Fumion<sup>®</sup> ELM-505, obtained from Fumatech (Germany) as 5 wt% methanol solution. Methanol (Emsure<sup>®</sup> grade of purity) was obtained from Merck (The Netherlands). Rhodamine 6G and DMSO- $d_6$  (99.5 atom % D) were obtained from Sigma-Aldrich (The Netherlands). <100> -oriented silicon wafers P/Boron were obtained from Okmetic (Finland). Quartz glass slides Nr. 1.5 were obtained from Menzel-Gläser (Germany). Nylon membrane 25 mm syringe filters (pore size 0.45  $\mu\text{m}$ ) were obtained from VWR International. Porous  $\alpha$ -alumina discs were purchased from Pervatech (The Netherlands). Nitrogen gas (4.5) was supplied by Linde (Germany). Deionized water (18.2  $\text{M}\Omega\cdot\text{cm}$ ) was obtained using a Milli-Q Advantage A10 system Millipore.

### 3.2.2 Film preparation

#### For spectroscopic ellipsometry

Films were spin-coated from SPEEK 5 wt% dissolved in methanol on pre-cut pieces of silicon wafers. Prior to spin-coating, the solutions were filtered using a syringe filter in order to remove residual contaminations. SPEEK in the 5 wt% methanol solution from Fumatech has a relatively high molecular weight and correspondingly high viscosity. The solution was diluted with methanol (SPEEK solution to fresh methanol volume ratio was 3.5:1) prior to spin-coating to decrease the viscosity, such that all for swelling experiments films are  $\sim 300$  nm thick.

Spin-coating was conducted under two distinct humidity conditions:

*Humid atmosphere:* Spin-coating was conducted in air, at ambient relative humidity. The spin speed was set at 2000 or 3000 rpm.

*Dry atmosphere:* Spin-coating was conducted under a large stream of dry nitrogen ( $RH=0\%$ ). The spin speed was always set at 2000 rpm.

The spinning time was set to 50 seconds. Directly after spin-coating, the films were conditioned under vacuum at  $140\text{ }^{\circ}\text{C}$  for 48 h. This procedure is implemented to induce non-covalent attachment of the film to the substrate and to prevent detachment of the film upon swelling.

Before water swelling experiments, all films were equilibrated directly after removal from a vacuum oven, at the ambient relative humidity degree. Subsequently, the films were characterized *ex-situ* using Spectroscopic Ellipsometry (*SE*). The initial thickness of the films used in the swelling experiments was in the range 280 – 350 nm.

### **For fluorescence microscopy**

Two methods were applied: (1) Films were spin-coated from a mixture of 3 wt% SPEEK in methanol and Rhodamine 6G on quartz glass slides at 2000 rpm. The molar ratio Rhodamine 6G/sulfonic acid groups was  $6 \cdot 10^{-9}$ . Alternatively, (2) films were spin-coated from 3 wt% SPEEK in methanol at 2000 rpm, without Rhodamine 6G in the solution. Subsequently, 0.1 ml of the Rhodamine 6G water solution was deposited, with the similar molar ratio as in the first method, on the film surface and left for 2 hours.

Spin-coating was done in humid and dry atmosphere, as described above for the film formation for spectroscopic ellipsometry. The thicknesses of the films for fluorescence microscopy were  $\sim 150$  nm.

### **Films on porous alumina supports**

Films were spin-coated on porous  $\alpha$ -alumina supports, which were coated with a single layer of  $\gamma$ -alumina (according to the procedure described by Luiten et al. [16]), from 10 wt% SPEEK dissolved in methanol, in a humid ambient ( $RH=60\%$ ) and dry atmosphere ( $RH=0\%$ ) at 2000 rpm. The thicknesses of the films were  $\sim 800$  nm.



### 3.2.3 Measurements

#### <sup>1</sup>H-NMR

The degree of sulfonation of the two SPEEK batches was determined via <sup>1</sup>H-NMR using a Ascend™ (Bruker) at a resonance frequency of 400 MHz in deuterated dimethyl sulfoxide DMSO-d<sub>6</sub>, using an approach similar to that described by Zaidi *et al.* [17].

#### Ellipsometry

Spectroscopic ellipsometry experiments were performed on two devices: alfa-SE and M-2000 (J.A. Woollam Co., Inc.). The size spot of the light beam was 2 mm and a 70° angle of incidence was applied for *ex-situ* and *in-situ* measurements. *In-situ* measurements were conducted in demineralized liquid water at a temperature of either 20 or 40 °C, using a custom-made temperature-controlled 70 mL-volume glass cell [18]. For water experiments in the glass cell, the delta offset was determined prior to measurements using a calibration wafer. The recording of the swelling data started in the first half minute after immersion in water. Modeling of the data obtained from SPEEK film measurements using CompleteEase 4.64 software (J.A. Woollam Co., Inc.) is described in detail in [14]. The ambient refractive index of water at 20 and 40 °C was taken from the H<sub>2</sub>O Pribil Temperature Library from the CompleteEase software.

The time-dependent swelling factor  $S_F(t)$  is defined as the thickness  $d$  at time  $t$  normalized with respect to the initial thickness:

$$S_F(t) = \frac{d(t)}{d_{\text{initial}}} \quad \text{Eq. 3.1}$$

The initial film thickness is measured by *ex-situ* ellipsometry prior to the swelling experiment.

#### TIRF microscopy

Total internal reflection fluorescence (TIRF) microscopy was performed using a Nikon Eclipse Ti microscope equipped with a 100× Oil, Plan Apo objective (numerical aperture 1.45, Olympus) and an Andor DU-885 camera in TIRF mode. The Rhodamine 6G was excited using a 488 nm laser with a readout speed of 35 MHz. The emission signal from the green dye was collected at 520 nm.

### 3.3 Results and Discussion

#### 3.3.1 Relation between anisotropy and swelling

Figure 3.1 shows the swelling dynamics for two distinct SPEEK films, prepared from the same polymer batch,  $DS$  84 %, and formed at different dates under humid conditions at 2000 rpm, upon exposure to liquid water at 40 °C. Prior to the exposure to water, the extent of optical anisotropy of the films is different. The differences in optical properties are due to dissimilarities in the relative humidity of the ambient, on the different dates of film formation and measurement. Despite the equal  $DS$ , the swelling dynamics and the final degree of swelling are extremely distinct for the two films. The film that has the higher initial anisotropy,  $\Delta n=0.028$ , swells slower and its swelling factor shows a maximum value of  $\sim 3.5$  followed by a continuous relaxation-induced decrease in film thickness. Such overshoot swelling dynamics have been observed for SPEEK and other charged polymers [19-21]. For the film with the lower initial optical anisotropy,  $\Delta n=0.023$ , the swelling dynamics are much faster. Most of the swelling occurs immediately, upon contact with water. Closer inspection of the shape of the curve reveals that this film also exhibits overshoot dynamics, albeit far less pronounced, with the maximum swelling factor of only  $\sim 1.7$ .

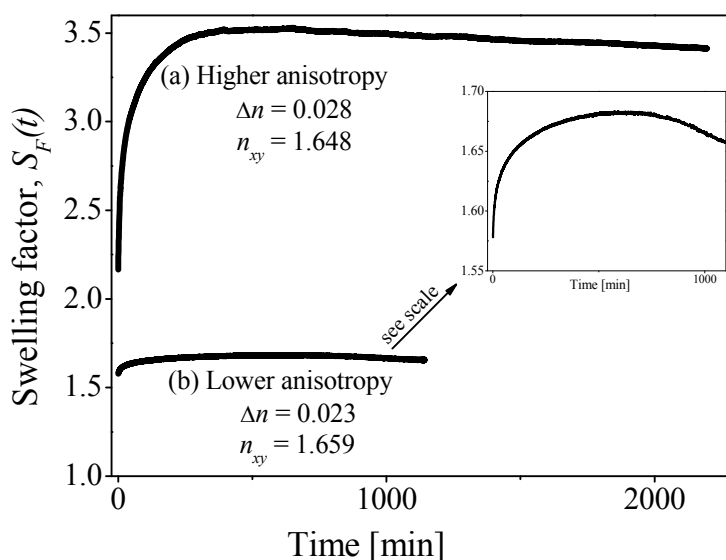


**Figure 3.1** Time-dependent water-induced swelling at 40 °C of  $\sim 300$  nm SPEEK films with a  $DS$  of 84 % and (a) relatively high optical anisotropy ( $\Delta n=0.028$ ), and (b) relatively low optical anisotropy ( $\Delta n=0.023$ ).

In the last years we have measured the swelling of several dozens of thin SPEEK films and found a positive correlation between the value of  $\Delta n$  and the extent of swelling. The observed differences in the swelling behavior can be related to two superimposed phenomena.

Firstly, the distinct swelling behavior can be associated with a different initial concentration of water in the film. Due to the sulfonic acid groups, SPEEK has a high affinity for water. A SPEEK film that is exposed to an ambient with higher relative humidity will have a higher concentration of sorbed water. It is known that a higher water concentration in a SPEEK film results in a reduction of density and anisotropy [14]. The higher initial concentration of water in the film is manifested by a lower value of  $\Delta n$  and less apparent swelling during exposure to liquid water.

Secondly, the distinct swelling behavior can be due to an inherent relation between optical anisotropy in a film and the swelling of this film. The theoretical prediction of penetrant induced swelling of polymers is generally based on free energy considerations [22]. Within such a context, the contributions to the free energy that ultimately determine the extent of swelling, are related to the changes in enthalpy and entropy upon mixing of polymer and penetrant, and an elastic contribution due to deformation of the network. The optical anisotropy in the thin films is associated with internal stresses, and consequently constitutes a distinct free energy status prior to swelling. After swelling with water at a high activity ( $\sim 1$ , or liquid water), the internal stresses, and hence anisotropy, either vanish or are very minor. This implies that the distinct initial free energy must result in a distinct extent of swelling.

For both phenomena, a larger extent of optical anisotropy will correspond to a larger extent of swelling, which complicates deconvolution of the two phenomena. This is illustrated by the swelling of a selection of four films at 40 °C and 2 films at 20 °C, in Figure 3.2. All films have been prepared from the batch with a *DS* of 84 % and have been formed under humid conditions. The four samples swollen at 40 °C have been obtained from three different sets, I, II and III, and the swelling of the films has been studied at different times under various relative humidity conditions. Only samples IIIa and IIIb are from the same set and their swelling is studied on the same day, i.e., under the same relative humidity conditions.

IIIa and IIIb differ in the extent of optical anisotropy, which has been induced by differences in the spinning conditions [14], 2000 and 3000 rpm for IIIa and IIIb, respectively. The two samples swollen at 20 °C have been obtained from two different sets, a and b. Sample

b with very low optical anisotropy,  $\Delta n=0.014$ , was exposed prior to swelling to an ambient with  $RH \gg 80\%$ .

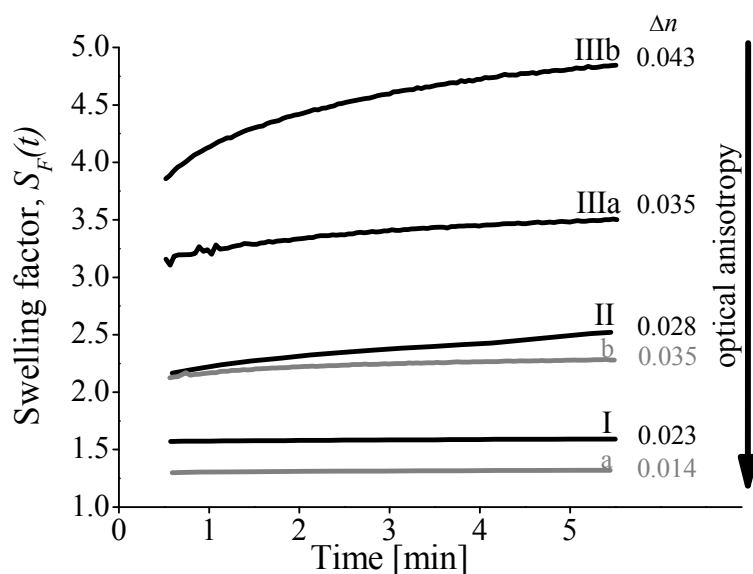


**Figure 3.2** Water-induced swelling recorded for 5 minutes of SPEEK films with a  $DS$  of 84 %, and with various initial optical anisotropy, at 20 °C (grey lines a and b) and 40 °C (black lines I, II, IIIa and IIIb). The initial anisotropy of  $\leq 0.014$  prior to swelling is achieved by film exposure to an ambient with  $RH \gg 80\%$ .

As we have generally found, the film with the lowest initial optical anisotropy shows the lowest degree of swelling. Because the humidity conditions during the swelling studies of these films are not well defined, it is not possible to quantify the relative contributions of the effect of initial relative humidity and the contribution of the initial stresses and density in the film, to the overall extent of swelling. When comparing samples I, IIIa and IIIb, the refractive indices of the materials are similar ( $n_{xy}=1.659, 1.658$  and  $1.661$ , respectively). This implies a comparable initial density of the samples. Hence, the higher degree of swelling must be predominantly due to initially higher internal stresses in this film. Such an observation is further supported when comparing samples IIIa and IIIb; for these samples, the synthesis and swelling conditions have been identical, except for the spinning speed. The consequent difference in optical anisotropy of the two films is accompanied by a significant difference in swelling. In this case, this divergent extent of swelling can be attributed to the difference in initial stresses in the two films.

Thus, the swelling factor in water of thin SPEEK films is dependent not only on the degree of sulfonation and water temperature, but also on the initial film properties that are strongly responsive to ambient conditions.

### 3.3.2 Effect of RH during spinning on thin film swelling

In the above section a correlation is discussed between the optical anisotropy and swelling of thin SPEEK films, prepared via spin-coating in a humid atmosphere. In a previous paper we have found that a spin-coating with a relatively concentrated (5 wt%) SPEEK alcohol solution at relatively low spin speed (2000 rpm) can result in SPEEK films with lower anisotropy as compared to films spun at 3000 rpm [14]. For less concentrated solutions and higher spinning speeds, the extent of optical anisotropy of thin SPEEK films is more or less insensitive to variations in the spinning conditions [14]. The anisotropy of the formed films has been also found to increase with a decrease in relative humidity of the ambient [14]. In this paper, a particular swelling behavior is observed when films are prepared by spin-coating in the absence of water ( $RH=0\%$  due to flushing with nitrogen). The thickness and optical anisotropy of these films is comparable with those of films formed in the presence of water. However, the swelling of the films upon exposure to liquid water is very different. This is illustrated in Figure 3.3, by the dynamic swelling of two films with a  $DS$  of 84 %, of which the optical anisotropy is comparable,  $\Delta n \sim 0.028$ . One film is prepared under relatively humid conditions ( $RH \sim 30\%$ ), the other film under dry nitrogen ( $RH=0\%$ ). The film formed under dry conditions shows significantly less swelling. The different swelling is considered to be the result of different molecular orientations in SPEEK, due to a different hydration state of the polymer during spin-coating in the absence/presence of water.

The hydration state of a polyelectrolyte, such as SPEEK, has prominent effects on the charge and molecular morphology. In the presence of water, hydration of the negatively charged sulfonic acid groups affects the structural separation of the polymer into hydrophilic and hydrophobic domains [23, 24]. The hydrophilic domains are responsible for the transport of water and ions, such as protons, and the hydrophobic domains give the polymer morphological stability [13, 25]. In the absence of water, the lack of hydration of the sulfonic acid groups allows them to come closer to each other. This facilitates more pronounced attractive non-covalent interactions between the aromatic rings that are present in the polymer backbone. These attractive interactions have been considered to result in an ordered arrangement of the aromatic rings that is referred to as  $\pi$ - $\pi$  stacking. Recently, Jarumaneeroj et

al. [26] reported reversible  $\pi$ - $\pi$  stacking in SPEEK films induced by the heating of this material. They reported a color change of the material: initially SPEEK is transparent to light in the visible range, upon heating to 190 °C a yellow color develops that is attributed to  $\Pi$ - $\Pi$  stacking. The reported color change is reversible; upon cooling in ambient or exposure to water, the material becomes transparent again.

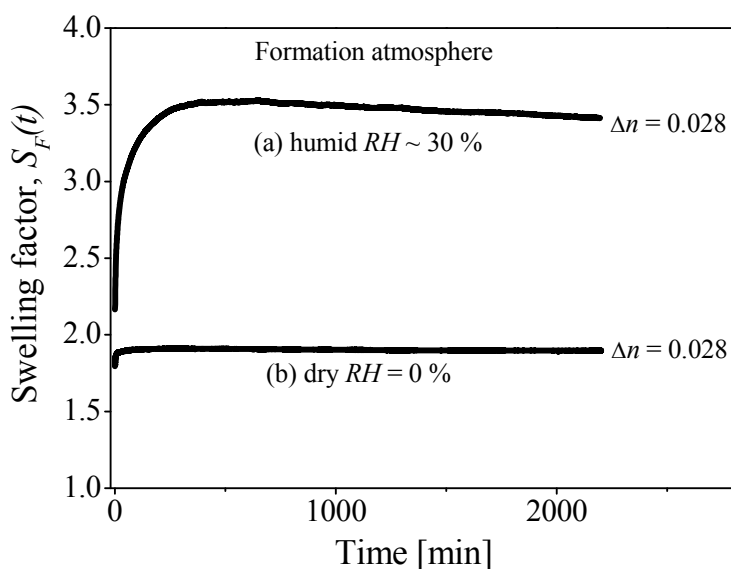


**Figure 3.3** Water-induced swelling dynamics at 40 °C of ~300 nm SPEEK films with a *DS* of 84 %, formed under (a) humid, *RH*~30 % and (b) dry, *RH*=0 % atmosphere. For both films, the extent of optical anisotropy is comparable,  $\Delta n \sim 0.028$ .

In Figure 3.4 the reversible color change, induced by the removal of water, is shown for a thin (~800 nm) SPEEK film on top of a porous ceramic  $\gamma/\alpha$ -alumina support. The film was prepared by spin-coating under humid conditions and initially it is colorless to the human eye. Figure 3.4a shows the film directly after incubation at 60 °C in a vacuum oven. The yellow color is indicative for the changed hydration state and corresponds to the color change reported by Jarumaneeroj et al. at high temperature [26]. The occurrence of the color change at relatively low temperature, in vacuum, implies that it is actually the removal of the water that causes the change in color, rather than an inherent thermochromic characteristic of SPEEK. Upon the removal of water, an ordered arrangement of the aromatic rings due to non-polar interactions is induced that is destroyed when water molecules are introduced again [26]. Upon exposure to the ambient, the sorption of water causes the film to become colorless again (Figure 3.4b). We have observed that SPEEK membranes with a thickness >20  $\mu\text{m}$ , also start to appear yellowish to the human eye, which is caused by slight absorption in the visible range. This

yellowish color becomes more apparent with increasing film thickness (the thicker the films, the higher the light absorption) and transforms to intense yellow, which is induced, as reported in [26], by benzene stacking, and is visible in Figure 3.4a.



**Figure 3.4** Photos of a SPEEK film  $\sim 800$  nm with a  $DS$  of 84 % coated on a  $\gamma/\alpha$ -alumina support (a) directly after incubation at a  $60$  °C in a vacuum oven and (b) after few minutes in a humid atmosphere.

An identical colour transformation was observed also for a SPEEK film on top of a porous ceramic  $\gamma/\alpha$ -alumina support formed under dry nitrogen. Yet the distinct swelling of films prepared under dry conditions (Figure 3.3) implies that in that case the molecular arrangement of the aromatic rings does not respond reversibly to the presence of water. In other words, the  $\pi$ - $\pi$  stacking in the films formed under dry conditions is partly irreversible.

Figure 3.5 shows the dynamic swelling of films that have been prepared in an identical manner, except for a difference in relative humidity during spinning. To investigate the reproducibility of this effect on another polymer batch, SPEEK with a  $DS$  of 68 % was used.

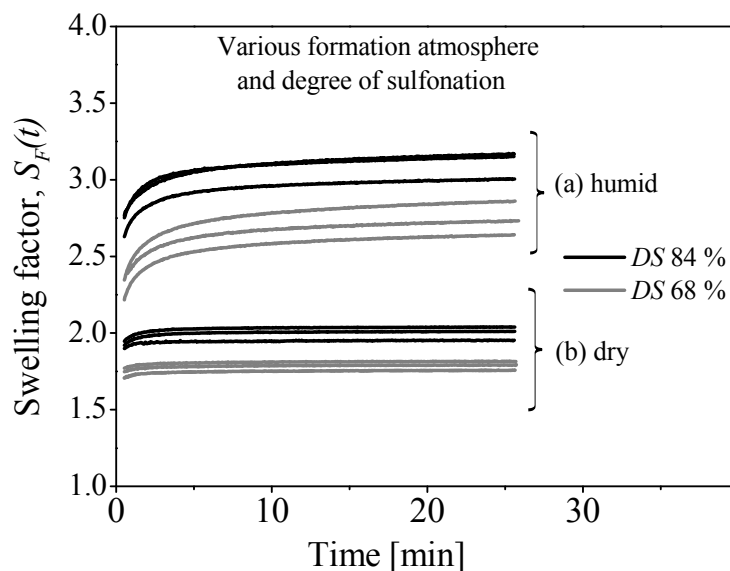


**Figure 3.5** Time-dependent water-induced swelling at 40 °C of ~ 300 nm SPEEK films with a  $DS$  of 84 % (black lines) and 68 % (grey lines), formed (a) in a humid  $RH \sim 30$  % and (b) dry  $RH = 0$  % atmosphere. Films are formed simultaneously, in an identical manner from the two methanol solutions of SPEEK  $DS$  68 and 84 %, except for a difference in humidity during spinning.

The experiment confirms the irreversible  $\pi$ - $\pi$  stacking in the films formed under dry conditions for two different batches. This is evidenced by significantly reduced swelling of these films prepared under dry conditions, as compared to swelling of the films prepared under humid conditions. Additionally, SPEEK films with a lower  $DS$  swell less than these with a higher  $DS$ , which is consistent with the literature [27].

As such, the internal structure and consequently, properties of thin SPEEK films can be altered without chemical modification, just by varying the humidity during their preparation process, which can have important implications for applications of films derived from SPEEK or other sulfonated polymers. For instance, in membrane applications, the stacking of the aromatic rings will affect the permeability of the films, because the stacking is associated with an impermeable crystalline structure of the polymer [28-30].



### Fluorescence microscopy

Total internal reflection fluorescence (TIRF) microscopy is used to reveal the effect of relative humidity on the distribution of sulfonic acid groups in SPEEK (Figure 3.6). The negatively charged sulfonic acid groups are visualized via marking them with the fluorescent cationic dye - Rhodamine 6G.

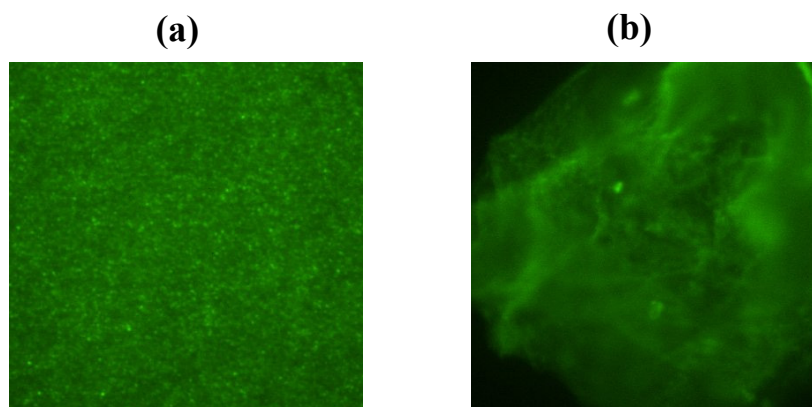


**Figure 3.6** Fluorescence microscopy images of SPEEK films (*DS* 84 %) labeled with Rhodamine 6G, formed in a (a) humid ambient and (b) dry atmosphere. The Rhodamine 6G was excited using 488 nm laser and the emission signal from the green dye was collected at 520 nm. Image size corresponds to a region of  $28 \times 28 \mu\text{m}^2$  for both images.

The fluorescent images represent the SPEEK films obtained by using the first experimental method described in the experimental section (film preparation). For the second film formation method, comparable images have been obtained. This confirms that the presence of the dye molecules does not interfere or alter the structural arrangements of SPEEK in a substantial manner. Figure 3.6a is representative for samples prepared under humid conditions. Such films show a homogenous distribution of the fluorescent cations, and thus of the sulfonic acid groups. When the film is formed under dry conditions, a cluster-like structure is observed (Figure 3.6b). Such clustering can originate from ordered molecular arrangements of the aromatic rings that are also associated with the change of color to yellow. The clustering produces hydrophobic domains that expel the charged functional groups. Despite of the ordering on the molecular scale, the material still combines hydrophilic domains (the sulfonic groups) and hydrophobic domains.

### **3.4 Conclusions**

Water-induced swelling in thin oriented sulfonated poly(ether ether ketone) films has been studied using *in-situ* spectroscopic ellipsometry. For films with a comparable degree of sulfonation, the swelling behavior is significantly correlated with the extent of optical anisotropy. Films with high optical anisotropy swell considerably more than more isotropic films. The correlation is attributed to two superimposed phenomena; a higher anisotropy can imply a lower initial water concentration at the start of the experiments, and a higher anisotropy is associated with higher internal stresses that imply a distinct free energy status. At very low water concentration, assembly of the aromatic rings in the backbone of the polymer can occur, which is manifested by a color change from clear to intense yellow. When the polymer is deprived of water during film formation, the stacking of aromatic rings is partly irreversible. This results in a lower propensity of the films to swell in water, signifying that control of the humidity during film formation allows to change the final film properties, without chemical modification.

### **Acknowledgements**

This work was performed in the cooperation framework of Wetsus, centre of excellence for sustainable water technology ([www.wetsus.nl](http://www.wetsus.nl)). Wetsus is co-funded by the Dutch Ministry of Economic Affairs and Ministry of Infrastructure and Environment, the European Union Regional Development Fund, the Province of Fryslân, and the Northern Netherlands Provinces. The authors would like to thank the participants of the research theme “Dehydration” for the fruitful discussions and their financial support.

## References

1. Kreuer, K.D., *On the development of proton conducting materials for technological applications*. Solid State Ionics, 1997. **97**(1-4): p. 1-15.
2. Huang, R.Y.M., et al., *Pervaporation separation of water/isopropanol mixture using sulfonated poly(ether ether ketone) (SPEEK) membranes: transport mechanism and separation performance*. Journal of Membrane Science, 2001. **192**(1-2): p. 115-127.
3. Gómez, P., et al., *Comparative behaviour of hydrophilic membranes in the pervaporative dehydration of cyclohexane*. Journal of Membrane Science, 2006. **279**(1-2): p. 635-644.
4. Sijbesma, H., et al., *Flue gas dehydration using polymer membranes*. Journal of Membrane Science, 2008. **313**(1-2): p. 263-276.
5. Toomey, R., D. Freidank, and J. Rühle, *Swelling behavior of thin, surface-attached polymer networks*. Macromolecules, 2004. **37**(3): p. 882-887.
6. Hou, H., M.L. Di Vona, and P. Knauth, *Building bridges: Crosslinking of sulfonated aromatic polymers—A review*. Journal of Membrane Science, 2012. **423–424**: p. 113-127.
7. Unnikrishnan, L., S. Mohanty, and S.K. Nayak, *Proton exchange membranes from sulfonated poly(ether ether ketone) reinforced with silica nanoparticles*. High Performance Polymers, 2013. **25**(7): p. 854-867.
8. Di Vona, M.L., et al., *SPEEK-TiO<sub>2</sub> nanocomposite hybrid proton conductive membranes via in situ mixed sol-gel process*. Journal of Membrane Science, 2007. **296**(1-2): p. 156-161.
9. Shao, P., et al., *Composite membranes with an integrated skin layer: preparation, structural characteristics and pervaporation performance*. Journal of Membrane Science, 2005. **254**(1-2): p. 1-11.
10. Dishari, S.K. and M.A. Hickner, *Antiplasticization and water uptake of nafion thin films*. ACS Macro Letters, 2012. **1**(2): p. 291-295.
11. Eastman, S.A., et al., *Effect of confinement on structure, water solubility, and water transport in Nafion thin films*. Macromolecules, 2012. **45**(19): p. 7920-7930.
12. Krishnan, K., et al., *Proton conductivity enhancement in oriented, sulfonated polyimide thin films*. Journal of Materials Chemistry A, 2014. **2**(19): p. 6895-6903.
13. Zhang, Y., et al., *Proton conductivity enhancement by nanostructural control of sulphonated poly(ether ether ketone) membranes*. International Journal of Hydrogen Energy, 2010. **35**(15): p. 8337-8342.
14. Koziara, B.T., K. Nijmeijer, and N.E. Benes, *Optical anisotropy, molecular orientations, and internal stresses in thin sulfonated poly(ether ether ketone) films*. Journal of Materials Science, 2015. **50**(8): p. 3031-3040.
15. Shibuya, N. and R.S. Porter, *Kinetics of PEEK sulfonation in concentrated sulfuric acid*. Macromolecules, 1992. **25**(24): p. 6495-6499.
16. Luiten, M.W.J., et al., *Robust method for micro-porous silica membrane fabrication*. Journal of Membrane Science, 2010. **348**(1-2): p. 1-5.
17. Zaidi, S.M.J., et al., *Proton conducting composite membranes from polyether ether ketone and heteropolyacids for fuel cell applications*. Journal of Membrane Science, 2000. **173**(1): p. 17-34.
18. Ogieglo, W., et al., *Temperature-induced transition of the diffusion mechanism of n-hexane in ultra-thin polystyrene films, resolved by in-situ Spectroscopic Ellipsometry*. Polymer (United Kingdom), 2013. **54**(1): p. 341-348.

19. Walker, M., et al., *Proton-conducting polymers with reduced methanol permeation*. Journal of Applied Polymer Science, 1999. **74**(1): p. 67-73.
20. Potreck, J., et al., *Sorption induced relaxations during water diffusion in S-PEEK*. Physical Chemistry Chemical Physics, 2009. **11**(2): p. 298-308.
21. Ogieglo, W., et al., *Relaxation induced optical anisotropy during dynamic overshoot swelling of zwitterionic polymer films*. Thin Solid Films, 2013. **545**: p. 320-326.
22. Flory, P.J., *Principles of Polymer Chemistry: Paul J. Flory*. 1953: Cornell University.
23. Gil, M., et al., *Direct synthesis of sulfonated aromatic poly(ether ether ketone) proton exchange membranes for fuel cell applications*. Journal of Membrane Science, 2004. **234**(1-2): p. 75-81.
24. Kreuer, K.D. and G. Portale, *A critical revision of the nano-morphology of proton conducting ionomers and polyelectrolytes for fuel cell applications*. Advanced Functional Materials, 2013. **23**(43): p. 5390-5397.
25. Kreuer, K.D., *On the development of proton conducting polymer membranes for hydrogen and methanol fuel cells*. Journal of Membrane Science, 2001. **185**(1): p. 29-39.
26. Jarumaneeroj, C., K. Tashiro, and S. Chirachanchai, *Shifting from hydrogen bond network to  $\pi$ - $\pi$  Stacking: A key mechanism for reversible thermochromic sulfonated poly(ether ether ketone)*. Macromolecular Rapid Communications, 2014. **35**(16): p. 1397-1401.
27. Li, L., J. Zhang, and Y. Wang, *Sulfonated poly(ether ether ketone) membranes for direct methanol fuel cell*. Journal of Membrane Science, 2003. **226**(1-2): p. 159-167.
28. Dahl, T., *The Nature of Stacking Interactions between Organic Molecules Elucidated by Analysis of Crystal Structures*. Acta Chemica Scandinavica, 1994. **48**: p. 96-106.
29. Sinnokrot, M.O., E.F. Valeev, and C.D. Sherrill, *Estimates of the Ab Initio Limit for  $\pi$ - $\pi$  Interactions: The Benzene Dimer*. Journal of the American Chemical Society, 2002. **124**(36): p. 10887-10893.
30. Freeman, B., Y. Yampolskii, and I. Pinnau, *Materials Science of Membranes for Gas and Vapor Separation*. 2006: Wiley.

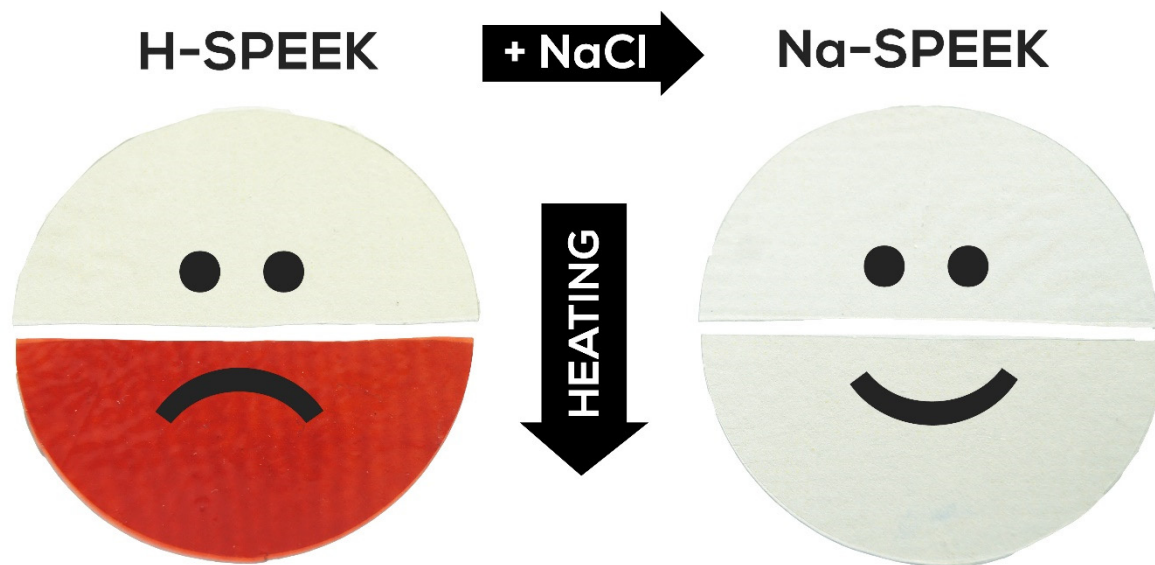


# Chapter 4

## Thermal stability of sulfonated poly(ether ether ketone) films: on the role of protodesulfonation

This chapter has been published as:

Koziara, B.T. and Kappert, E.J.; Ogieglo, W.; Nijmeijer, K.; Hempenius, M.A.; Benes, N.E., *Thermal stability of sulfonated poly(ether ether ketone) films: on the role of protodesulfonation*. *Macromolecular Materials and Engineering* **2015**, doi: 10.1002/mame.201500075.

**Abstract**

Thin film and bulk, sulfonated poly(ether ether ketone) (SPEEK) have been subjected to a thermal treatment at 160 – 220 °C for up to 15 hours. Exposing the films to 160 °C already causes partial desulfonation, and heating to temperatures exceeding 200 °C results in increased conjugation in the material, most likely via a slight cross-linking by H-substitution. It is well-known that the sulfonate proton plays a major role in the desulfonation reactions, and exchanging the protons with other cations can inhibit both protodesulfonation as well as electrophilic cross-linking reactions of the sulfonate group with other chains. Yet the implications of such ion-exchange for the thermal processing of sulfonated polymer films has not been recognized. Our study demonstrates that the ion exchange stabilizes thin films and bulk SPEEK up to temperatures exceeding 200 °C, opening up ways for the thermal processing of SPEEK in the temperature range of 160 to 220 °C without adverse effects.

## 4.1 Introduction

Sulfonated poly(ether ether ketone) (SPEEK, Figure 4.1) is an anionic polymer that finds wide use as high-performance membrane polymer that can be applied in water purification [1-3], in proton exchange membrane (PEM) fuel cells [4-6] and in dehydration of industrial gases [7-9]. For multiple reasons, SPEEK membranes are exposed to higher temperatures. PEM fuel cells have operating advantages at higher temperatures [10, 11]. Additionally, during membrane preparation high temperature treatments are suggested to remove residual high boiling point solvents after membrane formation [12], bring the material above its glass transition temperature to remove its thermal history [4], or to perform temperature-promoted crosslinking [13, 14]. Whereas temperatures up to 200 °C are not uncommon in these procedures [15], they can have detrimental effects on the integrity of SPEEK [16].

Generally, thermal changes to SPEEK are reported to occur via three separate processes [17, 18]: the removal of absorbed water and solvent ( $T = 50 - 150$  °C); temperature-promoted crosslinking, annealing and/or removal of the sulfonic acid group ( $T = 150 - 400$  °C); and backbone decomposition ( $T > 400$  °C). Especially the second temperature range is of interest, as it is associated with both desired and undesired reactions. Desulfonation is one of the major undesired reactions, because it affects the sulfonation degree and may enhance degradation reactions. Because the desulfonation reaction typically takes place through a protodesulfonation mechanism, the thermal stability of the sulfonate group is strongly dependent on the presence of a proton that takes the place of the sulfonate leaving group on the aromatic ring [19]. In the absence of a proton, desulfonation will not occur. Membrane performance studies and thermogravimetric analysis on bulk material, in which the sulfonate proton was exchanged by a sodium ion, showed indications of an enhanced thermal stability [12, 15, 16, 20]. Nonetheless, the effect of exchanging the sulfonate proton for a different counter-ion on the thermal processing has hitherto not been fully appreciated and studied systematically for SPEEK films.

In this study, we have assessed the thermal stability of SPEEK thin films and bulk membranes in the temperature range of 160 to 250 °C over a time scale of 15 hours, and have compared the stability of the proton-form H-SPEEK with that of the sodium-form Na-SPEEK. Thermogravimetric analysis (TGA) on the bulk membranes indicates an enhanced stability of



the material in the sodium-form. By performing thermo-ellipsometric analysis (TEA), the stability of thin films has been studied in detail by tracking the thermally induced changes in the UV absorption spectrum of the material. These results indicate that already temperatures as low as 160 °C induce changes to H-SPEEK. Exchanging the proton by a sodium ion significantly enhances the thermal stability of the SPEEK films, allowing for thermal treatment at temperatures exceeding 200 °C without adverse effects.

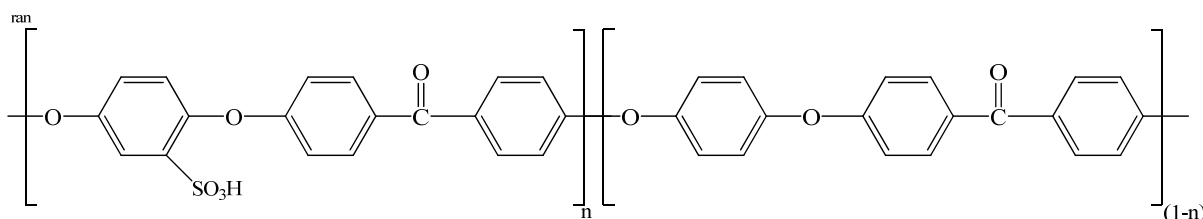


**Figure 4.1** Structural formula of SPEEK with a degree of sulfonation  $n$ .

## 4.2 Experimental

### 4.2.1 Materials and sample preparation

Poly(ether ether ketone) (PEEK) was purchased from Victrex.  $\text{CaF}_2$  pellets were obtained from Crystran.  $\text{NaCl}$  (99.5% for analysis) was obtained from Acros Organics. Methanol (Emsure<sup>®</sup>) and sulphuric acid 95-98% (EMPROVE<sup>®</sup>) were purchased from Merck.  $\text{DMSO-d}_6$  (99.5% atom D) for  $^1\text{H-NMR}$  measurements was obtained from Sigma-Aldrich. Silicon wafers (100-oriented) were obtained from Okmetic. Water was deionized to 18.2  $\text{M}\Omega\cdot\text{cm}$  using a Milli-Q Advantage A10 system (Millipore). Nitrogen was dried with molecular sieve water absorbents, followed by removal of oxygen using an oxygen trap (outlet concentration < 1 ppb  $\text{O}_2$ ).

#### PEEK sulfonation

Sulfonated poly(ether ether ketone) was obtained by sulfonation of PEEK in sulphuric acid following the procedure described by Shibuya and Porter [21]. The obtained SPEEK was in the acidic form, where  $\text{H}^+$  is the counter ion; from hereon, it will be referred to as H-SPEEK. The degree of sulfonation was determined by  $^1\text{H-NMR}$  to be 84 % following the procedure in literature [22] (see section  $^1\text{H-NMR}$  for the details on the calculation).

### **SPEEK conversion to sodium form**

SPEEK with sodium as the counter ion, referred to as Na-SPEEK, was made by immersing H-SPEEK in a 2M NaCl solution, ensuring a Na<sup>+</sup> excess of >500x. Each hour, the NaCl solution was substituted by a fresh solution, to ensure complete conversion of the proton to the sodium form. After three hours, the Na-SPEEK was rinsed with deionized water and dried for 48 hours at 30 °C under vacuum. Part of the Na-SPEEK was converted back to the proton form. This back-converted SPEEK will be referred to as H<sup>\*</sup>-SPEEK, to distinguish it from H-SPEEK. H<sup>\*</sup>-SPEEK was made by immersing Na-SPEEK in a stirred 1M HCl solution for 17 hours, ensuring a proton excess of > 200x. Afterwards, H<sup>\*</sup>-SPEEK was rinsed with deionized water multiple times and dried for 48 hours at 30 °C under vacuum.

### **Preparation of freestanding H-SPEEK and Na-SPEEK films**

A 10 wt% solution of H-SPEEK in methanol was cast onto a glass plate. After methanol evaporation under atmospheric conditions for 24 hours, the membranes were detached from the glass plate by immersion into deionized water. Subsequently, the membranes were dried for 48 hours at 30 °C under vacuum. Na-SPEEK membranes were obtained by immersing H-SPEEK membranes in a 2M NaCl solution, following the same procedure as described above for the SPEEK powder.

### **Preparation of H-SPEEK and Na-SPEEK thin films on silicon substrates**

A 5 wt% solution of H-SPEEK or Na-SPEEK in methanol was spin-coated onto 2x2 cm<sup>2</sup> silicon wafers at 2000 rpm for 50 seconds. The spin-coated thin films were dried for 48 hours at 30 °C under vacuum.

## **4.2.2 Characterization**

### **Thermogravimetric analysis**

Thermogravimetric analysis (TGA) was performed on a STA 449 F3 Jupiter<sup>®</sup> (Netzsch) fitted with a TG-only sample holder. Measurements were performed under 70 mL min<sup>-1</sup> nitrogen at a heating rate of 20 °C min<sup>-1</sup> from room temperature to 1200 °C. A temperature correction by melting standards and a blank correction with an empty cup were carried out prior to the measurements. A sample mass of ~50 mg was used, the exact mass being determined accurately by an external balance.

Gases evolving during the thermogravimetric analysis were transferred to a mass spectrometer (MS, QMS 403 D Aëolos<sup>®</sup>, Netzch). TGA and MS start times were synchronised, but no correction was applied for the time offset caused by the transfer line time (estimated < 30 sec, systematic offset). First, a bar graph scan for mass-to-charge ratio ( $m/z$ ) 1-100 amu was performed to determine the evolving  $m/z$ -numbers. The detected  $m/z$ -numbers were selected and recorded more accurately in multiple-ion-detection mode, with a dwell time of 0.5 sec per  $m/z$ -value and a resolution of 50.

### Photographs of heated SPEEK

Photographs of SPEEK were taken of fresh, freestanding films of H-SPEEK and Na-SPEEK, and of freestanding films of H-SPEEK and Na-SPEEK that were heated for 15 hours at  $190 \pm 10$  °C in a furnace under ultrapure nitrogen.

### ATR-FTIR

Fourier Transform Infrared Spectroscopy (FTIR) in Attenuated Total Reflection (ATR) mode was performed on freestanding films using a Tensor 27 Spectrometer equipped with a diamond crystal (Bruker Optics Inc., Germany), prior to and after a thermal treatment of the films under ultrapure nitrogen. The spectra were run against an empty background, baseline corrected using a rubberband baseline correction with a single iteration, and normalized before plotting.

### <sup>1</sup>H-NMR

The <sup>1</sup>H-NMR spectra were recorded on an Ascend<sup>™</sup> (Bruker) at a resonance frequency of 400 MHz. For each analysis, 5 mg of polymer was dissolved in 1 ml of DMSO-d<sub>6</sub>. NMR data were acquired for 16 scans. From the <sup>1</sup>H-NMR spectra, the degree of sulfonation was calculated following the procedure outlined in literature [22]. In this method, the degree of sulfonation is calculated from the ratio of the surface areas of the peaks stemming from the proton neighbouring the sulfonic acid to that of the other protons.

### UV-VIS absorption spectroscopy

UV-VIS spectra were recorded on a Cary 300 Spectrophotometer (Varian) with a spectral range of 200 – 800 nm, a resolution of 1 nm and a scan rate of 600 nm/min, on a solution of SPEEK in ethanol in a quartz cuvette.

## **Spectroscopic Ellipsometry**

Spectroscopic ellipsometry measurements were conducted on a M2000X ellipsometer (J.A. Woollam Co.) in the full wavelength range of 210 – 1000 nm. For measurements using the CaF<sub>2</sub>-substrate, the ellipsometer was used in transmission mode, and the background was taken in air. For room temperature measurements using silicon wafers as substrate, measurements were performed at 70° angle of incidence. Temperature-controlled experiments were performed on layers on silicon wafers. For these measurements, the M2000X was equipped with a HTC200 HeatCell™ accessory. Temperature calibration was performed using melting point standards [23]. Measurements were performed at a 70° angle of incidence. During experiments, the hot stage was continuously purged with nitrogen. The thermal treatment program consisted of a two hour dwell at room temperature, followed by heating the material to the desired temperature with a heating rate of 2.5 °C min<sup>-1</sup>. The dwell time was 15 hours, and after the dwell the sample was cooled to room temperature at 2.5 °C min<sup>-1</sup>.

### **Analysis of ellipsometry data**

Analysis of the obtained optical spectra was performed using CompleteEase® (version 4.86, J.A. Woollam Co.). The used optical constants for silicon were taken from the built-in library, and the thickness of the native oxide was fixed at 2 nm.

Parameterization of the optical dispersion of SPEEK was performed using Kramers-Kronig consistent B-Splines [24]. In order to obtain the optical dispersion reproducibly, the following steps were taken. First, the layer thickness was determined by fitting a Cauchy optical dispersion in the transparent range ( $\lambda = 500 - 1000$  nm). Taking into account optical anisotropy in thin SPEEK films [25] was not required to accurately model the absorption spectra. With fixed thickness, the layer was parameterized by B-Splines, with the node resolution set to 0.15 eV, the B-Splines forced to be Kramers-Kronig consistent, and  $\epsilon_2$  forced to be a positive number. Subsequently, the wavelength range of the B-Spline was expanded with increments of 0.15 eV, until it spanned the full wavelength range of the measurement. Finally, all parameters, i.e. thickness and optical dispersion, were fit using the B-Spline function.

For the temperature-controlled measurements, exactly the same approach was followed, with the exception that the temperature-dependent optical model for silicon was selected.

### **Conversion of extinction coefficient to absorption coefficient**

In order to be able to directly compare the results of spectroscopic ellipsometry, transmission intensity of spectroscopic ellipsometry, and UV-VIS analysis, the extinction coefficient  $k$  (-) was converted to the absorption coefficient  $\alpha$  ( $\text{nm}^{-1}$ ) by  $\alpha = 4\pi k/\lambda$ , with  $\lambda$  (nm) being the wavelength of the light. The transmission intensity  $I$  (-) was converted to the absorbance  $A$  (-) by  $A = -\ln(I/I_0)$ , with  $I_0$  (-) being the intensity of the incident beam before transmission.

## 4.3 Results and Discussion

### 4.3.1 Influence of the counter-ion on the thermal stability of SPEEK

Figure 4.2 shows the mass loss and evolved gases that are detected upon heating of H-SPEEK, Na-SPEEK, H<sup>\*</sup>-SPEEK and PEEK. In these spectra, the identical low mass loss below 200 °C is accompanied by the release of water and can be attributed to removal of absorbed water from the material. For H-SPEEK, mass loss associated with removal of water, CO<sub>2</sub> and SO<sub>2</sub> sets on at 250 °C and reaches a peak at 350 °C. There are two possible sulfur sources for the evolution of SO<sub>2</sub>: the sulfonate group or residual sulfuric acid. The presence of the latter has been proposed for SPEEK with high degrees of sulfonation [6]. Indeed, the release of SO<sub>2</sub> takes place close to the boiling point of H<sub>2</sub>SO<sub>4</sub> [26]. To verify this hypothesis, Na-SPEEK, for which the SO<sub>2</sub> release at 250 °C was absent, was converted back to H<sup>\*</sup>-SPEEK, using hydrogen chloride to avoid the sulfuric counter ion. The mass loss spectrum obtained for the H<sup>\*</sup>-form is strikingly similar to that of the original H-form, thus rejecting the hypothesis that residual H<sub>2</sub>SO<sub>4</sub> is the source of SO<sub>2</sub> formation. Hence, it can be concluded that the sulfonate group is the origin of the SO<sub>2</sub>, and that exchange of the proton by sodium prevents the reaction that produces SO<sub>2</sub>. The absence of this SO<sub>2</sub>-loss in the sodium-exchanged Na-SPEEK is a direct evidence of the enhanced thermal stability of the Na-SPEEK compared to H-SPEEK, and matches previous experiments [16, 20].

Between 450 and 650 °C, all SPEEK-forms show a strong mass loss, associated with the evolution of CO<sub>2</sub> and SO<sub>2</sub>, followed by a release of aromatic compounds. The evolution of SO<sub>2</sub> indicates that sulfur-containing groups were still present at these temperatures in both materials. Around 750 °C, a final mass loss step takes place that is accompanied by the release of CO<sub>2</sub>. A similar step is observed in the case of PEEK. This implies that the CO<sub>2</sub> loss is due to degradation of the polymer backbone, and is independent on the sulfonation history of the polymer.

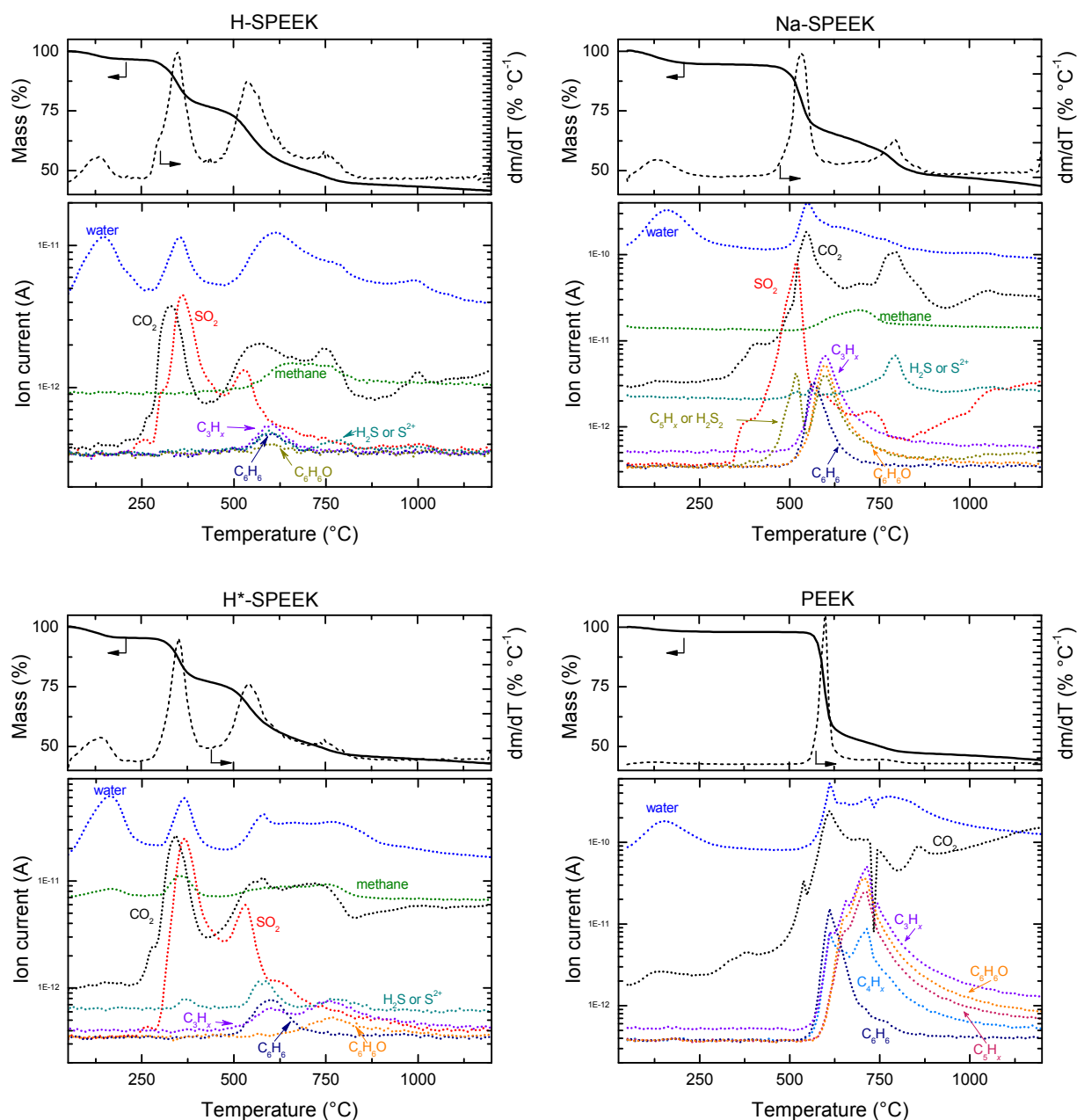
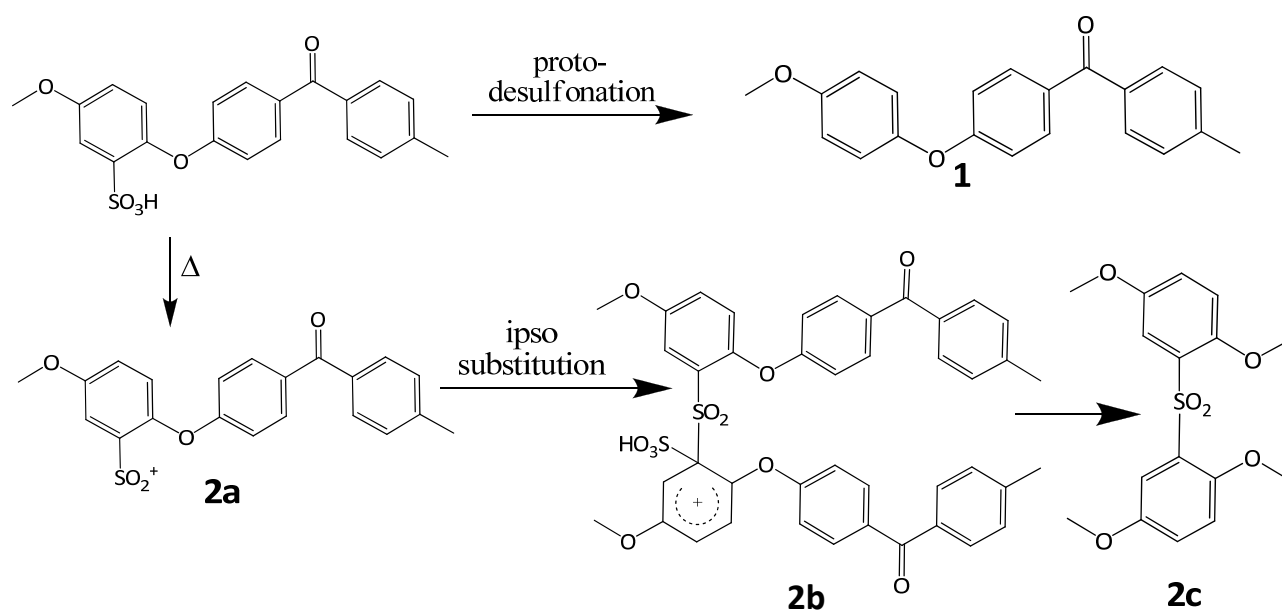


**Figure 4.2** TGA-MS spectra of H-SPEEK (top left), Na-SPEEK (top right), H\*-SPEEK (bottom left) and PEEK (bottom right), all recorded with a heating rate of  $20\text{ }^{\circ}\text{C min}^{-1}$  under a nitrogen atmosphere.

For H-SPEEK, the release of  $\text{SO}_2$  in two distinct steps with onsets at  $\sim 250\text{ }^{\circ}\text{C}$  and  $\sim 500\text{ }^{\circ}\text{C}$  is an indication for the presence of sulfur in two different forms in the material. The majority of the  $\text{SO}_2$ -release occurs in the first step (note that the log-scale over-emphasises gases present in smaller amounts). Previous studies on SPEEK decomposition only reported  $\text{SO}_2$  release in a unimodal peak between  $200$  and  $400\text{ }^{\circ}\text{C}$  (a temperature shift of some tens of degrees could

be the result of differences in heating rate), although not all studies include an evolved-gas analysis up to a temperature of 500 °C [13, 15, 17, 27].

Scheme 4.1 summarizes the two possible routes for  $\text{SO}_x$  loss from the material: protodesulfonation or ipso substitution. If a sulfone ( $\text{R-SO}_2\text{-R}$ ) bridge is formed by ipso substitution, this sulfone bridge can in turn decompose at higher temperatures, yielding the release of a second  $\text{SO}_x$  species. Whether  $\text{SO}$ ,  $\text{SO}_2$ , or  $\text{SO}_3$  is released from the material, depends on the reaction mechanism. Thermal protodesulfonation is typically said to yield an  $\text{SO}_3$  group, although a two-stage process with cleavage of a  $\text{SO}_2$  group has been registered in mass spectrometry [28]. Upon ipso substitution,  $\text{SO}_2$  release would be expected. It has to be noted that the ipso substitution reaction was found to depend strongly on the presence of traces of solvent: it was found to occur in the presence of DMSO [13, 15], but not with NMP, DMAc, or DMF [29]. A third possible reaction, H-substitution, results in cross-linking as well, but will not cause  $\text{SO}_2$  release [13]. It will, however, result in the formation of cross-links inside the material under release of water, and can therefore be the origin for the different forms of sulfur in the material.



**Scheme 4.1** Two possible reactions involving loss of  $\text{SO}_x$ : **1**. protodesulfonation, and **2**. formation of a  $\text{SO}_2^+$  electrophile (**2a**) followed by cross-linking via ipso-substitution on the sulfonic acid moiety (**2b** and **2c**), as suggested by Di Vona et al. [13].



Discerning between the two possible mechanisms for the first SO<sub>2</sub> loss, which are given in Scheme 4.1, is not straightforward. Both routes are effectively blocked by the sodium exchange. In addition, SO<sub>2</sub> and SO<sub>3</sub> are difficult to discern by MS, because SO<sub>3</sub> fragments upon electron impact to [SO<sub>2</sub>]<sup>+</sup> and [SO<sub>3</sub>]<sup>+</sup> (ratio [SO]<sup>+</sup>: [SO<sub>2</sub>]<sup>+</sup>: [SO<sub>3</sub>]<sup>+</sup> is ~2.1:1.2:1) [30]. Mikhailenko et al. have suggested that the release of CO<sub>2</sub> prior to the SO<sub>2</sub> release could indicate the formation of an electrophile (RSO<sub>2</sub><sup>+</sup>) available for cross-linking via ipso or H-substitution, under the release of a hydroxyl radical that can directly react with the main chain [27]. However, as no further evidence for these degradation reactions is seen, and the CO<sub>2</sub> could also have been sorbed in the proton-rich watery environment present in the material, we consider this reaction unlikely in our system.

The combination of visual observation, NMR, and FTIR has been used to conclusively assert the thermally induced effects, and to better understand the differences between H-SPEEK and Na-SPEEK. Figure 4.3 visualizes the differences between the proton and sodium forms after thermal treatment of both films. Here, the films are shown before and after heating to 190 ± 10 °C for 15 hours. Before thermal treatment, both films are transparent, and the H-SPEEK has a yellowish appearance. After heating the material, the strong color change into red in the H-SPEEK confirms the substantial chemical changes in the material. Although at this temperature, the TGA results do not reveal significant mass changes of the material, nor the release of gaseous degradation products, the long dwell time can significantly increase the progress of the reaction [31]. The red color of the treated H-SPEEK is a manifestation of the development of chromophoric groups. Partially, this could result from desulfonation, which would cause the color to shift to the brown-greyish color of PEEK. Because of the intense red color, this reaction alone cannot be responsible for the color change. Most likely, a heating-induced cross-linking reaction through H-substitution increases the conjugation of the π-bonds, resulting in an increased light absorption. After the thermal treatment, H-SPEEK has lost its flexibility and has turned into a brittle material. The color change after the long-term treatment is irreversible. This is in contrast to the reversible color changes that have been reported previously for short-term treatments in [32] that are attributed to π-π stacking induced by the removal of water at elevated temperatures.

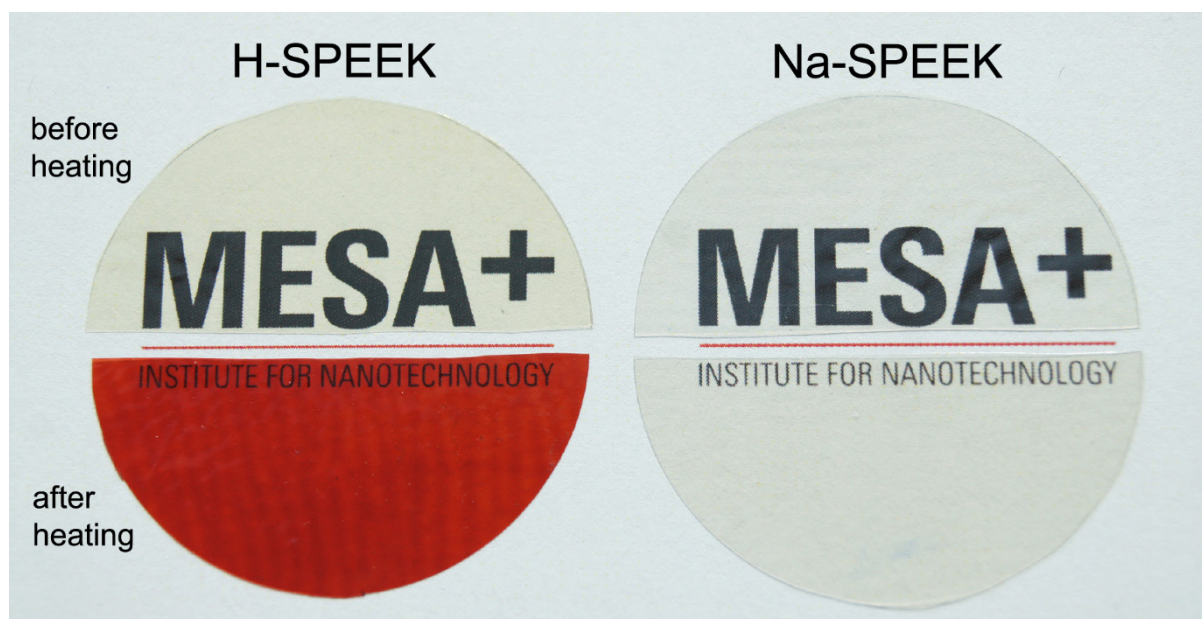


**Figure 4.3** Photographs of H-SPEEK (left) and Na-SPEEK (right) before heating (top) and after heating (bottom) in nitrogen at 190 °C for 15 hours.

Although the effects of thermal treatment on the color of the H-SPEEK appear dramatic, the changes in the infrared spectrum upon this treatment are only limited. Figure 4.4 shows the infrared spectrum for both H-SPEEK and Na-SPEEK prior to and after thermal treatments. Again, changes are seen upon thermal treatment of H-SPEEK, whereas Na-SPEEK remains unchanged upon heating to 190 °C.

Our sodium exchange allows for direct identification of the peaks involving the sulfonate group, which are indicated by an asterisk in Figure 4.4. In combination with the peak changes upon sulfonation indicated in [29], this allows for accurate identification of phenyl and sulfonate peaks. The full band assignment is given in Table 4-S1 in the Supporting Information. Here, the most important peaks are found at 1490  $\text{cm}^{-1}$  and 1471  $\text{cm}^{-1}$ . The change in the ratio between these peaks upon heating shows the identical trend as for a chemically obtained lower degree of sulfonation of PEEK [29]. This conclusion is further supported by the changes in the peaks at 1078  $\text{cm}^{-1}$ , 1020  $\text{cm}^{-1}$ , and 767  $\text{cm}^{-1}$ , which are all peaks associated with either sulfonic acid groups or the substitution of sulfonate groups on a phenyl ring. Heating does not introduce new peaks, except for the peaks at 1375  $\text{cm}^{-1}$  (w) after heating to 300 °C and at 1104  $\text{cm}^{-1}$  (w) and 1737  $\text{cm}^{-1}$  (w) after heating to 300 °C and 400 °C, respectively.

All these peaks fall outside the typical range for sulfone cross-links ( $R-SO_2-R$ ) that is given as  $1370-1290$  and  $1170-1110\text{ cm}^{-1}$ , and which should be very strong [33]. Therefore, we conclude that, if any, the amount of sulfone cross-links formed in the H-SPEEK upon heating is too low to be obvious from the infrared analysis.

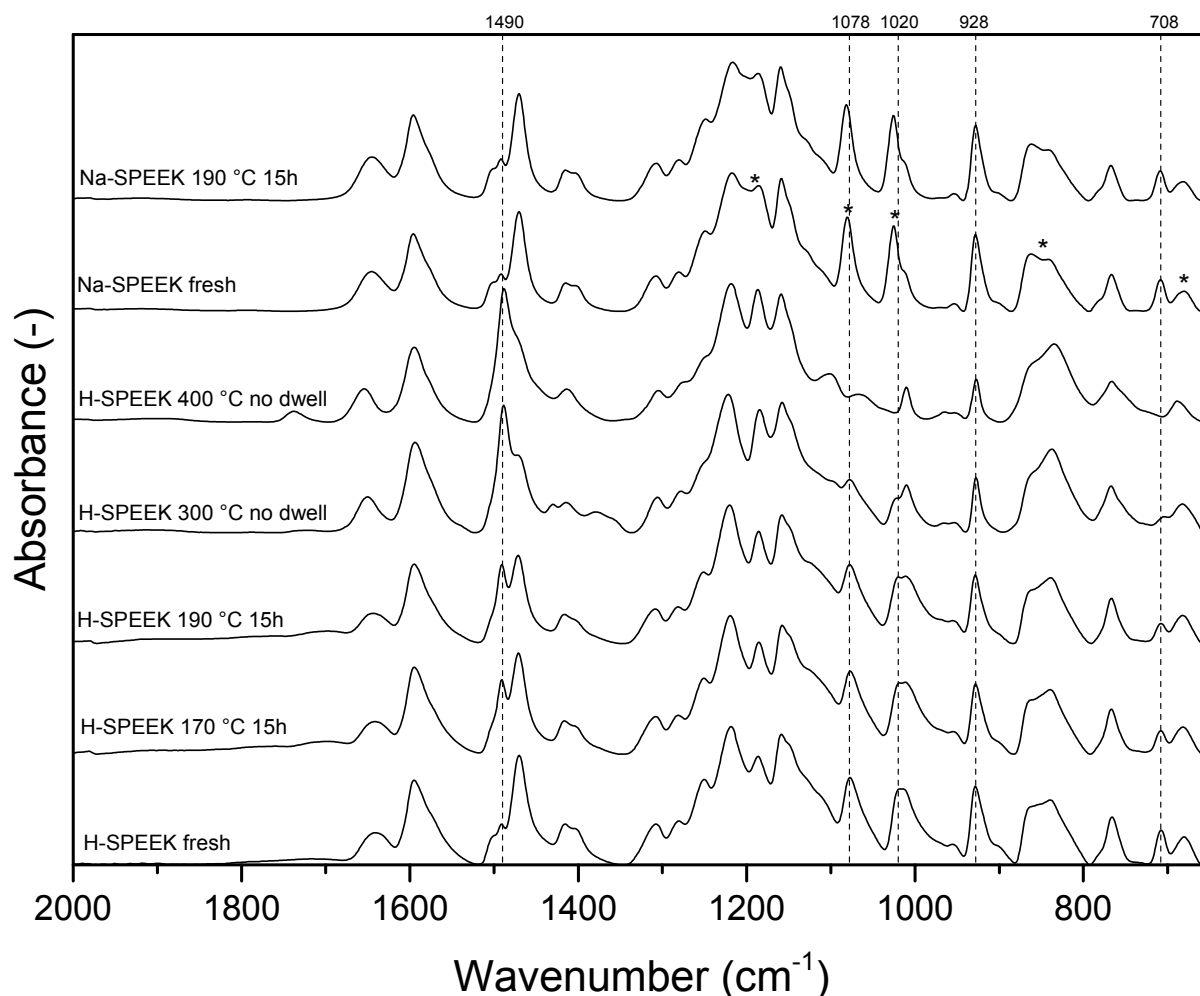


**Figure 4.4** ATR-FTIR spectra of H-SPEEK and Na-SPEEK treated at different temperatures. The peaks marked by an asterisk (\*) in the spectrum of fresh Na-SPEEK show a difference from the fresh H-SPEEK spectrum, and therefore likely involve the sulfonate group. The band assignment is given in Table 4-S1 and the spectra in the wavelength range  $4000-2000\text{ cm}^{-1}$  are given in Figure 4-S7 in the Supporting Information.

The thermally induced changes in the  $^1\text{H}$ -NMR-spectrum of SPEEK, shown in Figure 4.5, are another demonstration of the distinct characteristics of the proton and sodium form of SPEEK. The NMR spectrum for H-SPEEK agrees well with results previously reported in literature [34]. As can be seen from the spectrum, the exchange of the sulfonate proton by a sodium ion results in a slight deshielding of the  $\text{H}_{\text{E}}$ -proton, resulting in a small downfield shift.

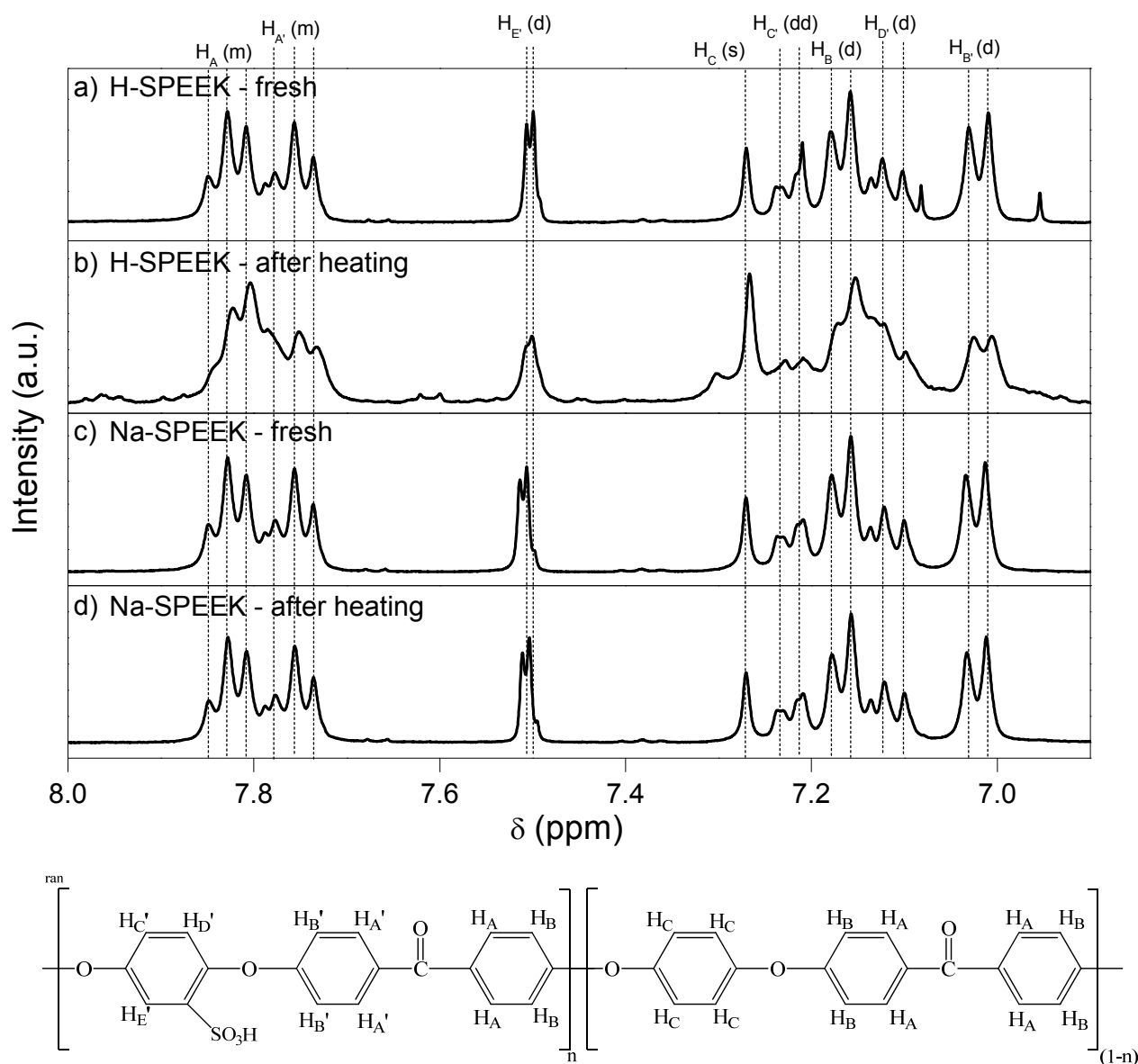


**Figure 4.5** Top panel:  $^1\text{H}$ -NMR spectra of H-SPEEK and Na-SPEEK before and after thermal treatment at 190 °C for 15 hours. Assignments given at the top of the graph are for fresh H-SPEEK. Bottom panel: structural formula of H-SPEEK with proton assignment.

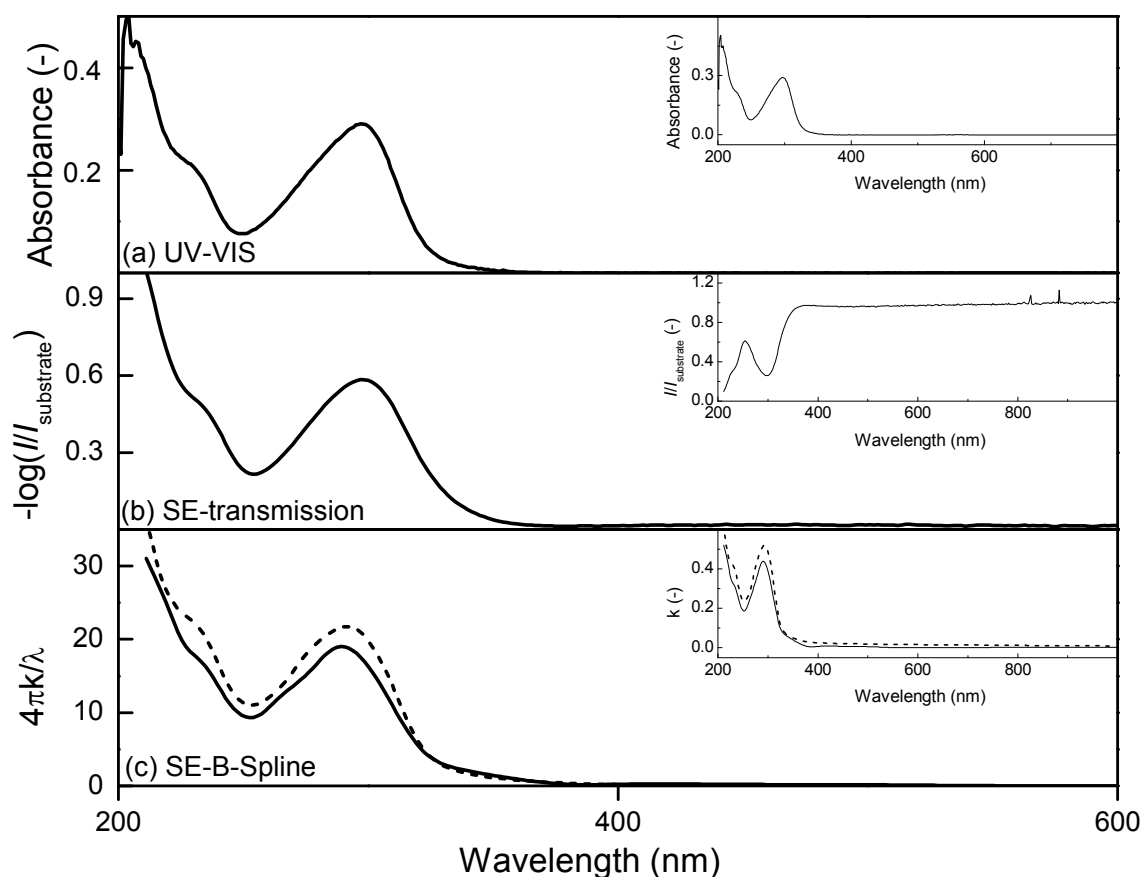
A similar effect is seen for the  $H_{B'}$ -protons. The sodium exchange did not influence any of the other peaks. For the sodium form, the thermal treatment step induced no changes at all in the material's structure. For correctly discerning the  $H_{A'}$  and  $H_A$ -protons, a 2D ( $^1H$  COSY) spectrum was recorded (see Supporting Information, Figures 4-S1 – 4-S3).

For H-SPEEK, definite changes are introduced by the thermal treatment, resulting in strong changes in the chemical environment of the protons. Although most peaks still remain visible, strong peak broadening has occurred. Peak broadening can be a result of reduced mobility of the studied molecules and can therefore be an indication of cross-linking reactions. Alternatively, it can be the result of a mixture of molecules for which the peaks overlap, for instance through cross-linking by H-substitution. As a single peak without overlap with other peaks, the  $H_C$ -peak is an ideal peak to study the effects of the thermal treatment. Upon desulfonation, the removal of one sulfonate group results in the creation of four  $H_C$ -protons at the expense of the  $H_{C'}$ ,  $H_{D'}$ , and  $H_{E'}$  peaks. In the case of a thermally induced ipso substitution reaction, the electron-withdrawing  $SO_3^-$  group gets exchanged for an  $SO_2$  group that is electron-withdrawing as well. Consequently, the changes in the  $^1H$ -NMR spectra would be minor peak shifts. The significant increase in the  $H_C$ -peak confirms the occurrence of desulfonation reactions. This conclusion is further supported by the decrease of the  $H_{A'}$ ,  $H_{B'}$ ,  $H_{D'}$  and  $H_{E'}$ -peaks, and in line with spectra of SPEEK at lower sulfonation degrees [22]. The 2D ( $^1H$  COSY) spectrum (see Supporting Information, Figures 4-S2 and 4-S3) confirms the presence of three new groups of coupled protons with apparent downfield shifts from the base material, indicating the occurrence of side reactions during the desulfonation.

From the NMR-spectrum of SPEEK, the degree of sulfonation can be determined [22]. For the untreated H-SPEEK and both untreated and treated Na-SPEEK, this calculation could be applied accurately. For all three SPEEK-types, the degree of sulfonation was determined to be unchanged at 84 %, indicating no structural changes in these polymers. For the heat-treated H-SPEEK, the apparent degree of sulfonation was calculated to be 78 % after heating at 160 °C for 15 h and 65 % after heating at 190 °C for 15 h. Because some changes in the spectrum could not be assigned to specific groups, wrong groups can be included in the peak integration, and these values should be considered with caution. For the treatment at 183 °C for 15 h, the loss of sulfonate groups from the material is supported by the detected release of  $SO_2$  (see Supporting Information, Figure 4-S8).

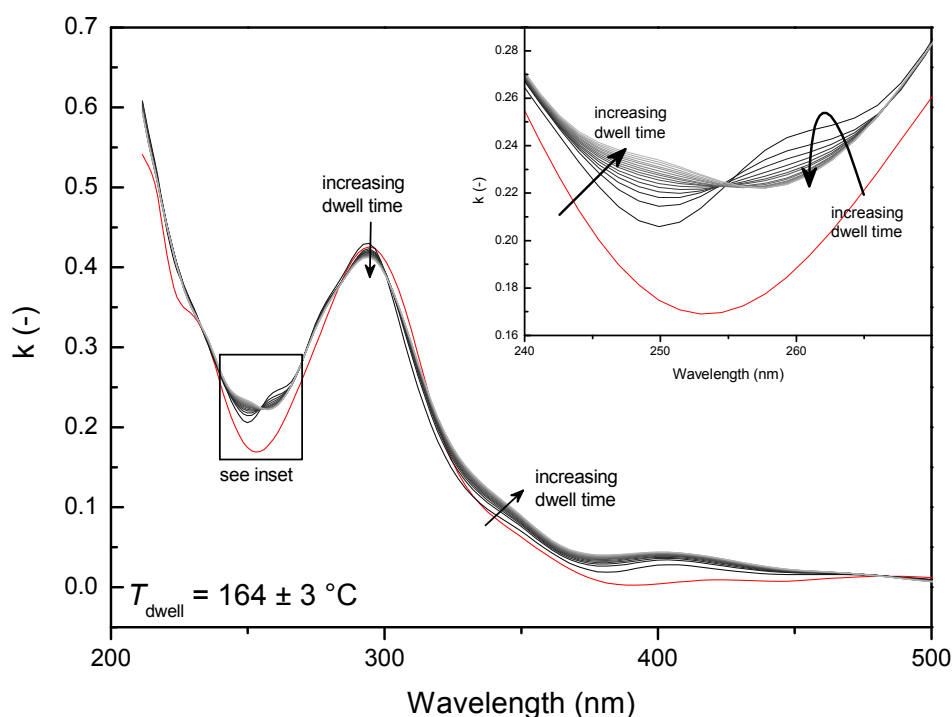
### 4.3.2 Long-term stability of thin films

Figure 4.6 shows the absorption spectra obtained by UV-VIS absorption spectroscopy, by transmission mode ellipsometry, and reflectance mode ellipsometry. The close agreement between the spectra establishes ellipsometry as a suitable technique to study the changes in the thin supported films. This is in particular beneficial for polymers, such as PEEK, that have low solubility in common solvents, and are therefore difficult to study with, e.g., UV-VIS. The close resemblance between the PEEK and H-SPEEK ellipsometry spectra indicates that the sulfonation of the polymer does not induce large changes in its light absorption properties.



**Figure 4.6** Absorption spectra of H-SPEEK (solid line) and PEEK (dashed line) determined by (a) UV-VIS on SPEEK dissolved in ethanol, (b) spectroscopic ellipsometry in transmission mode, and (c) spectroscopic ellipsometry B-spline modeling. All data were converted to a parameter that is linearly proportional to the absorbance. The inserts show the original data over the whole wavelength range.

The changes in the absorption spectrum of H-SPEEK upon prolonged exposure to a temperature of 164 °C are given in Figure 4.7. The red line corresponds to untreated H-SPEEK and has the same shape as in Figure 4.6. The prolonged exposure to 164 °C for 15 h induced multiple changes in the absorption spectrum. The increase in absorbance at wavelengths higher than 320 nm, and the slight decrease of the peak at  $\lambda = 300$  nm, are in line with earlier observations made by temperature-controlled UV-VIS [32]. Notable is the development of two peaks at 250 and 260 nm. The peak at 250 nm shows a progressive growth with increasing dwell times; the peak at 260 nm first appears but later disappears during the prolonged exposure to this temperature. The clear development of individual peaks corresponds to changes in the structure of SPEEK. Absorptions around 250 nm are generally associated with  $n-\pi^*$  transitions or with  $\pi-\pi^*$  transitions in conjugated systems [35]. It is therefore difficult to assign this peak specifically, as it can be due to non-bonding electrons of oxygen in either the sulfonate, the ether, or the carbonyl groups, or due to an increase in conjugation within the material because of thermal cross-linking.



**Figure 4.7** Absorption spectra of H-SPEEK under nitrogen before thermal treatment (red) and after 0 (black) to 15 hours (light grey) of dwell at  $164 \pm 3$  °C, obtained by in-situ ellipsometry. The change between the untreated and the 0 hour dwell samples is induced by the heating ramp.

Given the results of the TGA-MS, FTIR, and NMR on the bulk SPEEK, a higher electron density in the aromatic rings resulting from protodesulfonation would be the most plausible explanation. Treatment of H-SPEEK at temperatures of 183 and 193 °C (see Supporting Information, Figures 4-S4 and 4-S5) resulted in similar, but more pronounced trends. For Na-SPEEK, treatment at 183 °C introduces only minor changes in the spectrum, indicating that the absence of the sulfonate proton prevents the thermal reactions from taking place (see Supporting Information, Figure 4-S4).

At a treatment temperature of ~220 °C (Figure 4.8) and higher (~250 °C, Supporting Information Figure 4-S6), the differences between the proton and sodium form are even more pronounced. Here, the region of interest is the wavelength range of 300 nm upwards, in which chromophoric behavior is typically limited to strongly conjugated structures [35]. For H-SPEEK, light absorption increases over nearly the full wavelength range, and strong changes take place around  $\lambda = 380$  nm. The increase in absorption is in line with the visual observations presented in Figure 4.3. For Na-SPEEK, the changes in the spectrum are limited to minor changes in the absorption in the 300 – 400 nm wavelength range.

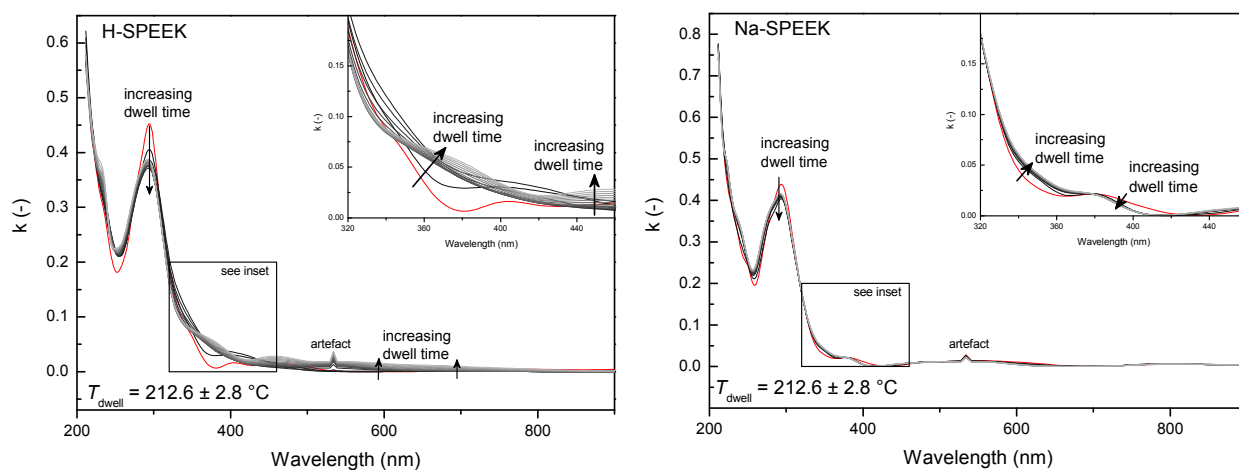


**Figure 4.8** The absorption spectrum of H-SPEEK (left) and Na-SPEEK (right) under nitrogen before thermal treatment (red) and after 0 (black) to 15 hours (light grey) of dwelling at  $213 \pm 3$  °C, obtained by in-situ ellipsometry. The change between the untreated and the 0 hour dwell samples is induced by the heating ramp.



## 4.4 Conclusions

The thermal stability of SPEEK (H-SPEEK) and its sodium-exchanged form (Na-SPEEK) have been studied at temperatures of 160 to 220 °C, in shorter heating rate experiments and for longer experiments by dwelling for 15 hours. For H-SPEEK, desulfonation reactions are found to occur already at temperatures as low as 160 °C, followed by increased conjugation in the material, most likely via slight cross-linking on phenyl rings by H-substitution at temperatures exceeding 200 °C.

The thermal stability of SPEEK is found to be strongly enhanced upon ion exchange of the sulfonate proton with a sodium ion. For the bulk polymer, this exchange shifts the onset of the first SO<sub>2</sub> removal to higher temperatures by 100 °C. This shift is attributed to the inhibition of the protodesulfonation reaction. Experiments, in which the Na-SPEEK is converted back to the proton form, eliminate residual sulfuric acid as a possible cause for sulfur release at 250 to 350 °C [6]. The absence of sulfonated solvents in our synthesis, and the fact that H<sub>2</sub>SO<sub>4</sub> could be excluded as a sulfur source, is a strong indication for the involvement of the sulfonate groups for both mass losses. For H-SPEEK, TGA-MS, FTIR, and <sup>1</sup>H-NMR are separately not conclusive whether the SO<sub>2</sub> loss from the material is due to protodesulfonation or cross-linking through sulfone bridges via ipso substitution. However, the fact that all three techniques individually show evidence for desulfonation and only limited evidence for the formation of sulfone bridging groups at temperatures exceeding 160 °C, suggest that the SO<sub>2</sub> loss is mainly due to the protodesulfonation mechanism. Although this would indicate a possibility of using a specifically designed thermal treatment program to obtain SPEEK with a targeted degree of desulfonation, the fact that not all sulfur can be removed from the material before main-chain degradation occurs, indicates that some sulfur moieties remain stable inside the material. As a result, full desulfonation of a SPEEK thin film into a PEEK thin film appears to be impossible.

## **Acknowledgements**

This work was performed in the cooperation framework of Wetsus, centre of excellence for sustainable water technology ([www.wetusus.nl](http://www.wetusus.nl)). Wetusus is co-funded by the Dutch Ministry of Economic Affairs and Ministry of Infrastructure and Environment, the European Union Regional Development Fund, the Province of Fryslân, and the Northern Netherlands Provinces. The authors would like to thank the participants of the research theme “Dehydration” for the fruitful discussions and their financial support.

The authors thank Jeroen Ploegmakers (Pentair, The Netherlands) for ICP-AES measurements.

## References

1. He, T., et al., *Preparation and characterization of nanofiltration membranes by coating polyethersulfone hollow fibers with sulfonated poly(ether ether ketone) (SPEEK)*. Journal of Membrane Science, 2008. **307**(1): p. 62-72.
2. Ba, C. and J. Economy, *Preparation and characterization of a neutrally charged antifouling nanofiltration membrane by coating a layer of sulfonated poly(ether ether ketone) on a positively charged nanofiltration membrane*. Journal of Membrane Science, 2010. **362**(1-2): p. 192-201.
3. Bowen, W.R., T.A. Doneva, and H.-B. Yin, *Separation of humic acid from a model surface water with PSU/SPEEK blend UF/NF membranes*. Journal of Membrane Science, 2002. **206**(1-2): p. 417-429.
4. Carbone, A., et al., *Sulphonated poly(ether ether ketone) membranes for fuel cell application: Thermal and structural characterisation*. Journal of Power Sources, 2006. **163**(1): p. 18-26.
5. Jörisen, L., et al., *New membranes for direct methanol fuel cells*. Journal of Power Sources, 2002. **105**(2): p. 267-273.
6. Kaliaguine, S., et al., *Properties of SPEEK based PEMs for fuel cell application*. Catalysis Today, 2003. **82**(1-4): p. 213-222.
7. Giuseppin, M.L.F., P.J. Smits, and G.W. Hofland, *Subcritical gas assisted drying of biopolymer material*. 2012, US 20120316331 A1.
8. Jia, L., et al., *Sulfonation of polyetheretherketone and its effects on permeation behavior to nitrogen and water vapor*. Journal of Applied Polymer Science, 1996. **60**(8): p. 1231-1237.
9. Sijbesma, H., et al., *Flue gas dehydration using polymer membranes*. Journal of Membrane Science, 2008. **313**(1-2): p. 263-276.
10. Zhang, J., et al., *High temperature PEM fuel cells*. Journal of Power Sources, 2006. **160**(2): p. 872-891.
11. Alberti, G., et al., *Polymeric proton conducting membranes for medium temperature fuel cells (110–160°C)*. Journal of Membrane Science, 2001. **185**(1): p. 73-81.
12. Khan, A.L., X. Li, and I.F.J. Vankelecom, *Mixed-gas CO<sub>2</sub>/CH<sub>4</sub> and CO<sub>2</sub>/N<sub>2</sub> separation with sulfonated PEEK membranes*. Journal of Membrane Science, 2011. **372**(1-2): p. 87-96.
13. Luisa Di Vona, M., et al., *Analysis of temperature-promoted and solvent-assisted cross-linking in sulfonated poly(ether ether ketone) (SPEEK) proton-conducting membranes*. Journal of Physical Chemistry B, 2009. **113**(21): p. 7505-7512.
14. Mikhailenko, S.D., et al., *Proton conducting membranes based on cross-linked sulfonated poly(ether ether ketone) (SPEEK)*. Journal of Membrane Science, 2004. **233**(1-2): p. 93-99.
15. Maranesi, B., et al., *Cross-Linking of Sulfonated Poly(ether ether ketone) by Thermal Treatment: How Does the Reaction Occur?* Fuel Cells, 2013. **13**(2): p. 107-117.
16. Jin, X., et al., *Sulfonated poly(aryl ether ketone)*. British Polymer Journal, 1985. **17**(1): p. 4-10.
17. Knauth, P., et al., *Thermogravimetric analysis of SPEEK membranes: Thermal stability, degree of sulfonation and cross-linking reaction*. Journal of Analytical and Applied Pyrolysis, 2011. **92**(2): p. 361-365.
18. Hou, H., M.L. Di Vona, and P. Knauth, *Building bridges: Crosslinking of sulfonated aromatic polymers—A review*. Journal of Membrane Science, 2012. **423–424**: p. 113-127.

19. Wanders, A.C.M. and H. Cerfontain, *Kinetics of the desulfonation of benzenesulfonic acid and the toluenesulfonic acids in aqueous sulfuric acid*. Recueil des Travaux Chimiques des Pays-Bas, 1967. **86**(11): p. 1199-1216.
20. Bailly, C., et al., *The sodium salts of sulphonated poly(aryl-ether-ether-ketone) (PEEK): Preparation and characterization*. Polymer, 1987. **28**(6): p. 1009-1016.
21. Shibuya, N. and R.S. Porter, *Kinetics of PEEK sulfonation in concentrated sulfuric acid*. Macromolecules, 1992. **25**(24): p. 6495-6499.
22. Zaidi, S.M.J., et al., *Proton conducting composite membranes from polyether ether ketone and heteropolyacids for fuel cell applications*. Journal of Membrane Science, 2000. **173**(1): p. 17-34.
23. Kappert, E.J., et al., *Temperature calibration procedure for thin film substrates for thermo-ellipsometric analysis using melting point standards*. Thermochemica Acta, 2015. **601**: p. 29-32.
24. Johs, B. and J.S. Hale, *Dielectric function representation by B-splines*. physica status solidi (a), 2008. **205**(4): p. 715-719.
25. Koziara, B.T., K. Nijmeijer, and N.E. Benes, *Optical anisotropy, molecular orientations, and internal stresses in thin sulfonated poly(ether ether ketone) films*. Journal of Materials Science, 2015. **50**(8): p. 3031-3040.
26. Lide, D.R., *CRC handbook of chemistry and physics : a ready-reference book of chemical and physical data*. 2001, Boca Raton, Fla.: CRC Press.
27. Mikhailenko, S.D., et al., *Properties of PEMs based on cross-linked sulfonated poly(ether ether ketone)*. Journal of Membrane Science, 2006. **285**(1-2): p. 306-316.
28. Fornarini, S., *Mass Spectrometry of Sulfonic Acids and their Derivatives*, in *Sulphonic Acids, Esters and their Derivatives (1991)*. 2006, John Wiley & Sons: New York. p. 73-133.
29. Xing, P., et al., *Synthesis and characterization of sulfonated poly(ether ether ketone) for proton exchange membranes*. Journal of Membrane Science, 2004. **229**(1-2): p. 95-106.
30. Briggs, J.P., R.R. Hudgins, and P.L. Silveston, *The fragmentation of SO<sub>3</sub> in electron impact ionization sources*. International Journal of Mass Spectrometry and Ion Physics, 1976. **20**(1): p. 1-5.
31. Vyazovkin, S., et al., *ICTAC Kinetics Committee recommendations for performing kinetic computations on thermal analysis data*. Thermochemica Acta, 2011. **520**(1-2): p. 1-19.
32. Jarumaneeroj, C., K. Tashiro, and S. Chirachanchai, *Shifting from hydrogen bond network to  $\pi$ - $\pi$  Stacking: A key mechanism for reversible thermochromic sulfonated poly(ether ether ketone)*. Macromolecular Rapid Communications, 2014. **35**(16): p. 1397-1401.
33. Pretsch, E., P. Bühlmann, and M. Badertscher, *IR Spectroscopy*, in *Structure Determination of Organic Compounds*. 2009, Springer Berlin Heidelberg. p. 1-67.
34. Robertson, G.P., et al., *Casting solvent interactions with sulfonated poly(ether ether ketone) during proton exchange membrane fabrication*. Journal of Membrane Science, 2003. **219**(1-2): p. 113-121.
35. Pretsch, E., P. Bühlmann, and M. Badertscher, *UV/Vis Spectroscopy*, in *Structure Determination of Organic Compounds*. 2009, Springer Berlin Heidelberg. p. 1-20.

## Supporting Information

### $^1\text{H}$ COSY NMR spectrum

Figure 4-S1 shows the  $^1\text{H}$ -COSY spectrum of fresh H-SPEEK for  $\delta = 6.9 - 8.0$ . From the off-diagonal elements, the homonuclear correlation of protons can be determined. From the figure, the following peaks could be coupled:

- $\delta 7.17$  to  $\delta 7.82$  (establishing that  $\delta 7.82$  belongs to the  $\text{H}_A$ -proton);
- $\delta 7.02$  to  $\delta 7.76$  (establishing that  $\delta 7.76$  belongs to the  $\text{H}_{A'}$ -proton);
- $\delta 7.22$  to  $\delta 7.50$  (confirming the coupling between  $\text{H}_{C'}$  and  $\text{H}_{E'}$ );
- $\delta 7.22$  to  $\delta 7.11$  (confirming the coupling between  $\text{H}_{C'}$  and  $\text{H}_{D'}$ );

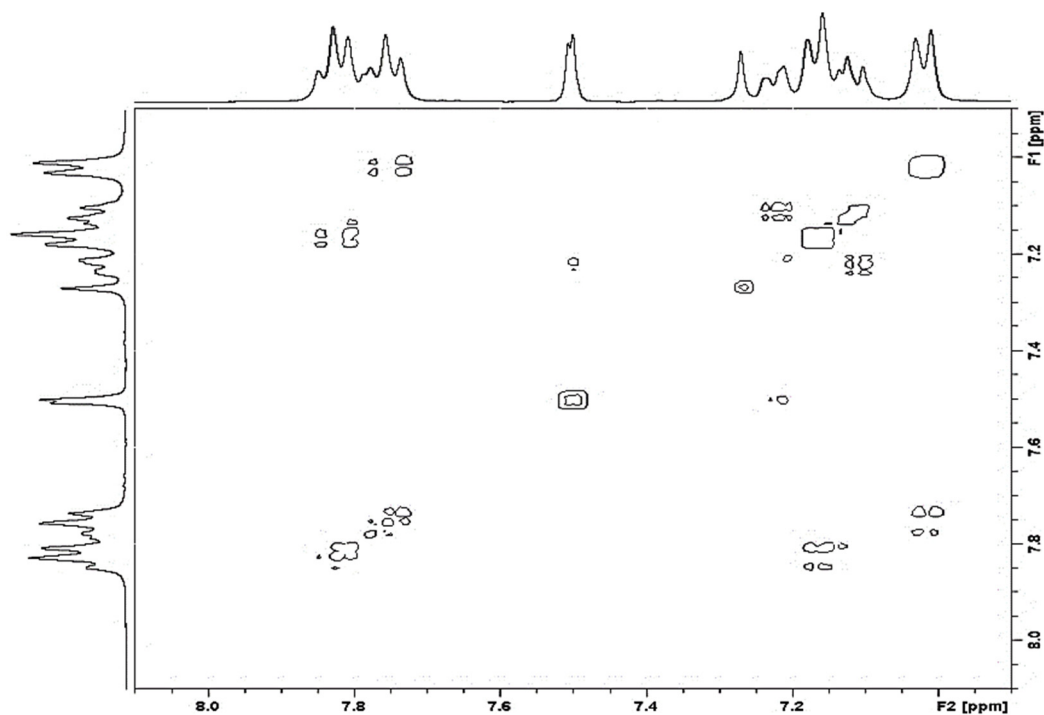
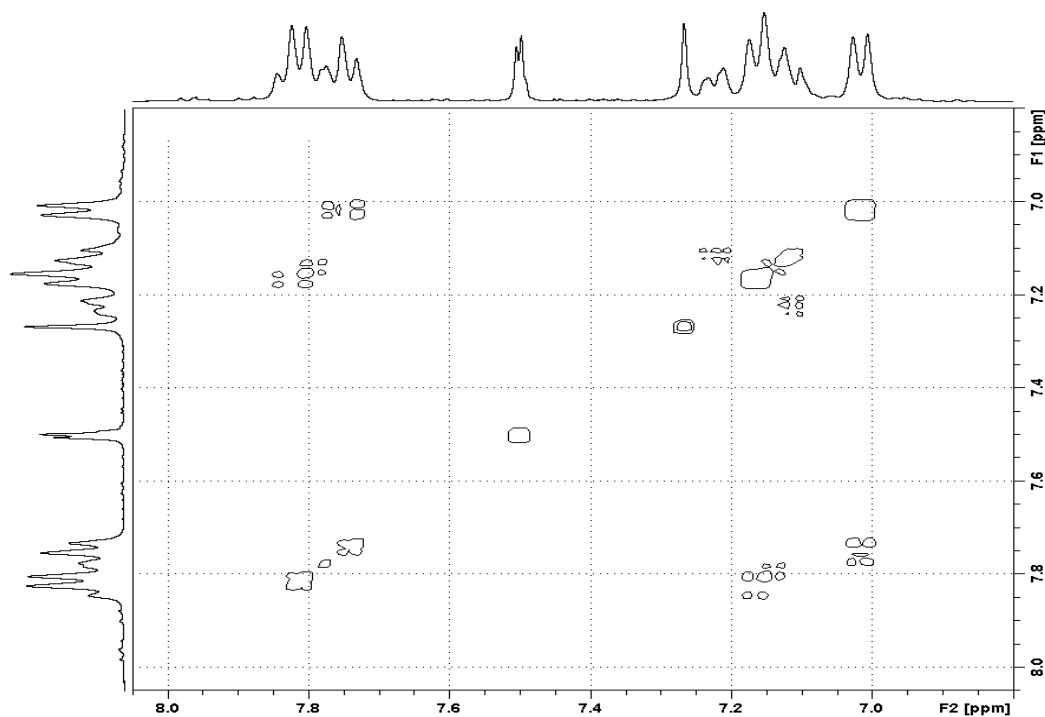


Figure 4-S1  $^1\text{H}$  COSY spectrum in  $\text{DMSO-d}_6$  at 400 MHz of fresh H-SPEEK.



**Figure 4-S2**  $^1\text{H}$  COSY spectrum in  $\text{DMSO-d}_6$  at 400 MHz of H-SPEEK treated at  $160\text{ }^\circ\text{C}$  for 15 hours.

Figure 4-S2 shows the  $^1\text{H}$ -COSY spectrum of H-SPEEK treated at  $160\text{ }^\circ\text{C}$  for 15 hours, for  $\delta = 6.9 - 8.1$ . Again, the spectrum shows the correlation between the peaks as given above for the fresh SPEEK. However, in the spectrum, additional correlations can be found:

- $\delta 6.85$  to  $\delta 7.55$
- $\delta 7.0$  to  $\delta 7.7$  and to  $\delta 7.95$
- $\delta 7.15$  to  $\delta 8.03$

Figure 4-S3 shows the  $^1\text{H}$ -COSY spectrum of H-SPEEK treated at 190 °C for 15 hours, for  $\delta = 6.9 - 8.5$ . Please note that the H-SPEEK was treated in a different batch as the H-SPEEK given in the article, and that as a result, the treatment temperature may be slightly different. Again, the spectrum shows the correlation between the peaks as given above for the fresh SPEEK. However, in the spectrum, additional correlations can be found:

- $\delta 6.93$  to  $\delta 7.6$
- $\delta 7.0$  to  $\delta 7.7$  and to  $\delta 7.95$
- $\delta 7.15$  to  $\delta 8.03$

Assigning these peaks to specific compounds is difficult, because of the numerous possible reactions that could occur in the material. The upfield shift of all these peaks is an indication of the increasing shielding of these protons. Furthermore, the correlation between the  $\delta 7.0$ ,  $\delta 7.67$  and  $\delta 7.95$  indicates that these groups are part of the same structure.

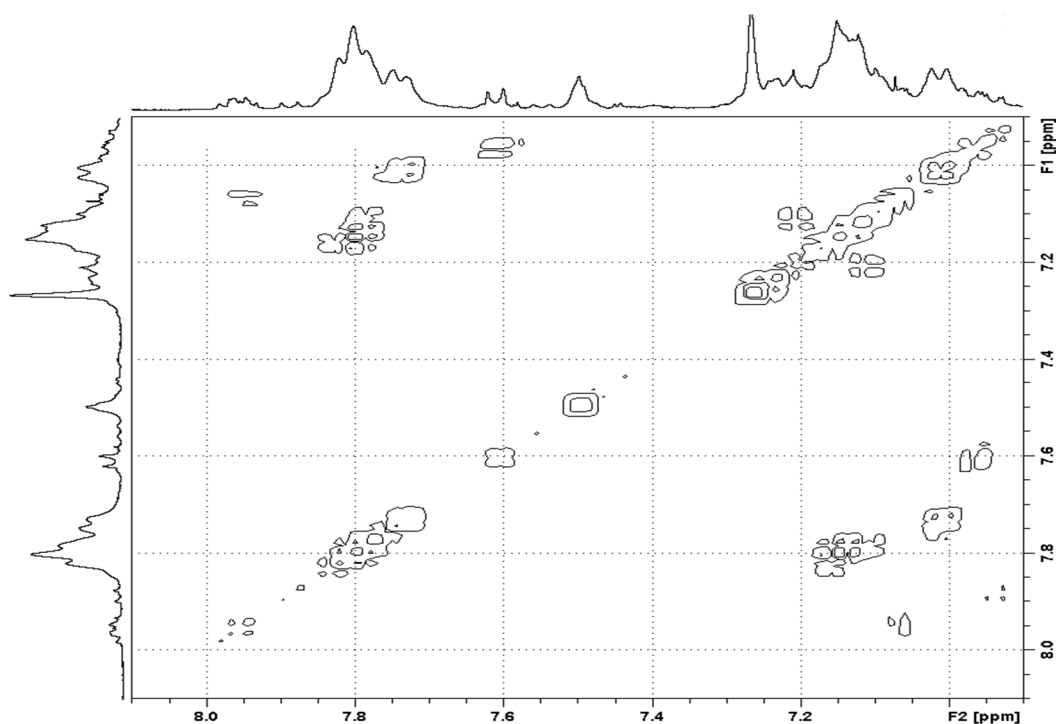
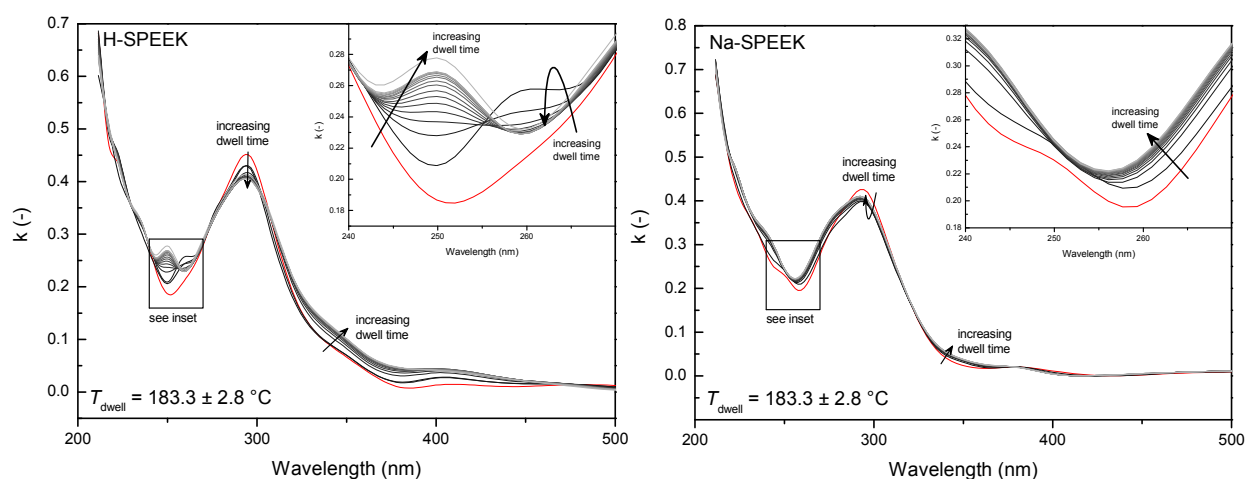


**Figure 4-S3**  $^1\text{H}$  COSY spectrum in  $\text{DMSO-d}_6$  at 400 MHz of H-SPEEK treated at 190 °C for 15 hours. The chemical shift is not locked to the solvent peak.

## Absorption spectra H-SPEEK and Na-SPEEK

In addition to the spectra already given in the manuscript, the spectra in the Figures 4-S4 – 4-S6 show the changes in the absorption of H-SPEEK and Na-SPEEK upon prolonged exposure to different temperatures between 180 and 250 °C.

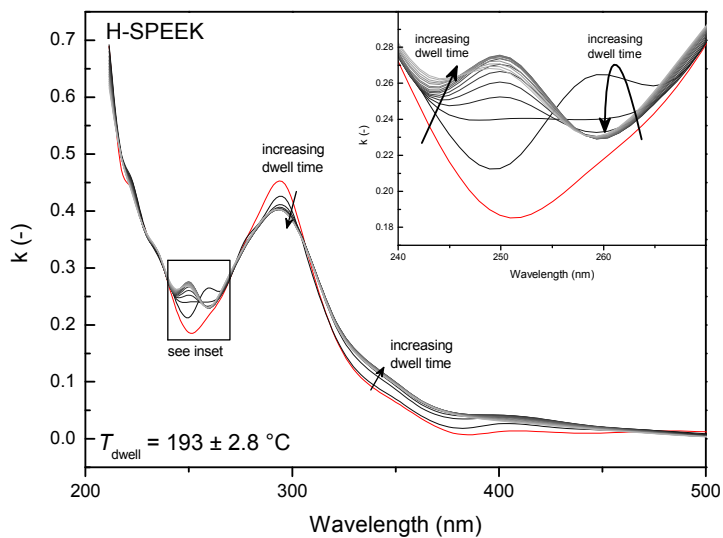
Figure 4-S4 shows that the changes in H-SPEEK follow the same trend for treatment at 163.8 and 183.3 °C. For the 183.3 °C treatment, the changes in the absorption peaks at ~250 nm is stronger, and a significant absorption peak develops over the course of a 15 hour treatment. For Na-SPEEK treated at the same temperatures, only minor changes are recorded.



**Figure 4-S4** The absorption spectrum of H-SPEEK (left) and Na-SPEEK (right) under nitrogen before thermal treatment (red) and after 0 (black) to 15 hours (light grey) of dwell at  $183.3 \pm 2.8$  °C. The change between the untreated and the 0 hour dwell samples is induced by the heating ramp.

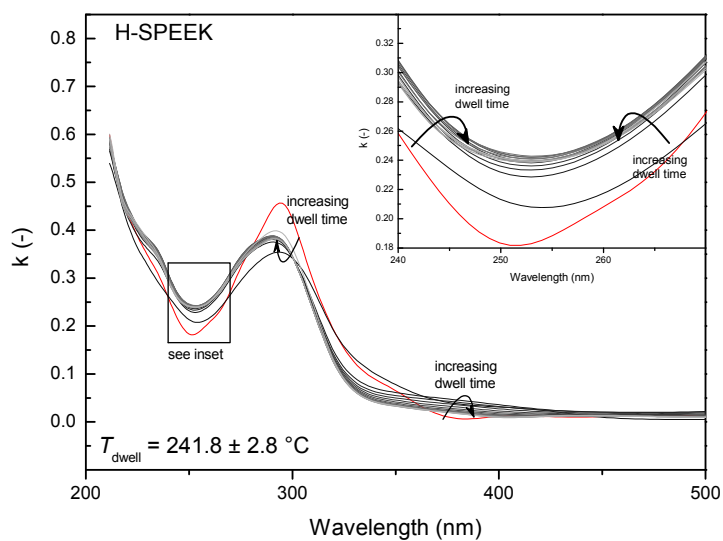


Figure 4-S5 shows that the changes in H-SPEEK at 193 °C are in line with those obtained at 183.3 °C. No significant differences are seen between the spectra.



**Figure 4-S5** The absorption spectrum of H-SPEEK under nitrogen before thermal treatment (red) and after 0 (black) to 15 hours (light grey) of dwell at  $193 \pm 2.8$  °C. The change between the untreated and the 0 hour dwell samples is induced by the heating ramp.

In addition to the figures in the manuscript, Figure 4-S6 substantiates the pronounced differences in the absorption spectra of H-SPEEK when heating to temperatures higher than 210 °C.



**Figure 4-S6** The absorption spectrum of H-SPEEK under nitrogen before thermal treatment (red) and after 0 (black) to 15 hours (light grey) of dwell at  $241.8 \pm 2.8 \text{ }^\circ\text{C}$ . The change between the untreated and the 0 hour dwell samples is induced by the heating ramp.

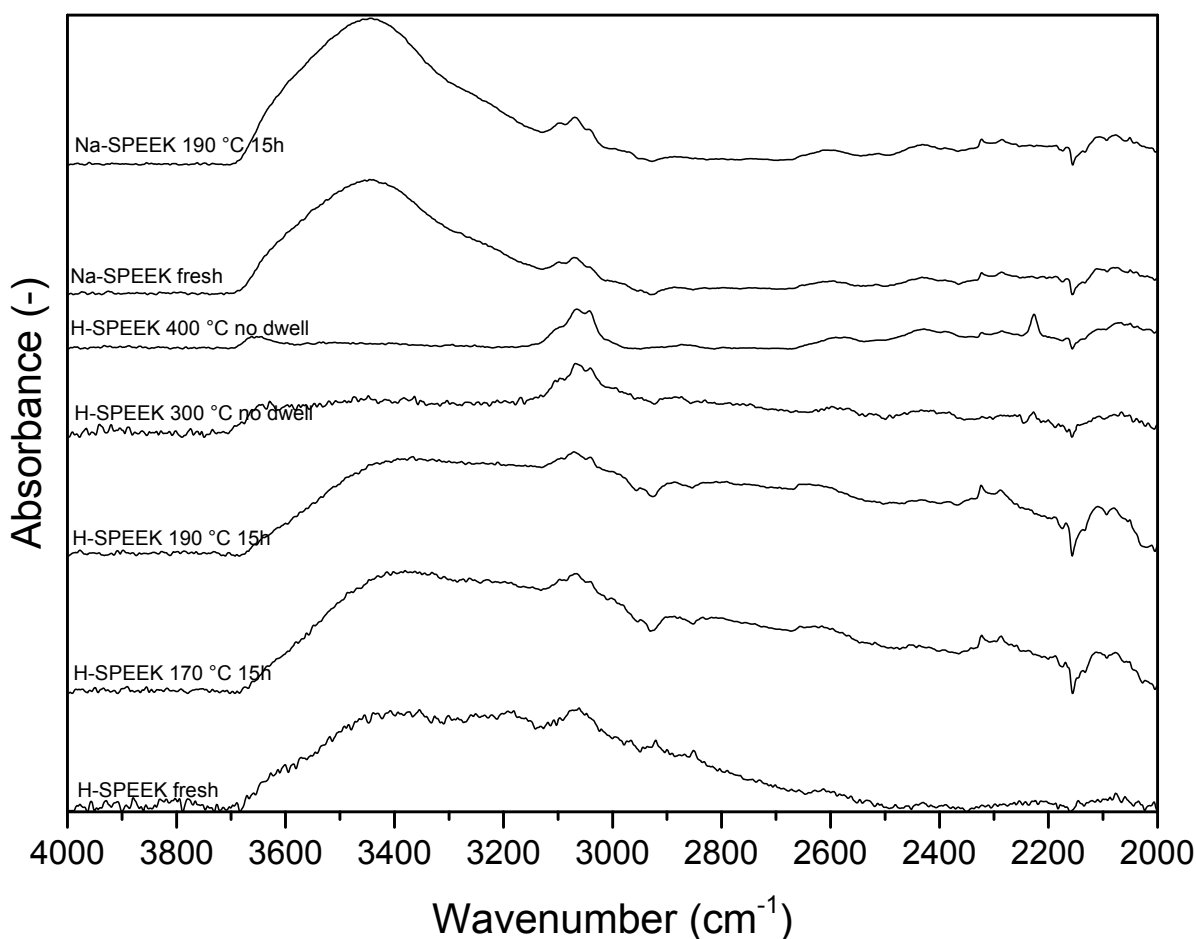
## Infrared band assignment

Table 4-S1 gives the infrared band assignment, based on general infrared bands in Pretsch et al.<sup>1</sup>, supplemented with characteristic peaks for SPEEK from Xing et al.<sup>2</sup> and Maranesi et al.<sup>3</sup>

**Table 4-S1:** Infrared band assignment for fresh SPEEK.

| Wavenumber<br>(intensity) | Group                                      | Extra information                                  |
|---------------------------|--|--|
| 3600-3200 (s, broad)      | -OH  | Stretching of O-H in water and/or acid             |
| 3100-3020                 | =C-H                                       | Stretching of aromatic hydrogens                   |
| 1644 (m)                  | C=O  | Symmetric stretching                               |
| 1595 (s)                  | Phenyl                                     | Skeletal in-plane <sup>3</sup>                     |
| 1490 (s)                  | Phenyl                                     | Skeletal in-plane <sup>2,3</sup>                   |
| 1472 (s)                  | Phenyl                                     | Skeletal in-plane <sup>3</sup>                     |
| 1416-1400 (m)             | Phenyl                                     | Symmetric stretching aromatic C-C <sup>3</sup>     |
| 1308 (m)*                 |  |  |
| 1281 (w, shoulder)*       |  | 1,2,4-substituted phenyl <sup>3</sup>              |
| 1251 (s)*                 |  | SO <sub>3</sub> H <sup>2,3</sup>                   |
| 1220 (s)*                 |  | 1,2,4-substituted <sup>2,3</sup>                   |
| 1186 (s)*                 |  |  |
| 1158 (s)*                 |  | Assigned to Ph-SO <sub>2</sub> -Ph in <sup>3</sup> |
| 1078 (m)                  | O=S=O                                      | In SO <sub>3</sub> H, Stretching <sup>2,3</sup>    |
| 1020-1005 (m)             | SO <sub>3</sub> H                          | Bending <sup>2,3</sup>                             |
| 955 (w)                   |  |  |
| 928 (s)                   |  | Most likely C-H or C-O-C                           |
| 863 (s)                   |  | Most likely C-H or C-O-C                           |
| 839 (m)                   |  | Most likely S-O (affected by Na-exchange)          |
| 767 (m)                   | All: Possibly ar C-H<br>δ, C-O-C γ, S-O st | Most likely C-H or C-O-C                           |
| 708 (w)                   |  |  |
| 682 (w)                   |  | Most likely S-O (affected by Na-exchange)          |

\* Strong overlap between the peaks, possibly all present in PEEK,<sup>2</sup> and therefore most likely vibrations in the phenyl rings and ether group. Because changes in these peaks are difficult to follow because of the strong overlap, specific assignment is difficult and could be inaccurate. Therefore, these peaks have not been assigned. Previously made assignments are given in the last column.



**Figure 4-S7** ATR-FTIR spectra of H-SPEEK and Na-SPEEK treated at different temperatures, in the wavenumber range of 4000-2000.

#### References

- (1) Pretsch, E.; Bühlmann, P.; Badertscher, M. *Structure Determination of Organic Compounds. Tables of Spectral Data.*; 4th, revis.; Springer: Heidelberg, 2009.
- (2) Xing, P.; Robertson, G. P.; Guiver, M. D.; Mikhailenko, S. D.; Wang, K.; Kaliaguine, S. *J. Membr. Sci.* **2004**, *229*, 95–106.
- (3) Maranesi, B.; Hou, H.; Polini, R.; Sgreccia, E.; Alberti, G.; Narducci, R.; Knauth, P.; Di Vona, M. L. *Fuel Cells* **2013**, *13*, 107–117.

### Detection of evolved SO<sub>2</sub> by ICP-AES

To determine whether the detected chemical changes in the H-SPEEK structure are the result of a reaction by the sulfonic acid groups, the amount of SO<sub>x</sub> in the gases that evolve during heating was measured. Gaseous products that were released during isothermal treatment of H-SPEEK at 183 °C were absorbed in water. ICP-AES was used to analyse the sulfur content in the water. Measurements were performed on a ICPE-9000 (Shimadzu). Samples were analyzed in triplicate and in axial direction.

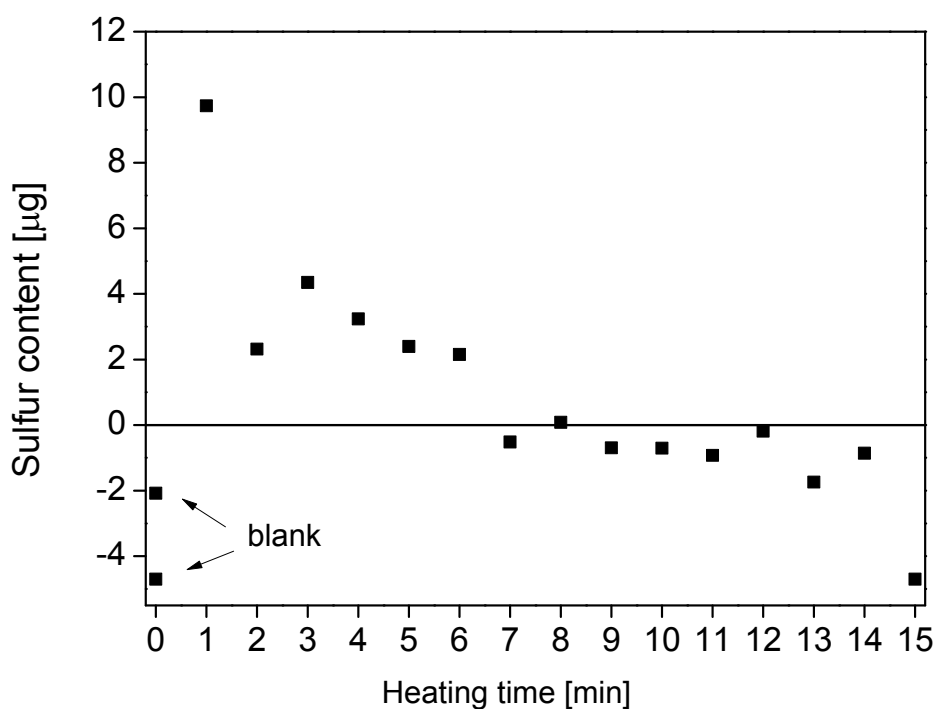


**Figure 4-S8** Overview of the evolved SO<sub>2</sub> per hour of the experiment as determined by ICP-AES at 183 °C.





# Chapter 5

Modification of thin sulfonated  
poly(ether ether ketone) films  
using ethylene glycol and glycerol



## **Abstract**

Chemical modification of thin films of sulfonated poly(ether ether ketone) (SPEEK) using polyols (i.e. ethylene glycol and glycerol), is investigated using spectroscopic ellipsometry. For a glycerol/SPEEK molar ratio  $>1$ , temperature treatment at 140 °C for 48 h induces structural changes and plasticization of the SPEEK films. The plasticization is evident from a depression in the glass transition temperature and a reduction in the optical anisotropy. When ethylene glycol is used instead of glycerol, less pronounced changes in the film properties are observed. After the chemical modification, the films are less susceptible to water-induced swelling, and no longer exhibit overshoot swelling dynamics. This reduced tendency to take up water is attributed predominantly to the reduced number of sulfonic acid groups, due to their reactions with the polyols.

## 5.1 Introduction

Reinforcement of membranes derived from sulfonated poly(ether ether ketone) (SPEEK) has been studied since decades [1-5]. SPEEK membranes have distinctive properties that can be beneficial in, for instance, fuel cells, redox flow batteries, and dehydration applications [6-10]. In these applications, SPEEK membranes are to be exposed to water or organic solvents, frequently at elevated temperatures. Strategies are required to moderate the extensive swelling that SPEEK membranes can exhibit under such conditions. Swelling generally has negative effects on membrane processes, because it deteriorates the mechanical stability and selectivity of the membranes.

The attentiveness for SPEEK membranes with moderated swelling tendency is evident from the fact that nowadays, great majority of research is concerned with modified materials compared to the number of articles devoted to pure SPEEK. Researchers, who have recently investigated the performance of pure SPEEK membranes in liquids, such as Winardi et al. [11], have also concluded that the swelling of the SPEEK is detrimental for membranes and hence, membrane strengthening is needed [11].

Numerous articles present a variety of methods to perform membrane reinforcement. Hou et al. have reviewed the methods to chemically modify membranes derived from sulfonated polymers [12]. Chemical modification includes formation of covalent and ionic bonds. Formation of covalent bonds can, for instance, be activated thermally [13] or by radiation [14, 15]. Ionic bonds can be formed when the acidic sulfonated polymers are mixed with basic (aminated) polymers [2]. Besides via chemical modification, the stability of SPEEK has been reported to improve after blending with other polymers, such as polytetrafluoroethylene [16], poly(vinylidene fluoride) [17], polysulfone [18], poly(ether sulfone) [19], sulfonated poly(ether sulfone) [20], sulfonated tetrafluoroethylene based fluoropolymer-copolymer (Nafion<sup>®</sup>) [21], sulphated poly(vinyl alcohol) [22], and the polyimide Matrimid<sup>®</sup> [23]. Furthermore, incorporation of various inorganic fillers in the SPEEK membrane matrix has been applied to improve mechanical stability of the membrane, thereby preventing excessive swelling. Some examples of the investigated fillers are: zirconium phosphate [24], zirconium oxide [25], titanium oxide [26], organically functionalized titanium oxide [27], silica additives [28] and sulfonated graphene oxide [29]. The enhancement of structural stability in SPEEK has also been accomplished in composite

SPEEK membranes by using a novel fusion technique for membrane formation [30]. This technique improved the compatibility between a selective SPEEK layer and a PMMA/PVDF substrate, resulting in suppressed swelling.

One of the chemical modification methods of SPEEK membranes is based on the thermally activated reaction of the polymer with aliphatic polyols, such as ethylene glycol and glycerol. This has been studied in detail by Mikhailenko et al. [31, 32], who have reported that the polyol molecules attach to the sulfonic acid groups and form oligomers that generate an interpenetrating network with the main SPEEK chains. [32]. SPEEK membranes modified with this method exhibited reduced swelling [32].

In the present study, we evaluate the chemical modification of thin supported SPEEK films with ethylene glycol and glycerol. The usage of ethylene glycol and glycerol is advantageous, because of the simple reaction procedure, activated at reasonably low temperatures of 130 – 150 °C [31]. Glycerol is also a non-toxic additive, commonly used in various processes [33]. In contrary to the previous studies, here anhydrous methanol is used as a casting solvent instead of an aqueous alcohol or acetone. The investigation of the properties and stability of thin supported films is of importance, as decreasing the membrane thickness to thin and ultra-thin films in composite hollow fiber membranes increases the permeance of species. Therefore, we study the effects of polyol content and temperature treatment on the structural modification of thin SPEEK films and the impact on swelling behavior. Measurements on unsupported SPEEK membranes are also conducted to verify the findings concerning thin films.

## 5.2 Experimental

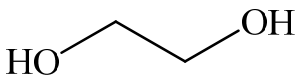
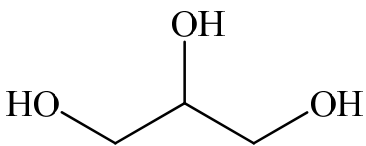
### 5.2.1 Materials

SPEEK with a degree of sulfonation (*DS*) of 84 % was obtained by sulfonation of PEEK using sulphuric acid [34]. Methanol (Emsure® grade of purity) and anhydrous glycerol were obtained from Merck (The Netherlands). Anhydrous ethylene glycol (99.8 %) was obtained from Sigma-Aldrich (The Netherlands). Milli-Q Advantage A10 system (Millipore) was used to produce deionized water of 18.2 MΩ·cm. Polished, <100> -oriented silicon wafers were obtained from Okmetic (Finland).

### 5.2.2 Sample preparation

Samples were formed from various 5 wt% SPEEK-methanol solutions: native SPEEK, SPEEK with the addition of ethylene glycol, EG (EG/SPEEK molar ratio: 0.5, 1, 2, 3 and 5) and with glycerol, GL (GL/SPEEK molar ratio: 0.5, 1, 2, 5 and 7). The chemical structure and physical properties of ethylene glycol and glycerol are shown in Table 5.1.

**Table 5.1** Properties of ethylene glycol and glycerol.

| Polyol               | Structure   | T <sub>b</sub><br>[°C] | M <sub>w</sub><br>[g·mol <sup>-1</sup> ] | Viscosity<br>[Pa·s] | Ref. |
|----------------------|---|------------------------|--|---------------------|------|
| Ethylene Glycol (EG) |  | 198                    | 62                                       | 0.02 (20 °C)        | [35] |
| Glycerol (GL)        |  | 290                    | 92                                       | 1.5 (20 °C)         | [33] |

#### Thin SPEEK films coated on a silicon wafer

Films were formed by spin-coating using above described solutions onto pre-cut pieces of silicon wafers at 2000 rpm for 50 s under atmospheric conditions. All films were prepared in duplicate and were treated under vacuum for 48 hours: one part was treated at 30 °C and the second part at 140 °C. The thickness of the thin films varied between 300 – 450 nm.

### **Unsupported SPEEK membranes**

Membranes were formed from the same solutions as for the thin films, by pouring the solutions into petri dishes. All membranes were prepared in duplicate. After solvent evaporation under atmospheric conditions for 24 hours, membranes were treated under vacuum for 48 hours: one part was treated at 30 °C and the second part at 140 °C. Subsequently, membranes were detached from the petri dishes by immersion into deionized water and dried under vacuum at 30 °C for 48 hours. The thickness of the unsupported membranes varied between 20 – 60 µm.

### **5.2.3 Sample characterization**

#### **Differential scanning calorimetry (DSC)**

DSC was performed on a Perkin Elmer DSC 8000 to determine the glass transition temperatures of unsupported membranes. Approx. 3.5 mg of the sample was placed in an aluminum sample holder. The sample was held for 1 minute at 50 °C, heated subsequently till 240 °C at 80 °C/min and cooled down to 50 °C. The cycle was repeated twice. The data from the second heating cycle were used for determination of the glass transition temperature,  $T_g$ , which is defined as the midpoint of the heat capacity transition. 3 different samples of each membrane were measured and the average value was taken.

#### **Thermogravimetric analysis (TGA)**

TGA was performed on a Perkin Elmer DSC 4000 to determine the thermal decomposition behavior of unsupported membranes. Approx. 3.5 mg of the sample was placed in a small aluminum sample holder. The sample was held for 1 minute at 30 °C and heated subsequently till 900 °C at a heating rate of 20 °C/min under constant nitrogen flow of 20 mL/min.

#### **Spectroscopic ellipsometry (SE)**

SE was used to determine the thickness, the optical properties and the swelling behaviour in 40 °C water of thin SPEEK films coated on a silicon wafer. Details on how SE is applied to characterize the thin SPEEK films are described in our previous study [36]. Details concerning swelling experiments of thin SPEEK films are described in Chapter 3.

An Alfa SE spectroscopic ellipsometer (J.A. Woollam Co., Inc.) was used for sample measurements and the CompleteEase 4.64 software (J.A. Woollam Co., Inc.) was used for

spectroscopic data modelling. The size spot of the light beam was 2 mm and the angle of incidence was 70°. The swelling experiments in water were conducted using a custom-made, temperature-controlled 70 ml-volume glass cell [37]. The recording of the data started in the first half minute after immersion in water.

Data are represented by the swelling factor  $S_F(t)$ , defined as:

$$S_F(t) = \frac{d_{swollen}}{d_{initial}} \quad \text{Eq. 5.1}$$

Here,  $d_{swollen}$  is the film thickness in water at time  $t$  and  $d_{initial}$  is the initial film thickness measured *ex-situ* prior to the swelling experiment.

## 5.3 Results and discussion

SPEEK membranes, with and without polyols treated at 30 °C, all possess a similar yellowish color. After thermal treatment at 140 °C under vacuum, the color of the films that do not contain a polyol, does not alter. In contrast, the films containing polyols become brownish. This color change is consistent with previous studies [31, 38]. It has been reported that polyols are covalently bound to SPEEK [32, 38, 39] and the color change is indicative of the fact that this chemical modification have occurred.

Here, we further analyze the differences in properties between native SPEEK membranes and SPEEK membranes with various contents of ethylene glycol (EG) and glycerol (GL). Membranes with unbound polyols (the ones treated at 30 °C) serve as a reference for chemically modified membranes (treated at 140 °C).

### 5.3.1 DSC

Changes in the glass transition temperature,  $T_g$ , of polymeric membranes after their chemical modification can be indicative of structural changes. Upon membrane reinforcement caused by the formation of cross-links, the glass transition temperature increases, due to decreased polymer chain mobility. More flexible networks show a depression in the glass transition temperature compared to more rigid ones.

Figure 5.1 compares the  $T_g$  of the native and modified SPEEK membranes prepared. The  $T_g$  of the native membranes was  $\sim 215$  °C. Changes in  $T_g$  were only observed for GL-modified membranes treated at 140 °C, in which the GL/SPEEK molar ratio was  $>1$ . In those membranes, a depression in  $T_g$  to values of 162 – 175 °C occurred. For the rest of the samples, the  $T_g$  did not vary significantly.

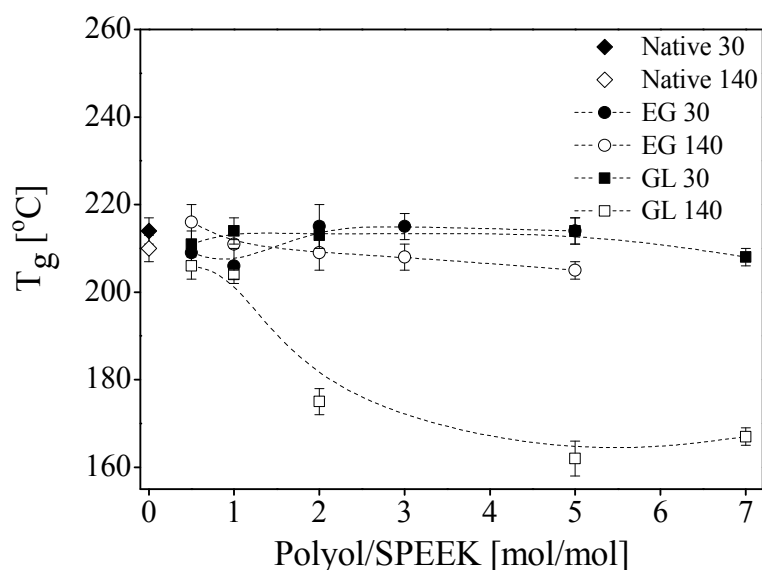
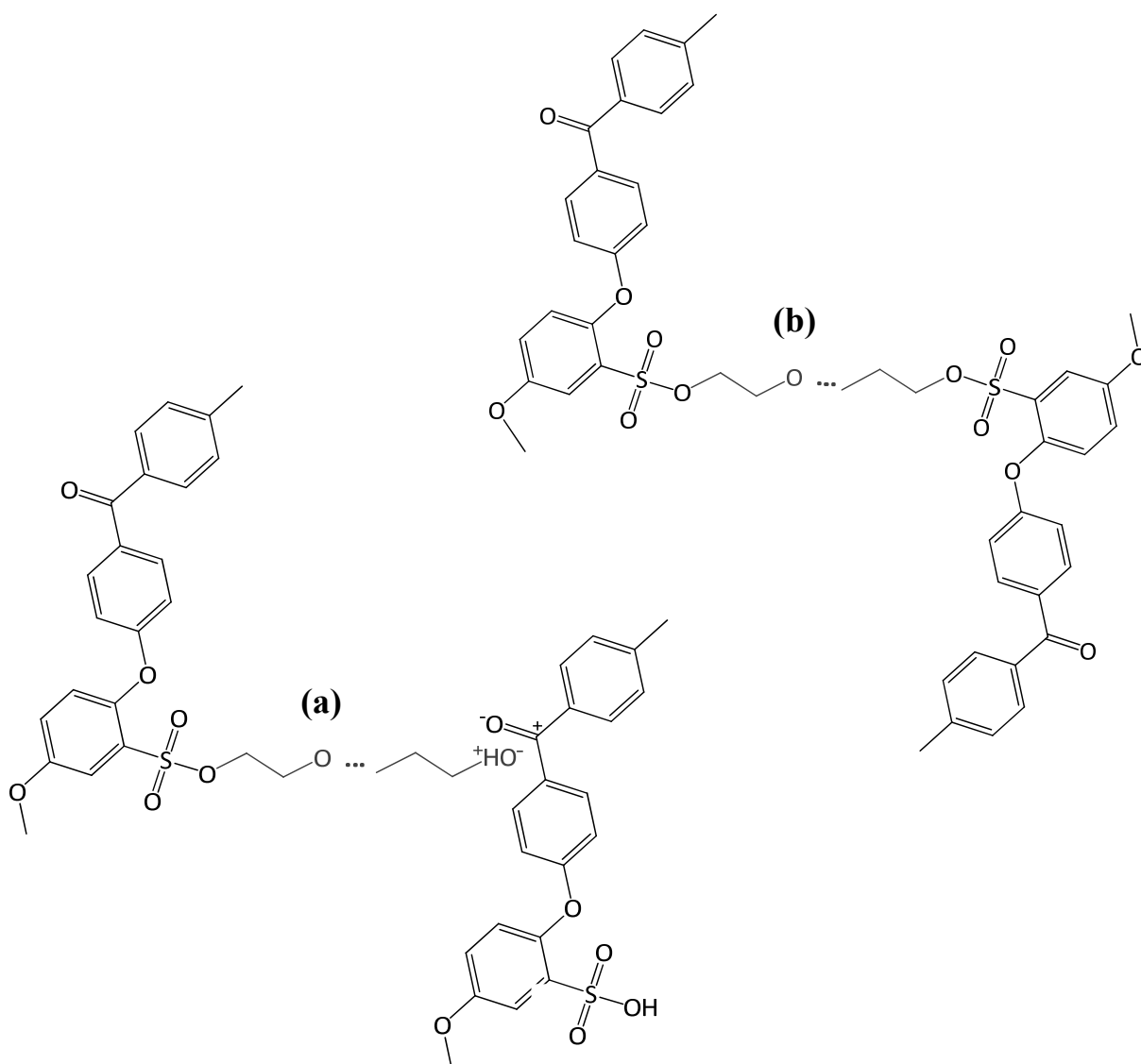


**Figure 5.1** Glass transition temperatures of native SPEEK membranes with a  $DS$  of 84 %, and ethylene glycol (EG)- and glycerol (GL)-modified ones, treated at 30 °C (closed symbols) or 140 °C (open symbols). The lines are added to guide the eye.

The absence of changes in  $T_g$  for the EG-modified membranes (EG-140) is in contrast to the study of Mikhailenko et al., in which SPEEK membranes with a similar degree of sulfonation and EG content, but formed from water/alcohol mixtures, showed a 15 °C increase in  $T_g$  in comparison to native membranes [32]. This  $T_g$  increase was attributed to the restrained chain mobility of SPEEK after grafting with EG. In more detail, as inferred by Mikhailenko et al. [32] and Gupta et al. [38], a polyol molecule attaches to SPEEK by a polyaddition reaction with the sulfonic acid groups and undergoes oligomerization that ultimately forms an interpenetrating network. Chains which are possibly terminated with the OH group, can interact with the ketone group of the other main chains (Scheme 5.1a) or can react with a second sulfonic acid group (Scheme 5.1b) [32]. Such long-chain networks reinforce the membrane matrix. Mikhailenko et al. termed this type of reinforcement using EG as ‘cross-linking by grafting’ [32]. In another study on the modification of resins using EG, a similar modification is referred to as ‘cross-linking by polyaddition reactions’ [40]. The corresponding interpenetrating networks are the reason for decreased polymer chain mobility and the increase of the glass transition temperature. In our samples, possibly due to the anhydrous conditions during membrane preparation, the formation of interpenetrating networks is different than when an aqueous solvent is used, and no effect on  $T_g$  is observed. This is in line with Mikhailenko et al. who have concluded (based on membrane stability experiments in various



organic solvents) that the final properties of modified SPEEK membranes and their degree of cross-linking, vary strongly with polyol and solvent used, which is caused by distinct solvent-polyol-sulfonic acid groups interactions influencing polyaddition reactions [31, 32]. The altered chemical structure of EG-modified membranes from our study will be nevertheless apparent from other measurements, as will be discussed later.



**Scheme 5.1** Schematic representation of the possible interpenetrating networks attached to SPEEK, which are formed from EG oligomers: (a) chains terminated with the OH group reacting with the ketone group of another main chain, (b) two main chains linked via sulfonic acid groups and EG oligomers [32, 37].

DSC studies on GL-modified membranes have not been presented elsewhere. An increased stability of GL-modified membranes in the previous study was concluded from the fact that the water uptake of those membranes was reduced [32]. The decreased  $T_g$  of the GL-modified membranes from our study (GL-140, Figure 5.1) indicates that the grafting reaction of glycerol molecules on sulfonic acid groups (in given formation conditions) results in the internal plasticization of SPEEK membranes. This outcome is not unexpected: GL is a highly flexible molecule that can form both intra- and intermolecular hydrogen bonds. This causes a high viscosity (see Table 5.1). GL is used as a plasticizer in many applications to induce flexibility [33].

The lack of plasticization effects in samples with unbound GL (GL-30) would be surprising since GL is a widely applied external plasticizer, used for instance to increase the flexibility of the sulfonated polystyrene [41]. Evidently, the DSC technique is not suitable to reveal the presence of unbound GL. Yet the plasticization of SPEEK, caused by unbound GL, will be visible from spectroscopic ellipsometry (SE) measurements, elaborated on later.

### 5.3.2 TGA

The thermal behavior of polymers can reveal differences in chemical structure between native and modified materials. Figure 5.2 shows the mass loss upon heating of the native SPEEK membranes and of the representative EG- and GL-modified ones treated at 140 °C with a polyol/SPEEK molar ratio of 5. The TGA data of membranes treated at 30 °C are not shown, because these do not deviate significantly from native ones.

A comprehensive analysis of the thermal decomposition of SPEEK with the same  $DS$  of 84 % has been discussed in more detail in Chapter 4. For conciseness, in this chapter only the relevant differences between native and chemically modified SPEEK membranes are discussed. The most relevant differences occur below ~ 400 °C. Above ~ 450 °C, all films exhibit a strong mass loss that can be associated with the degradation of aromatic compounds.

Below 200 °C, the mass loss is attributed to removal of physically sorbed water. A lower mass loss occurred at that range for the grafted membranes (EG-5-140 and GL-5-140) as compared to the native one. This is because grafted samples take up less water from the ambient, since they have less hydrophilic sulfonic acid groups than native samples. Furthermore, in native SPEEK, above 250 °C the release of CO<sub>2</sub> and SO<sub>2</sub> starts, as has been shown in Chapter 4. For the grafted samples, the onset of degradation is shifted towards lower temperatures, as visible in Figure 5.2. This is consistent with the observations of Mikhailenko et al. They determined, based on the TGA-MS measurements that the release of CO<sub>2</sub> and SO<sub>2</sub> takes place at lower temperatures as compared to the native SPEEK [32]. Additionally, the evolution of CO<sub>2</sub> in the grafted membranes has been detected at 50 °C earlier than that of SO<sub>2</sub> [32]. This indicates that the splitting of the sulfonic acid groups with attached polyols occurs easier as compared to pure sulfonic acid groups. Distinct susceptibility of EG and GL molecules to split upon heating could also explain their different thermal behavior (decomposition of GL shifted towards lower temperatures) between 250 and 400 °C, as shown in Figure 5.2.

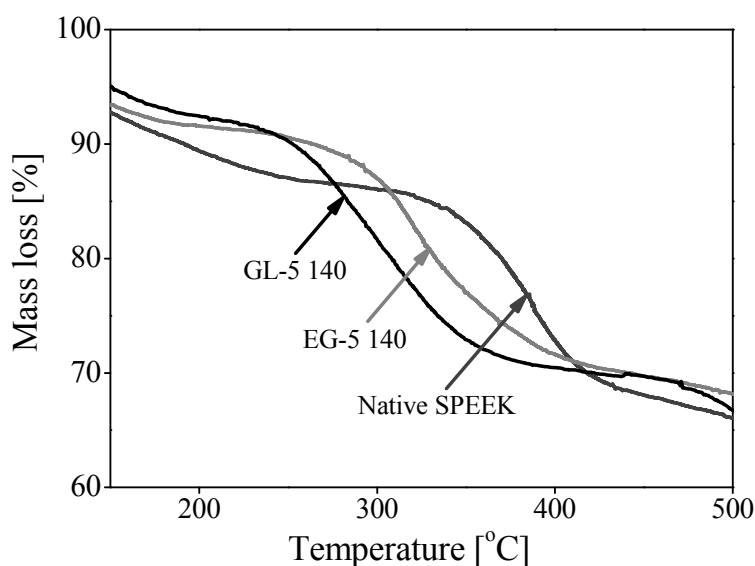


**Figure 5.2** Mass loss of the native SPEEK membrane and of the representative SPEEK membranes treated at 140 °C with a polyol/SPEEK molar ratio of 5.

### 5.3.3 Optical anisotropy

Changes in the optical anisotropy,  $\Delta n$ , in modified materials as compared to native ones can be a further indication of changes in chemical structure [42]. Optical anisotropy arises in oriented and stressed polymers. In SPEEK, optical anisotropy is affected by the presence of the sulfonic acid groups [36]. Sulfonic acid groups cause stiffness of SPEEK [38] and an increase in the glass transition temperature compared to PEEK [43]. Chemical modification is the method to induce internal plasticization of oriented and rigid materials [44], which can be visible from the reduced  $\Delta n$  value [42].

Figure 5.3 shows the  $\Delta n$  of the thin SPEEK films investigated in this research. The  $\Delta n$  values of the native films were  $\sim 0.028$ . Significant changes were observed in GL-modified films treated at 140 °C, in which the GL/SPEEK molar ratio was  $>1$ . In those films, a depression in  $\Delta n$  to values of 0.005 – 0.01 occurred. For the rest of the samples, the  $\Delta n$  values did not differ significantly. These results are consistent with our DSC measurements. Samples with significantly changed  $\Delta n$  correspond to samples having significantly affected  $T_g$ .

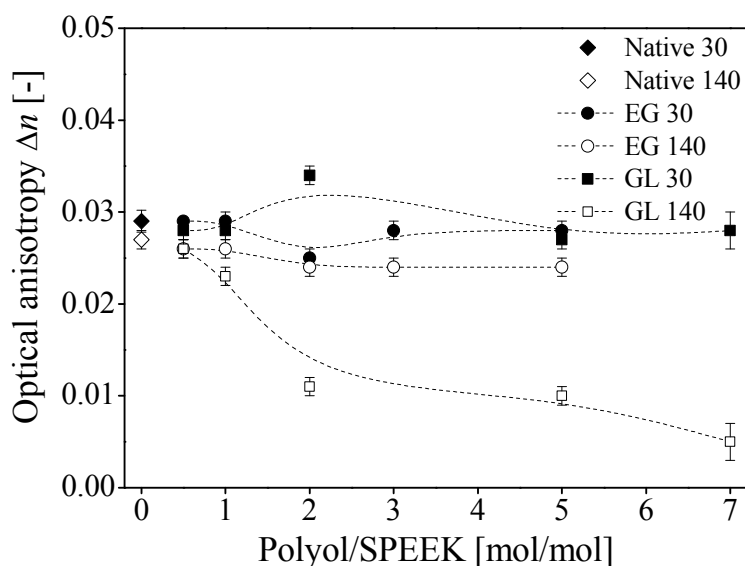


**Figure 5.3** Optical anisotropy of native thin SPEEK films ( $DS$  84 %) and ethylene glycol (EG)- and glycerol (GL)-modified ones, coated on a silicon wafer and treated at 30 °C (closed symbols) or 140 °C (open symbols). The average value is taken from two samples, each sample is measured at 4 different spots. The lines are added to guide the eye.

As mentioned before, plasticization of thin SPEEK films with unbound GL (GL-30) also occurs and is detectable using SE on samples that have been aged for a certain time. The  $\Delta n$  of samples which are measured directly after preparation procedure, is similar to that of native films (as shown in Figure 5.3), but it declines with time after diffusion of GL molecules and polymer relaxation.

Here, the swelling behavior of modified thin SPEEK films will be evaluated.

### 5.3.4 Swelling

#### *Short-exposure swelling*

Figure 5.4 shows the swelling dynamics for thin SPEEK films exposed to 40 °C water, recorded for 30 minutes. Due to a problem with the equipment alignment, only the swelling of grafted films was performed. The swelling behavior of native films with a  $DS$  of 84 % has been found to be more complex, as shown in our previous study (Chapter 3). Here, we will shortly discuss the most relevant findings in connection to the properties of the chemically modified films. Also, films treated at 30 °C cannot be exposed to water because of layer delamination. The treatment at 140 °C for 48 h allows adhesion of a SPEEK film to a substrate and prevents delamination upon contact with water.

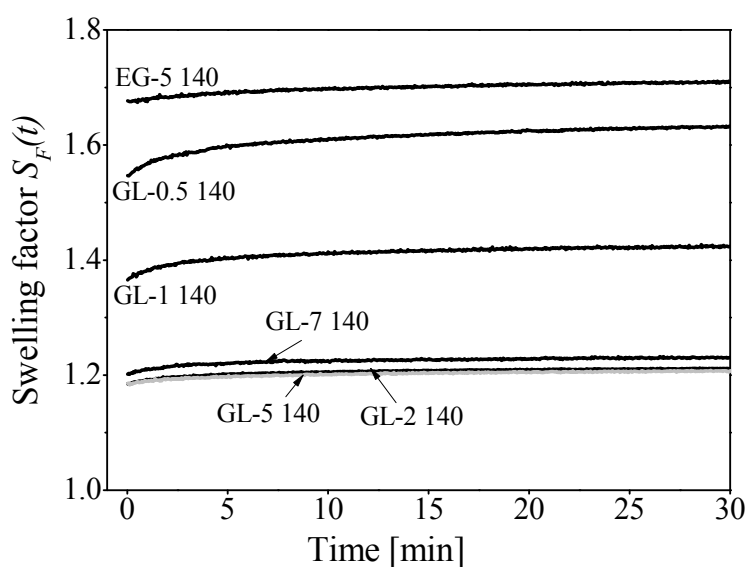


**Figure 5.4** Short-exposure time-dependent swelling at 40 °C water of thin SPEEK films.

The performed swelling experiments are sufficient to observe differences between various samples. The swelling factor is reduced for GL-140 samples as compared to the EG-5-140 sample. For GL-modified samples, a GL/SPEEK molar ratio of 2 is sufficient to cause the same swelling reduction as for a ratio of 7. Possibly, this is caused by the maximum occupation of the functional sulfonic acid groups at a molar ratio of 2. The swelling reduction is not caused by a structural reinforcement or cross-linking, since the GL-140 films exhibited decreased  $T_g$  as compared to the EG-5-140 sample. The reduced swelling and water uptake are caused by the chemical change at the cost of the sulfonic acid groups and consequential reduction of the affinity for water. Mikhailenko et al. also explained that for GL-modified membranes (no data on  $T_g$ ), the water uptake was less than for native samples, but the swelling was still high, which they attributed to incomplete cross-linking [32].

#### *Long-exposure swelling*

We assumed that the temperature treatment, next to the casting solvents, can be a factor impacting the grafting reaction of polyols. Therefore, a quick experiment was performed to verify this hypothesis. An additional EG-5 sample was prepared, which was treated under vacuum at 145 °C for 48 h, instead at 140 °C. To stay brief, a modification was initiated that in turn reduced the optical anisotropy in this sample to a value of  $\sim 0.01$ . The effect on  $T_g$  for this sample is not known. Figure 5.5 shows the long-time swelling behavior of the additionally synthesized EG-5-145, and a new sample, GL-3-140. Clearly, ethylene glycol and glycerol require different temperature treatment to cause significant structural changes in SPEEK, in order to reduce swelling. In Chapter 3, the minimum and maximum swelling factor recorded at 40 °C for two different native SPEEK films after 2000 min was  $\sim 1.7$  and 3.5, respectively. In Figure 5.5, the swelling factor is shown to be reduced to  $\sim 1.2$ -1.4. Within 4000 min, the slow polymer relaxation towards increasing film thickness occurs in both samples, due to the sorption of water and reorganization of the polymers chains, probably coupled with rinsing out of unbound polyols. Such swelling profile in these chemically modified films is different as compared to what is observed in native thin SPEEK films. The native films, prepared in an identical manner as in this study, exhibit overshoot swelling and negative relaxations after  $\sim 500$  min (Chapter 3).

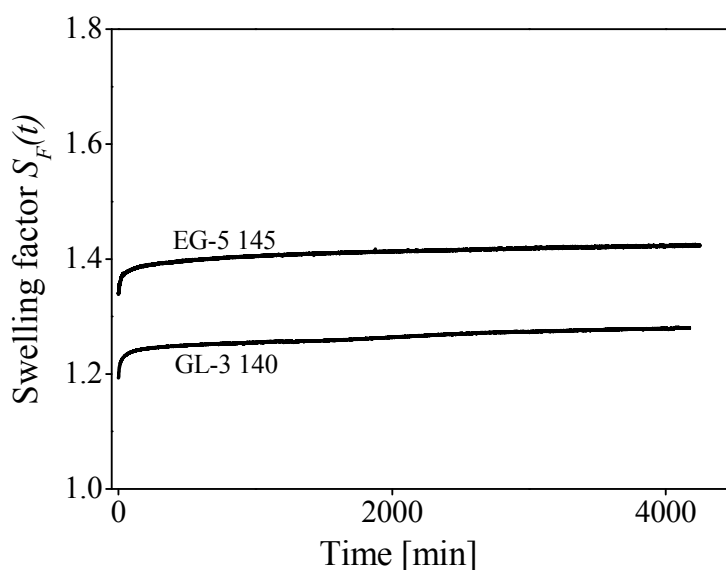


**Figure 5.5** Long-exposure time-dependent swelling at 40 °C water of additionally synthesized samples.

In the last years, we performed swelling experiments on several GL-modified films (GL/SPEEK molar ratio of 3) and found that the time dependent swelling factor at 40 °C water is reproducible (initial value of ~ 1.2 with slow positive relaxations). Thus, the swelling of those films can be controlled, in contrary to that of native thin SPEEK films. In native thin SPEEK films, due to various properties (described in Chapter 3), the swelling process is more complex, and it is impossible to correlate the exact swelling factor to the degree of sulfonation and/or water temperature only.

In summary, DSC, TGA and SE studies confirm changes in chemical structure of SPEEK films after introducing EG or GL. We show that with SE the property changes can be easily monitored and therefore, optimum conditions, such as polyol content and temperature treatment, and the effect on swelling performance can be adjusted.

## **5.4 Conclusions**

Swelling reduction of chemically modified thin SPEEK films has been investigated with spectroscopic ellipsometry. Chemical modification by grafting on functional sulfonic acid groups in SPEEK has been accomplished using polyols (i.e. ethylene glycol and glycerol). Ethylene glycol and glycerol require different temperatures to initiate a grafting reaction that causes significant structural changes, and consequently, reduction of swelling. Thin films with the lowest swelling factor exhibited a depression in the glass transition temperature. This indicates that the mechanism to reduce swelling, accomplished in our study, is chemical modification at the cost of sulfonic acid groups (reducing the affinity for water) rather than the chemical reinforcement by cross-linking or extended grafting.

## **Acknowledgements**

This work was performed in the cooperation framework of Wetsus, centre of excellence for sustainable water technology ([www.wetusus.nl](http://www.wetusus.nl)). Wetsus is co-funded by the Dutch Ministry of Economic Affairs and Ministry of Infrastructure and Environment, the European Union Regional Development Fund, the Province of Fryslân, and the Northern Netherlands Provinces. The authors would like to thank the participants of the research theme “Dehydration” for the fruitful discussions and their financial support.



## References

1. Walker, M., et al., *Proton-conducting polymers with reduced methanol permeation*. Journal of Applied Polymer Science, 1999. **74**(1): p. 67-73.
2. Li, W., et al., *Blend membranes consisting of sulfonated poly(ether ether ketone) and polysulfone bearing 4-nitrobenzimidazole for direct methanol fuel cells*. Journal of the Electrochemical Society, 2009. **156**(2): p. B258-B263.
3. Mikhailenko, S.D., S.M.J. Zaidi, and S. Kaliaguine, *Electrical properties of sulfonated polyether ether ketone/polyetherimide blend membranes doped with inorganic acids*. Journal of Polymer Science Part B: Polymer Physics, 2000. **38**(10): p. 1386-1395.
4. Kerres, J., et al., *Synthesis and characterization of novel acid-base polymer blends for application in membrane fuel cells*. Solid State Ionics, 1999. **125**(1-4): p. 243-249.
5. Rangasamy, V.S., et al., *Preparation and characterization of composite membranes based on sulfonated PEEK and AlPO<sub>4</sub> for PEMFCs*. Solid State Ionics, 2012. **216**: p. 83-89.
6. Sijbesma, H., et al., *Flue gas dehydration using polymer membranes*. Journal of Membrane Science, 2008. **313**(1-2): p. 263-276.
7. Kreuer, K.D., *Ion conducting membranes for fuel cells and other electrochemical devices*. Chemistry of Materials, 2014. **26**(1): p. 361-380.
8. Gómez, P., et al., *Comparative behaviour of hydrophilic membranes in the pervaporative dehydration of cyclohexane*. Journal of Membrane Science, 2006. **279**(1-2): p. 635-644.
9. Jia, L., et al., *Sulfonation of polyetheretherketone and its effects on permeation behavior to nitrogen and water vapor*. Journal of Applied Polymer Science, 1996. **60**(8): p. 1231-1237.
10. Roelofs, K.S., et al., *Behavior of sulfonated poly(ether ether ketone) in ethanol-water systems*. Journal of Applied Polymer Science, 2009. **111**(6): p. 2998-3009.
11. Winardi, S., et al., *Sulfonated poly(ether ether ketone)-based proton exchange membranes for vanadium redox battery applications*. Journal of Membrane Science, 2014. **450**: p. 313-322.
12. Hou, H., M.L. Di Vona, and P. Knauth, *Building bridges: Crosslinking of sulfonated aromatic polymers—A review*. Journal of Membrane Science, 2012. **423-424**: p. 113-127.
13. Hande, V.R., et al., *Crosslinking of sulphonated poly(ether ether ketone) using aromatic bis(hydroxymethyl) compound*. Journal of Membrane Science, 2008. **322**(1): p. 67-73.
14. Zhong, S., C. Liu, and H. Na, *Preparation and properties of UV irradiation-induced crosslinked sulfonated poly(ether ether ketone) proton exchange membranes*. Journal of Membrane Science, 2009. **326**(2): p. 400-407.
15. Song, J.-M., et al., *The effects of EB-irradiation doses on the properties of crosslinked SPEEK membranes*. Journal of Membrane Science, 2013. **430**: p. 87-95.
16. Bi, C., et al., *Hydrophilic treatment poly(tetrafluoroethylene) reinforced sulfonated poly(ether ether ketone) composite membrane for proton exchange membrane fuel cell application*. Journal of Power Sources, 2009. **194**(2): p. 838-842.
17. Sung, K.A., et al., *Stability enhancement of polymer electrolyte membrane fuel cells based on a sulfonated poly(ether ether ketone)/poly(vinylidene fluoride) composite membrane*. Journal of Power Sources, 2011. **196**(5): p. 2483-2489.
18. Richard Bowen, W., T.A. Doneva, and H.B. Yin, *Polysulfone - Sulfonated poly(ether ether) ketone blend membranes: Systematic synthesis and characterisation*. Journal of Membrane Science, 2001. **181**(2): p. 253-263.

19. Manea, C. and M. Mulder, *Characterization of polymer blends of polyethersulfone/sulfonated polysulfone and polyethersulfone/sulfonated polyetheretherketone for direct methanol fuel cell applications*. Journal of Membrane Science, 2002. **206**(1-2): p. 443-453.
20. Ling, X., et al., *Preparation and characterization of sulfonated poly(ether sulfone)/sulfonated poly(ether ether ketone) blend membrane for vanadium redox flow battery*. Journal of Membrane Science, 2012. **415–416**: p. 306-312.
21. Luo, Q., et al., *Preparation and characterization of Nafion/SPEEK layered composite membrane and its application in vanadium redox flow battery*. Journal of Membrane Science, 2008. **325**(2): p. 553-558.
22. Yang, T., *Composite membrane of sulfonated poly(ether ether ketone) and sulfated poly(vinyl alcohol) for use in direct methanol fuel cells*. Journal of Membrane Science, 2009. **342**(1-2): p. 221-226.
23. Khan, A.L., X. Li, and I.F.J. Vankelecom, *SPEEK/Matrimid blend membranes for CO2 separation*. Journal of Membrane Science, 2011. **380**(1-2): p. 55-62.
24. Silva, V.S., et al., *Performance and efficiency of a DMFC using non-fluorinated composite membranes operating at low/medium temperatures*. Journal of Power Sources, 2005. **145**(2): p. 485-494.
25. Silva, V.S., et al., *Proton electrolyte membrane properties and direct methanol fuel cell performance: I. Characterization of hybrid sulfonated poly(ether ether ketone)/zirconium oxide membranes*. Journal of Power Sources, 2005. **140**(1): p. 34-40.
26. Zhao, S., et al., *Electric field processing to control the structure of titanium oxide/sulfonated poly(ether ether ketone) hybrid proton exchange membranes*. Journal of Membrane Science, 2013. **437**: p. 65-71.
27. Di Vona, M.L., et al., *Composite polymer electrolytes of sulfonated poly-ether-etherketone (SPEEK) with organically functionalized TiO2*. Journal of Membrane Science, 2011. **369**(1-2): p. 536-544.
28. Sambandam, S. and V. Ramani, *SPEEK/functionalized silica composite membranes for polymer electrolyte fuel cells*. Journal of Power Sources, 2007. **170**(2): p. 259-267.
29. Heo, Y., H. Im, and J. Kim, *The effect of sulfonated graphene oxide on Sulfonated Poly(Ether Ether Ketone) membrane for direct methanol fuel cells*. Journal of Membrane Science, 2013. **425–426**: p. 11-22.
30. Shao, P., et al., *Composite membranes with an integrated skin layer: preparation, structural characteristics and pervaporation performance*. Journal of Membrane Science, 2005. **254**(1-2): p. 1-11.
31. Mikhailenko, S.D., et al., *Proton conducting membranes based on cross-linked sulfonated poly(ether ether ketone) (SPEEK)*. Journal of Membrane Science, 2004. **233**(1-2): p. 93-99.
32. Mikhailenko, S.D., et al., *Properties of PEMs based on cross-linked sulfonated poly(ether ether ketone)*. Journal of Membrane Science, 2006. **285**(1-2): p. 306-316.
33. Pagliaro, M. and M. Rossi, *The Future of Glycerol*. 2nd ed. 2010: Royal Society of Chemistry
34. Shibuya, N. and R.S. Porter, *Kinetics of PEEK sulfonation in concentrated sulfuric acid*. Macromolecules, 1992. **25**(24): p. 6495-6499.
35. Yue, H., et al., *Ethylene glycol: properties, synthesis, and applications*. Chemical Society Reviews, 2012. **41**(11): p. 4218-4244.
36. Koziara, B.T., K. Nijmeijer, and N.E. Benes, *Optical anisotropy, molecular orientations, and internal stresses in thin sulfonated poly(ether ether ketone) films*. Journal of Materials Science, 2015. **50**(8): p. 3031-3040.

37. Ogieglo, W., et al., *Temperature-induced transition of the diffusion mechanism of n-hexane in ultra-thin polystyrene films, resolved by in-situ Spectroscopic Ellipsometry*. Polymer (United Kingdom), 2013. **54**(1): p. 341-348.
38. Gupta, D. and V. Choudhary, *Studies on novel heat treated sulfonated poly(ether ether ketone) [SPEEK]/diol membranes for fuel cell applications*. International Journal of Hydrogen Energy, 2011. **36**(14): p. 8525-8535.
39. Gupta, D. and V. Choudhary, *Sulfonated poly(ether ether ketone)/ethylene glycol/polyhedral oligosilsesquioxane hybrid membranes for fuel cell applications*. International Journal of Hydrogen Energy, 2012. **37**(7): p. 5979-5991.
40. Kiguchi, T., H. Aota, and A. Matsumoto, *Crosslinking polymerization leading to interpenetrating polymer network formation. I. Polyaddition crosslinking reactions of poly(methyl methacrylate-co-2-methacryloyloxyethyl isocyanate)s with ethylene glycol resulting in polyurethane networks*. Journal of Polymer Science Part A: Polymer Chemistry, 2003. **41**(4): p. 606-615.
41. Lundberg, R.D., H.S. Makowski, and L. Westerman, *DUAL PLASTICIZATION OF SULFONATED POLYSTYRENE IONOMER*. Pap presented at the Natl Meet, 176th, 1978. **19**(2): p. 310-313.
42. Zhang, Z., et al., *Novel approach to reducing stress-caused birefringence in polymers*. Journal of Materials Science, 2004. **39**(4): p. 1415-1417.
43. Reyna-Valencia, A., S. Kaliaguine, and M. Bousmina, *Tensile mechanical properties of sulfonated poly(Ether Ether Ketone) (SPEEK) and BPO4/SPEEK membranes*. Journal of Applied Polymer Science, 2005. **98**(6): p. 2380-2393.
44. Cadogan, D.F. and C.J. Howick, *Plasticizers*, in *Kirk-Othmer Encyclopedia of Chemical Technology*. 2000, John Wiley & Sons, Inc.





# Chapter 6

## Dehydration of supercritical carbon dioxide using hollow fiber membranes: simulations in Aspen Plus<sup>®</sup> and economic evaluation

This chapter is an extension of the paper:

Lohaus, T.; Scholz, M.; Koziara, B.T.; Benes, N.E.; Wessling, M., *Drying of supercritical carbon dioxide with membrane processes*. The Journal of Supercritical Fluids **2015**, 98, 137-146.

## Abstract

Dehydration of supercritical carbon dioxide using hollow fibers has been simulated in Aspen Plus<sup>®</sup>, and an economic evaluation has been performed. High energy consuming adsorption by zeolites is currently used to perform the dehydration process. Membrane technology can be a promising alternative. In this membrane process of supercritical carbon dioxide dehydration, carbon dioxide has been also used as a sweep gas. Two types of systems have been investigated: 1) simple systems with a single membrane unit, in which carbon dioxide is released to the atmosphere; 2) hybrid systems with two membrane units, in which the permeate stream is partially recirculated. The flow rate and the pressure of a sweep gas determine the effectiveness of water removal from the permeate side. More effective sweeping results in lower required membrane surface area. In a small pilot plant (feed of 2,000 kg/h) and at certain conditions, simple systems can be more beneficial than hybrid systems. For a larger scale process (feed of 100,000 kg/h), high emissions of carbon dioxide make the hybrid systems a favorable option. High water permeance (250,000 GPU), and consequently, low required membrane surface area, can reduce the annual costs by 20 %. Still, the need for carbon dioxide recirculation causes that the main costs come from compressors used in the recirculation lines.

## 6.1 Introduction

Supercritical fluids (SCF) find applications in many technological processes [1, 2]. For several reasons, carbon dioxide (scCO<sub>2</sub>) is the predominant SCF. Carbon dioxide is non-toxic and can replace hazardous organic solvents. Its easily accessible critical point (73.8 bar, 31.1 °C), low price, non-toxicity, and large scale production, all together make applications attractive [3]. Successfully commercialized applications include extraction processes [4], processing of polymers [5] and textile dyeing [6]. The most common are extractions implemented in the food industry, such as decaffeination of coffee and tea, recovery of flavors, fragrances and essential oils from natural sources [7].

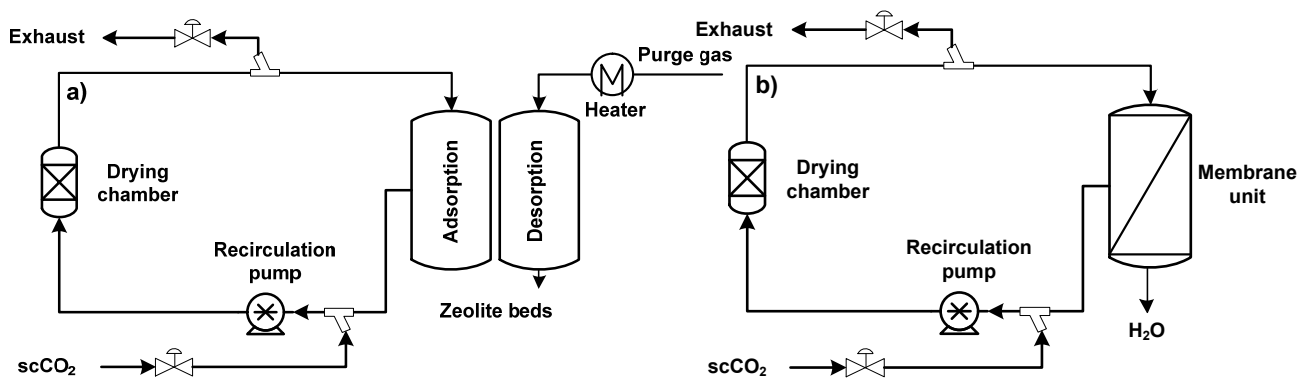
The high demand for the recovery of scCO<sub>2</sub> after extractions has made membrane technology a potential regeneration technique. Membrane processes can be more energy efficient compared to other separation methods, such as pressure swing, adsorption or absorption [8]. Several studies have investigated the separation of carbon dioxide from the extracts, and permeation behavior of high pressure and supercritical carbon dioxide through various membrane materials has been studied. For instance, Chiu et al. studied a caffeine rejection using nanofiltration and polycarbonate membranes [9]. Sarmiento et al. studied the retention of essential oils using commercial reverse osmosis membranes [10]. Semenova et al. studied the separation of ethanol from scCO<sub>2</sub> using polyimide Kapton® membranes [11]. Patil et al. studied the permeation of sub and supercritical CO<sub>2</sub> using polyvinyl alcohol (PVA) and polyamide copolymer (PA) membranes, and considered the effect of cross-linking on membrane stability [12]. Verkerk et al. studied permeation of sub and supercritical carbon dioxide through microporous silica membranes [13].

Another industrially important process, which implements scCO<sub>2</sub>, is the extraction of water [1, 14]. Extraction of water, or drying, is applied in the food industry as the alternative for hot air drying and freeze drying. The last two techniques possess various disadvantages. Hot air drying can damage the microstructure of sensitive products and can cause the loss of nutrients [15]. Freeze drying is suitable for sensitive products, but requires long drying times and high energy consumption [16]. Supercritical carbon dioxide is intended for drying of sensitive products; due to the low surface tension, no capillary stresses are induced in the food structure [17].



Currently, the regeneration of carbon dioxide used in a drying process is performed by adsorption of water on zeolites [18]. However, in a continuous drying process, shown in Scheme 6.1a, such an approach is undesired. Premature saturation of zeolites might occur before the food in a drying chamber is sufficiently dried. A premature saturation of zeolites forces a premature depressurization of the recirculation system. Additionally, regeneration of the zeolites is energy demanding, since it is performed by heating to high temperatures to supply the required high enthalpy of desorption. Temperatures up to 600 °C are required to completely restore the adsorption capacity of the zeolites [19]. Therefore, regeneration of  $\text{scCO}_2$  via membrane technology is a promising method. This process is shown in Scheme 6.1b.

The separation of carbon dioxide and water can be performed using highly water selective membranes. Membranes derived from the glassy polymer, sulfonated poly(ether ether ketone) (SPEEK), are considered to be appropriate for this application. SPEEK membranes have already been tested in a low pressure gas dehydration processes by Sijbesma et al. [20] and Liu et al. [21]. Their experiments showed excellent selectivity for water over gases (nitrogen, carbon dioxide) and high water permeance. Experimental data concerning high pressure dehydration performance have not been yet reported in the literature.



**Scheme 6.1** Food drying process using supercritical carbon dioxide with (a) zeolite beds [1] and with (b) an alternative for zeolites - a membrane unit, as dehydration units.

However, removal of water from gases using membranes is also challenging. In a typical gas separation, the diffusion of gases passing the membrane is spontaneous. Those gases do not residue at the permeate side, so no extra removal step is required for their collection. On the contrary, in a gas dehydration process, permeating water condenses and remains at the permeate side. Increased water concentrations at the permeate side decreases the driving force. Therefore, efficient and continuous water removal has to be implemented, such as the incorporation of sub-pressure or of sweep gas on the permeate side. A disadvantage of the first option is the high energy consumption needed to maintain a sub-pressure, combined with the increased driving force for permeation of feed gases that lead to decreased selectivity. On the other hand, incorporation of a sweep gas different than the feed gases, is accompanied by the back-diffusion of such a sweep gas and consequently contamination of the feed. A promising option is thus the usage of a sweep medium, which is present in the feed as well.

Therefore, in this study, we simulate and analyze a membrane recovery process for supercritical carbon dioxide loaded with water, in which the sweep medium is also carbon dioxide. The simulation is performed in Aspen Plus<sup>®</sup> using a membrane gas permeation model. The impact of a flow rate and pressure of a sweep gas, and of membrane permeance/selectivity is elaborated on. Two types of systems are investigated: 1) simple system with a single membrane unit, 2) hybrid system with two membrane units and recirculation of the permeate stream. Depending on the operating time, both systems can be beneficial in terms of economy. For long term operation and high feed flows, hybrid systems are more feasible.

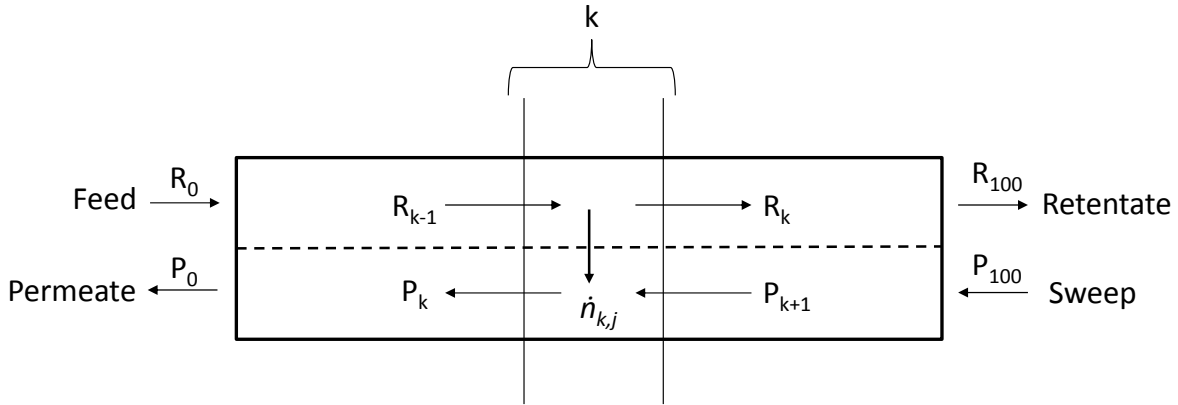
The configuration of the hybrid system used in this study is taken from the paper of Lohaus et al., in which six various hybrid configurations have been simulated in the similar dehydration process of supercritical carbon dioxide, and of which an economic evaluation has been made [22]. The chosen hybrid configuration was the most economical system and less sensitive to changes in membrane selectivity.

## 6.2 Modelling and process details

### 6.2.1 Hollow fiber gas permeation model

A model for a hollow fiber membrane module was used, in which the selective polymeric dense layer is coated on the shell side of a porous fiber. Transport through the membrane is described with the solution-diffusion mechanism. The initial 3-End configuration model (feed, retentate and permeate) was developed in Aspen Custom Modeler<sup>®</sup> (ACM) by Scholz et al. for the separation of carbon dioxide/propane and carbon dioxide/methane mixtures [23]. Because the feed pressure in those processes was low (<15 bar), preferential, inside-out operation was applied. To simulate a high pressure separation of water/carbon dioxide, this initial model has been accordingly adjusted by Lohaus et al. [22]. The 3-End configuration has been adapted to a 4-End configuration, to include an additional sweep stream on the permeate side. Inside-out operation at high feed pressure would damage the selective layer coated on the shell side of the fiber, and therefore, the outside-in operation has been used. Simulations were performed in Aspen Plus<sup>®</sup>. This modelling tool provides a large integrated model library for calculations of unit operations, such as the ones used in this work: compressors, turbines and flash vessels. Membrane operations are not included, but require modelling in Aspen Custom Modeler<sup>®</sup>. Models created in Aspen Custom Modeler<sup>®</sup> can be subsequently integrated with Aspen Plus<sup>®</sup>. Further information about Aspen Plus<sup>®</sup> can be found in [24].

The model divides the length of the module into 100 elements. The balance equations for all elements are solved simultaneously. Boundary conditions link the framing elements to the feed, retentate, permeate and sweep ports. The model is built in a counter current flow (Scheme 6.2).



**Scheme 6.2** Schematic representation of a 4-End hollow fiber model, which is divided into 100  $k$  elements and operates in a counter current flow.

The model includes the thermodynamic non-idealities that play a fundamental role in predicting the operating performance. The real fluid behavior and determination of fugacity coefficients are required for high pressure applications [25]. The real fluid properties at the chosen process conditions were determined using the Predictive Soave-Redlich-Kwong (PSRK) method. The choice of this property method was rationalized by the good agreement of the isothermal saturation curve at 50 °C up to 100 bar generated by the PSRK method with the experimental data reported in [26-31]. Accurate fugacity coefficients are essential, as these determine the driving force and therefore, the transmembrane fluxes, according to:

$$N_{k,j} = P_j \cdot \underbrace{(x_{k,j} \cdot p_{(Feed)} \cdot \phi_{k,j}^{(Ret)} - y_{k,j} \cdot p_{(Perm)} \cdot \phi_{k,j}^{(Perm)})}_{\text{driving force}} \quad \text{Eq. 6.1}$$

where  $N_{k,j}$  is the transmembrane flux in element  $k$  for component  $j$  [mol m<sup>-2</sup> h<sup>-1</sup>],  $P_j$  is the permeance of component  $j$  [mol m<sup>-2</sup> h<sup>-1</sup> bar<sup>-1</sup>];  $x_{k,j}$  and  $y_{k,j}$  are mole fractions in element  $k$  for component  $j$  at the retentate and permeate side, respectively [-];  $\phi_{k,j}^{(Ret)}$  and  $\phi_{k,j}^{(Perm)}$  are fugacity coefficients in element  $k$  for component  $j$  at the retentate and permeate side, respectively [-];  $p_{(Feed)}$  and  $p_{(Perm)}$  are the pressure on the feed and permeate side, respectively [bar]. Based on a water mole flow rate and flux over the membrane, the required membrane surface area,  $A$  [m<sup>2</sup>], is calculated from:

$$A = \frac{\dot{n}_{(H_2OFeed)} - \dot{n}_{(H_2ORet)}}{N_{H_2O}} \quad \text{Eq. 6.2}$$

where  $\dot{n}_{(H_2OFeed)}$  and  $\dot{n}_{(H_2ORet)}$  are the mole flow rates of water in the feed and retentate stream, respectively [ $\text{mol h}^{-1}$ ] and  $N_{H_2O}$  is the transmembrane flux of water [ $\text{mol m}^{-2} \text{h}^{-1}$ ].

The dehydration degree,  $D$  [%], of the final stream, termed in this research as a product stream, is defined as:

$$D = \frac{\dot{n}_{(H_2OProduct)}}{\dot{n}_{(H_2OFeed)}} \cdot 100\% \quad \text{Eq. 6.3}$$

where  $\dot{n}_{(H_2OProduct)}$  and  $\dot{n}_{(H_2OFeed)}$  are the mole flow rates of water in the final product stream and in the feed stream, respectively [ $\text{mol h}^{-1}$ ]. The dehydration degree was set to 95 %. The previous study of Lohaus et al. showed that to reach dehydration degrees >95 %, required membrane surface areas considerably increase, making the process much less profitable [22].

The Joule-Thompson effect is included and accounts for the temperature decrease caused by the decompression of permeating carbon dioxide. Generally, temperature changes influence membrane permeability and selectivity. In membranes derived from glassy polymers, with decreasing temperatures, the permeability declines and selectivity increases [32]. To simplify current simulations, a constant membrane performance at a temperature range of 30 – 50 ° C was assumed. The temperature changes had though an impact on heating and cooling demand for the streams, and were included in the simulations.

The membrane performance was also independent on pressures and concentrations along the fiber. As an alternative, the water permeance was varied from high to low values. A high water permeance of 250,000 GPU<sup>1</sup> was estimated based on permeability values reported for SPEEK membranes at low pressures and using a thin selective layer of 400 nm [22]. However, according to the research of Metz et al. [33], significantly lower water permeances can be obtained due to the boundary layer resistance on the feed side, caused by concentration

---

<sup>1</sup> GPU (Gas Permeation Unit) =  $10^{-6} \text{ cm}^3(\text{STP}) \text{ cm}^{-2} \text{ s}^{-1} \text{ cmHg}^{-1} = 0.1205 \text{ mol m}^{-2} \text{ h}^{-1} \text{ bar}^{-1}$

polarization. In such case, water permeance of 5,000 GPU is realistic [33]. Additionally, an increase in the feed pressure results in a larger resistance of the stagnant feed boundary layer, lowering the total water vapor flux [33]. Such layer is difficult to be reduced in gaseous and gas-like supercritical systems, because of poor mixing. Therefore, low water permeances can be also expected in supercritical carbon dioxide. The base membrane selectivity was chosen to be 5,000, which is realistic for a swollen SPEEK membrane.

Parameters, which are fixed in the process, are listed in Table 6.1, and dimensions of the hollow fiber used are listed in Table 6.2. The amount of hollow fibers required to perform the dehydration, can be calculated based on the required membrane surface area, obtained from the performed simulations.

The feed flow, membrane permeance and membrane selectivity were varied and are discussed in section - Results and discussion.

**Table 6.1** Fixed process parameters.

| <b>Parameter</b>                    | <b>Unit</b> | <b>Value</b>    |
|-------------------------------------|-------------|-----------------|
| Feed mass fraction H <sub>2</sub> O | -           | 0.0017          |
| Feed mass fraction CO <sub>2</sub>  | -           | 0.9983          |
| Feed mol fraction H <sub>2</sub> O  | -           | 0.0043          |
| Feed mol fraction CO <sub>2</sub>   | -           | 0.9957          |
| Feed pressure                       | bar         | 100             |
| Feed temperature                    | °C          | 50              |
| Sweep gas                           | -           | CO <sub>2</sub> |

**Table 6.2** Dimensions of the hollow fiber used.

| <b>Parameter</b>                | <b>Unit</b> | <b>Value</b>          |
|---------------------------------|-------------|-----------------------|
| Outer fiber diameter            | m           | $3.2 \cdot 10^{-4}$   |
| Thickness of the porous support | m           | $0.59 \cdot 10^{-4}$  |
| Thickness of the dense layer    | m           | $0.004 \cdot 10^{-4}$ |
| Fiber length                    | m           | 1                     |

### 6.2.2 Economic evaluation

In the economic evaluation, the operating and investment costs are included and recalculated as annual operating expenditures (OPEX) and annualized capital expenditures (CAPEX) [€/year]. The parameters used in the economic evaluation are listed in Table 6.3.

**Table 6.3** Parameters for the economic evaluation.

|                                  | <b>Parameter</b>                          | <b>Unit</b>      | <b>Value</b> | <b>Ref.</b> |
|----------------------------------|---|------------------|--------------|-------------|
| <b>Plant</b>                     | Annual operating hours                    | h/year           | 8,000        |             |
|                                  | Interest rate                             | %                | 8            |             |
|                                  | Depreciation period                       | year             | 8            |             |
|                                  | Update factor ( <i>UF</i> )               | -                | 5.041        | [34]        |
|                                  | Exchange rate (\$ in €)                   | \$/€             | 1.28         | [35]        |
| <b>Operating costs</b>           | Electrical energy price                   | €/kWh            | 9            | [36]        |
|                                  | Heat price                                | €/kWh            | 4.6          | [37]        |
|                                  | Coefficient of performance ( <i>COP</i> ) | -                | 4.16         | [38]        |
|                                  | CO <sub>2</sub> price                     | €/kg             | 10           | [est]       |
| <b>Membrane investment costs</b> | Membrane price                            | €/m <sup>2</sup> | 55           | [37]        |
|                                  | Peripheral factor                         | -                | 1.86         | [37]        |
|                                  | Membrane lifetime                         | year             | 4            | [est]       |

The operating costs include the energy demand for compression of the streams, cooling for compressors, heating of streams and the demand for carbon dioxide.

### **Annual operating costs**

Compression costs are calculated from:

$$Compression_{annual} = Compression\ demand \cdot Annual\ operating\ hours \cdot Electrical\ energy\ price$$

Cooling costs are calculated using the coefficient of performance (COP):

$$Cooling_{annual} = Cooling\ demand \cdot Annual\ operating\ hours \cdot Electrical\ energy\ price / COP$$

Heating costs are calculated from:

$$Heating_{annual} = Heating\ demand \cdot Annual\ operating\ hours \cdot Heat\ price$$

Costs of carbon dioxide are calculated from:

$$Carbon\ dioxide_{annual} = Demand\ for\ carbon\ dioxide \cdot Annual\ operating\ hours \cdot CO_2\ price$$

The compression, cooling and heating demand [kW] and the demand for carbon dioxide [kg/h] are obtained from simulations and are listed in Table 6.6 and 6.7 for particular systems. Annual operating hours [h], electrical energy price and heat price [€/kWh], CO<sub>2</sub> price [€/kg] and COP [-] are listed in Table 6.3.



## Investment costs

The investment costs include the equipment and the membrane costs. Equipment costs are calculated using Guthrie's method as described in Biegler et al. [39]. This method considers the equipment size based on mass and energy balances for each unit. In this research, mass and energy balances are obtained from simulations and are listed in Table 6.6 and 6.7 for particular systems. The base equipment costs,  $BC$  [\$], of compressors and turbines, are calculated with an exponential method from:

$$BC = C_0 \left( \frac{S}{S_0} \right)^\alpha \quad \text{Eq. 6.4}$$

where  $C_0$  are base (reference) costs [\$],  $S_0$  are base capacities (base energy consumption) [bhp],  $S$  is the energy consumption of a given unit [bhp] and  $\alpha$  is a correlation factor [-]. The base equipment costs,  $BC$ , for pressure vessels (flashes), are calculated from:

$$BC = C_0 \left( \frac{l}{l_0} \right)^\alpha \left( \frac{d}{d_0} \right)^\beta \quad \text{Eq. 6.5}$$

where  $C_0$  are base (reference) costs [\$],  $l_0$  and  $d_0$  are the base vessel length and diameter, respectively [m],  $l$  and  $d$  are the length and diameter of a particular vessel, respectively [m], and  $\alpha$  and  $\beta$  are correlation factors [-]. The diameter and length of a flash vessel are calculated based on the volume flow of condensed water leaving the flash vessel [ $\text{m}^3/\text{s}$ ]. In the calculations, the unit of brake horse power (bhp) is converted to kilowatt (kW) and dollar (\$) is converted to euro (€). The reference costs are given in prices from the year 1968 and have to be updated to account for inflation and cost development. The update factor  $UF$  is calculated from the Chemical Engineering Plant Costs Index ( $CEPCI$ ) from 2012 and 1968:

$$UF = \frac{CEPCI_{2012}}{CEPCI_{1968}} = \frac{572.7}{113.5} = 5.041 \quad \text{Eq. 6.6}$$

The total investments costs have to be corrected with the module factor,  $MF$ , that accounts for components, such as labor, piping, control systems, shipping, taxes and supervision. The value of  $MF$  depends on the bare costs and is taken from Biegler et al. [39]. For more accurate calculations, Hirschberg et al. [40] proposes to add a value of 2 to the  $MF$  values from Biegler et al. [39].

Further, the costs have to be corrected with the material and pressure correction factor, *MPF* that accounts for a material used, high pressures and special designs. The total investments costs, *C<sub>total</sub>*, are finally given as:

$$C_{total} = BC \cdot UF (MF + MPF - 1) \quad \text{Eq. 6.7}$$

All above described parameters and factors regarding compressors, flashes and turbines, are taken from Biegler et al. [39] and are listed in Table 6.4.

**Table 6.4** Parameters for the investment cost estimation using Guthrie’s method for different units.

| Units                            | <i>MPF</i> | <i>MF</i> | <i>d<sub>o</sub></i> [m] | <i>l</i> [m] | <i>C<sub>o</sub></i> [\$] | <i>S<sub>o</sub></i> [bhp] | <i>α</i> | <i>β</i> |
|----------------------------------|------------|-----------|--------------------------|--------------|---------------------------|----------------------------|----------|----------|
| <b>Compressors</b>               | 1.29       | 5.11      | -                        | -            | 23,000                    | 100                        | 0.77     | -        |
| <b>Turbines</b>                  | 1.15       | 5.11      | -                        | -            | 23,000                    | 100                        | 0.77     | -        |
| <b>Flash vessels<sup>2</sup></b> | 9.175      | 6.23      | 0.91                     | 1.2          | 1,000                     | -                          | 0.81     | 1.05     |

Regarding the membrane, the lifetime of 4 years is assumed, thus, within 8 years it has to be replaced once. The total investments costs for the membrane, *C<sub>total (membr)</sub>* are given from:

$$C_{total(membr)} = P_{membr} \cdot A_{membr} \cdot f \cdot 2 \quad \text{Eq. 6.8}$$

where *P<sub>membr</sub>* is the membrane price per m<sup>2</sup> [€/m<sup>2</sup>], *A* is the membrane area [m<sup>2</sup>] and *f* is a cost factor for peripheral costs.

<sup>2</sup> Vertical fabrication

## Calculation of annual operating expenditures (OPEX) and annualized capital expenditures (CAPEX)

The annual expenditures are calculated from:

$$OPEX_{annual} = \Sigma \text{Operating costs}_{annual}$$

$$CAPEX_{annual} = \Sigma \{ \text{Investment costs} \cdot (1+i)^n \cdot i / [(1+i)^n - 1] \} / n$$

where  $i$  is the interest rate of 0.08 and  $n$  is depreciation period of 8 years (Table 6.3). CAPEX calculations include that the membrane unit operates for 4 years instead of 8, so that it has to be replaced once.

### NPV – Net Present Value

Simple and hybrid systems are characterized by various payment schedules. They have different investment and operating costs. Calculation of  $NPV$  values [€/year] allows to determine, after which operating year one system becomes more beneficial than the other. The  $NPV$  calculation methods at specified conditions are described in Biegler et al. [39]. The system with the lowest  $NPV$  cost is superior. Here,  $NPV$  is calculated from:

$$NPV_n = \{ \text{Investment costs} \cdot (1+i)^n \cdot i / [(1+i)^n - 1] \} + n \cdot \text{Operating costs}_{annual} / n$$

where  $i$  is the interest rate of 0.08 and  $n$  is the operating time [years]. Basically, the  $NPV_n$  is the sum of  $OPEX_{annual}$  and  $CAPEX_{annual}$  calculated assuming  $n$  operating years. The  $n$  was varied from 1 to 8 years. Calculations include that the membrane unit has to be replaced in the 5-th operating year.

## 6.3 Results and discussion

### 6.3.1 Sweep stream

The effective removal of water from the permeate side is essential in the dehydration process. Therefore, the pressure and flow rates of sweep streams have to be accordingly adjusted.

With a high sweep pressure, the transmembrane pressure is low. The low transmembrane pressure enhances membrane stability and increases selectivity for water over carbon dioxide. However, as shown in Table 6.5 (data taken from Wiebe [41]), water solubility in carbon dioxide decreases with increasing pressure. At a certain pressure (dependent on the temperature), the water solubility increases again. Still, the greatest saturation abilities for carbon dioxide are at low pressures. The usage of pressurized carbon dioxide as a sweep stream would require large amounts of this fluid to dissolve water. Therefore, in all simulations, the sweep pressure was chosen to be 1, 1.1 or 2.5 bar.

**Table 6.5** Solubility of water in carbon dioxide as a function of pressure and temperature. Data are taken from Wiebe [41].

| Pressure [bar] | Solubility of water in carbon dioxide [g/dm <sup>3</sup> <sub>(STP)</sub> ] |          |         |         |
|----------------|---|----------|---------|---------|
|                | 25 °C   | 31.04 °C | 50 °C   | 75 °C   |
| 1              | 0.023   | 0.032    | 0.093   | 0.242   |
| 25             | 0.00132   | 0.00183  | 0.00498 | 0.00855 |
| 50             | 0.00104   | 0.00129  | 0.00308 | -       |
| 60             | -   | -        | 0.00287 | -       |
| 75             | -   | -        | 0.00281 | -       |
| 100            | 0.00267   | 0.00293  | 0.00361 | 0.00666 |

The sweep flow rate has a direct influence on the driving force for water permeation and therefore, on the required membrane surface area. Higher water fluxes through the membrane are obtained at larger sweep streams, because of the reduced water activity at the permeate side. However, a large sweep stream causes high operating costs, as will be shown later. Therefore,

the optimum conditions have been adjusted for particular simulations such that the dehydration degree of 95 % is reached, and the operating costs for carbon dioxide are sensible. The role of the sweep stream on the driving force along the length of the fiber is elaborated on in more detail in the research of Lohaus et al. [22].

Here, we discuss the operating principle of the simple and the hybrid systems, which are schemed in Figure 6.1 and 6.2, respectively. Temperatures and pressures of particular streams are presented in the figures.

### 6.3.2 Operating principle of the simple system

The simple system consists of a single membrane unit and a refill. *Feed* at 100 bar and 50 °C enters the membrane unit, *A*, in counter current to *Sweep* of 1 bar and 50 °C, respectively. The expansion of permeating carbon dioxide causes a temperature decrease of *Permeate* by few degrees. *Permeate* is released to the atmosphere. The losses of carbon dioxide in *Retentate* are compensated by *Refill*. *Refill*, which is delivered at 1.2 bar at 50 °C, is compressed to 100 bar before mixing with *Retentate*. A mixture of *Retentate* and *Compressed Refill* is termed as *Product*. This system is characterized by high CO<sub>2</sub> emissions, and therefore, by high operating costs (OPEX), whereas investment costs, or annualized investments cost (CAPEX), are low.

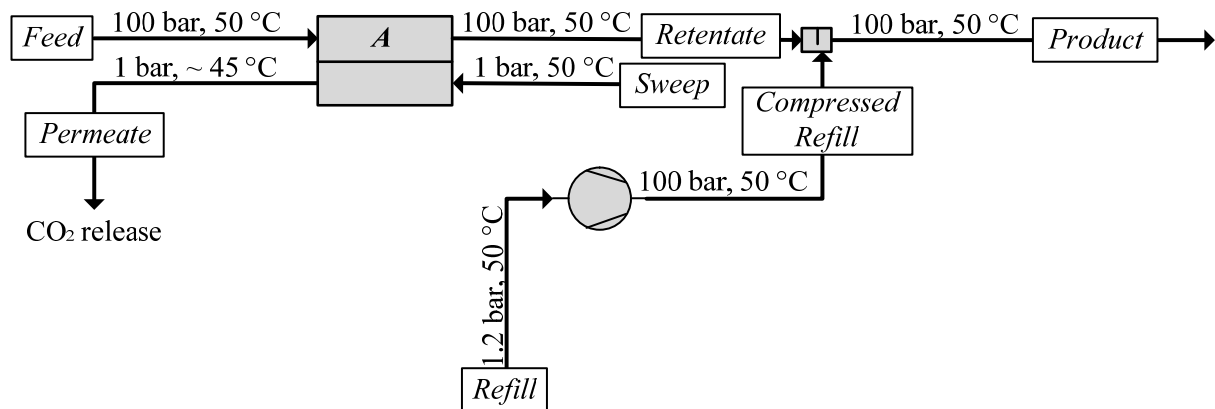


**Figure 6.1** Scheme of a simple system process and the distribution of the pressure/temperature values of the particular streams.

### **6.3.3 Operating principle of a hybrid system**

To prevent high  $CO_2$  emissions, a hybrid system is considered. This system is characterized by high investment costs (CAPEX) but reasonably lower operating costs (OPEX). The hybrid system has two membrane units, two compressors, a turbine and a flash vessel. Water from the feed is removed via the first membrane unit. The water collected by the sweep gas in the first membrane unit, is further removed from this sweep stream, mainly via condensation steps, and finally, via the second membrane unit.

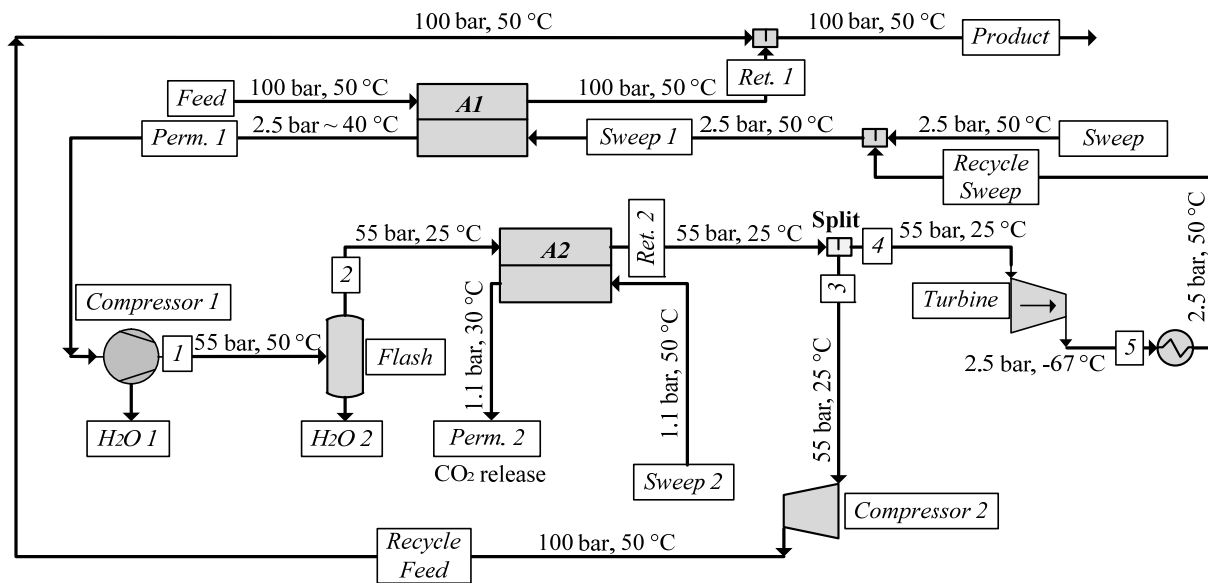


**Figure 6.2** Scheme of a hybrid system process and a distribution of the pressure/temperature values of the particular streams.

*Feed* at 100 bar and 50 °C enters the first membrane unit, *A1*, in counter current to *Sweep 1* of 2.5 bar and 50 °C. *Sweep 1* is a mixture of freshly supplied *Sweep* and *Recycle Sweep*, both at 2.5 bar and 50 °C. *Permeate 1*, of which the temperature decreases to ~ 40 °C due to carbon dioxide expansion, is compressed to 55 bar in *Compressor 1*. Due to compression, condensation of water occurs. In this compression step, the majority of water from *Permeate 1* is removed. The stream of condensed water coming from *Compressor 1* is termed as *Stream H2O 1*. The compressed stream leaving *Compressor 1* is indicated in the scheme as *Stream 1*. *Stream 1* at 50 °C is passed subsequently to the *Flash* vessel of a lower temperature, 25 °C. Due to decreased temperature, condensation of water occurs. The stream of condensed water coming from the *Flash* vessel is termed as *Stream H2O 2*. The compressed stream leaving the *Flash* vessel is indicated in the scheme as *Stream 2*. *Stream 2* is passed further to the second membrane unit, *A2*, in counter current to *Sweep 2* of 1.1 bar and 50 °C. *Permeate 2* leaves the *A2* at 1.1 bar and ~30 °C, and is released to the atmosphere. *Retentate 2* from the *A2* is split into two streams – *Stream 3* and *Stream 4*. The split ratio is defined as:

$$Split = \frac{Stream\ 4}{Stream\ 3}$$

*Stream 3* is compressed to 100 bar in *Compressor 2*. The stream leaving the *Compressor 2* is indicated in the scheme as *Recycle Feed*. *Recycle Feed* is mixed subsequently with *Retentate 1*. A mixture of *Retentate 1* and *Recycle Feed* gives the final stream, termed as *Product*. The second fraction of *Retentate 2*, *Stream 4*, is expanded to 2.5 bar. There, an additional benefit is obtained from implementing a *Turbine* that generates electricity. The stream leaving the *Turbine* is indicated in the scheme as *Stream 5*. The temperature of *Stream 5* is -67 °C due to carbon dioxide decompression. This stream after heating till 50 °C is further termed as *Recycle Sweep*. A mixture of *Recycle Sweep* and freshly supplied *Sweep* gives stream *Sweep 1*. In that way, the loop is closed.

The operating principle of the simple and hybrid systems has been discussed. The results from the simulations are shown in Table 6.6 and 6.7 for the simple and hybrid systems, respectively. The simulation results comprise of the required membrane area and energy demand for compression and cooling of compressors. For a hybrid system, there is additionally a turbine that generates electricity and the demand for heating of streams leaving the turbine. Table 6.8 shows investment and operating costs for particular simulations. In the Supporting information, Table 6-S1 and 6-S2 show the compositions of particular streams (mass balances) for the simple and hybrid systems, respectively.

Simulation results are divided into two parts. First, we consider a low feed flow of 2,000 kg/h that corresponds to a small pilot plant. High water permeance of 250,000 GPU and selectivity of 5,000 are used. Systems at those conditions are referred to as S1 and H1. These simulations clearly represent the operating differences between a simple and a hybrid system.

Second, we consider a larger process with a feed flow of 100,000 kg/h. Various water permeances and selectivities are used. Consequently, in S2 and H2, high water permeance of 250,000 GPU and selectivity of 5,000 are maintained, as in the systems S1 and H1. In S3 and H3, water permeance is significantly reduced to 5,000 GPU, but the selectivity of 5,000 is maintained. In S4, S5 and H4, H5, the low water permeance of 5,000 GPU is maintained, but the selectivity is varied. These simulations clearly represent factors that mostly determine investment and operating costs, and show the impact of a membrane unit on the process.



**Table 6.6** Varied process parameters and simulation results for simple systems.

| Simple system      |                                    |          |           |         |         |         |
|--------------------|------------------------------------|----------|-----------|---------|---------|---------|
|                    |                                    | Low feed | High feed |         |         |         |
|                    | Design number                      | S1       | S2        | S3      | S4      | S5      |
| Process parameters | Feed [kg/h]                        | 2,000    | 100,000   | 100,000 | 100,000 | 100,000 |
|                    | P H <sub>2</sub> O [GPU]           | 250,000  | 250,000   | 5,000   | 5,000   | 5,000   |
|                    | P CO <sub>2</sub> [GPU]            | 50       | 50        | 1       | 0.2     | 0.2     |
|                    | Selectivity [-]                    | 5,000    | 5,000     | 5,000   | 25,000  | 25,000  |
|                    | Sweep [kg/h]                       | 62       | 3,100     | 3,100   | 3,100   | 5,000   |
| Simulation results | Membrane A [m <sup>2</sup> ]       | 1.3      | 64.6      | 3,256   | 10,020  | 1,173   |
|                    | Compressor [kW]                    | 2.5      | 121.9     | 121.9   | 75.5    | 8.84    |
|                    | Cooling <sub>Compressor</sub> [kW] | 3.7      | 164.8     | 164.8   | 102.1   | 12.0    |

**Table 6.7** Varied process parameters and simulation results for hybrid systems.

| Hybrid system                   |                                     |          |           |         |                 |                    |
|---------------------------------|-------------------------------------|----------|-----------|---------|-----------------|--------------------|
|                                 |                                     | Low feed | High feed |         |                 |                    |
|                                 | Design number                       | H1       | H2        | H3      | H4 <sup>3</sup> | H5                 |
| Process parameters              | Feed [kg/h]                         | 2,000    | 100,000   | 100,000 | 100,000         | 100,000            |
|                                 | P H <sub>2</sub> O [GPU]            | 250,000  | 250,000   | 5,000   | 5,000           | 5,000              |
|                                 | P CO <sub>2</sub> [GPU]             | 50       | 50        | 1       | 1.5             | 0.5                |
|                                 | Selectivity [-]                     | 5,000    | 5,000     | 5,000   | 3,333           | 10,000             |
|                                 | Sweep [kg/h]                        | 1.69     | 84.5      | 84.5    | 56.6            | 84.5               |
|                                 | Sweep 2 [kg/h]                      | 1.4      | 70        | 70      | 46.9            | 70                 |
|                                 | Split [-]                           | 0.59     | 0.59      | 0.59    | 0.59            | 0.785 <sup>4</sup> |
| Simulation results              | Membrane A1 [m <sup>2</sup> ]       | 5.2      | 260       | 13,000  | 13,000          | 13,000             |
|                                 | Membrane A2 [m <sup>2</sup> ]       | 0.16     | 8         | 400     | 400             | 400                |
|                                 | Compressor 1 [kW]                   | 16.5     | 824.1     | 824.1   | 1,229.7         | 808.3              |
|                                 | Cooling <sub>Compressor1</sub> [kW] | 20.7     | 1,034.5   | 1,034.5 | 1,523.8         | 1,045.8            |
|                                 | Compressor 2 [kW]                   | 0.8      | 39.5      | 39.5    | 58.6            | 20.1               |
|                                 | Cooling <sub>Compressor2</sub> [kW] | 2.0      | 97.0      | 97.0    | 144.1           | 49.4               |
|                                 | Cooling <sub>Flash</sub> [kW]       | 2.5      | 124.0     | 124.0   | 184.0           | 120.0              |
|                                 | Turbine power [kW]                  | 2.5      | 122.9     | 122.9   | 182.5           | 158.9              |
| Heating <sub>Turbine</sub> [kW] | 5.6                                 | 281.9    | 281.9     | 418.6   | 364.6           |                    |

<sup>3</sup> Dehydration degree of the product reached in this system is 97 %, instead of 95 %.<sup>4</sup> With the split of 0.59, the dehydration degree of the product would be 51 %.

**Table 6.8** Investment and operating costs and the turbine benefit calculated based on simulation results.

| <b>Simple system</b>                  |         |           |           |           |           |
|---------------------------------------|---------|-----------|-----------|-----------|-----------|
|                                       | S1      | S2        | S3        | S4        | S5        |
| Investment costs [€]                  | 6,175   | 126,140   | 224,743   | 395,212   | 52,685    |
| Operating costs [€/year]              | 69,426  | 3,462,351 | 3,463,486 | 3,089,147 | 4,071,321 |
| Turbine benefit [€/year]              | -       | -         | -         | -         | -         |
| <b>Hybrid system</b>                  |         |           |           |           |           |
|                                       | H1      | H2        | H3        | H4        | H5        |
| Investment costs [€]                  | 185,776 | 3,808,438 | 6,495,557 | 7,845,971 | 6,552,552 |
| Operating costs <sup>5</sup> [€/year] | 17,334  | 866,716   | 866,665   | 1,279,084 | 838,895   |
| Turbine benefit [€/year]              | -1,770  | -88,479   | -88,530   | -131,383  | -114,410  |

### 6.3.4 Simulation results and economic evaluation

#### Low feed flow systems

##### System S1 and H1

Based on variable process parameters and the simulation results listed in Table 6.6 and 6.7, and investment and operating costs listed in Table 6.8, the annual costs are calculated. Figure 6.3 compares the annual operating (OPEX) and capital (CAPEX) costs for S1 and H1.

The simple system S1 is characterized by low capital costs and high operating costs. A great demand on CO<sub>2</sub> results from the lack of recycle streams and consequently, from releasing of carbon dioxide to the atmosphere. On the other hand, the hybrid system H1 is characterized by higher capital and lower operating costs compared to S1. The greatest capital costs in H1 are for compressors (mainly Compressor 1 used to compress the permeate stream from the first membrane unit, A1 – Table 6.7) and a turbine. A flash vessel is of minor expenses and is not visible in the graph. In both systems, due to the very high water permeance, the required membrane surface area is very low and therefore, the costs are not visible in the graph. Operating costs for H1 are mainly caused by electricity costs and cooling demand for the compressors. Heating of the stream leaving the turbine is not so pronounced, and CO<sub>2</sub> emissions are reduced compared to system S1.

<sup>5</sup> Including turbine benefit

### NPV for S1 and H1

The net present value (NPV) of the systems indicates which system is superior at specific operating times. Figure 6.4 shows the breaking point at the ~3.5 years of operation. System S1 has low investment but high operating costs. However, when a dehydration process is operated for less than 3.5 years, system S1 is more economical compared to the hybrid system H1. System H1 has the higher investment but lower operating costs, and is more beneficial assuming operating times longer than 3.5 years.

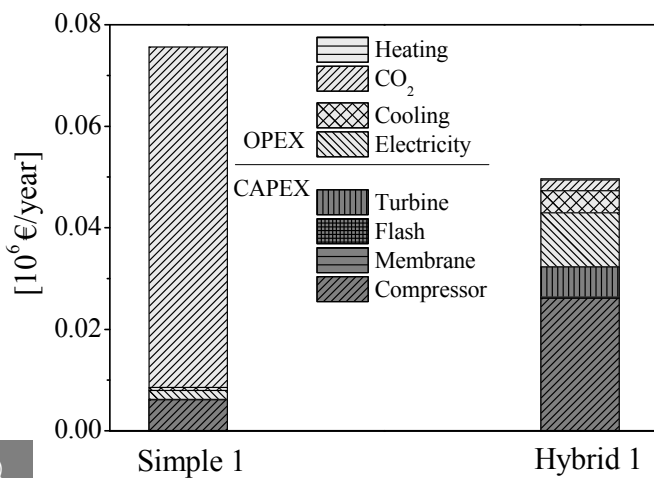


**Figure 6.3** Annual costs for the low feed, simple (S1) and hybrid (H1) systems for a period of 8 years.

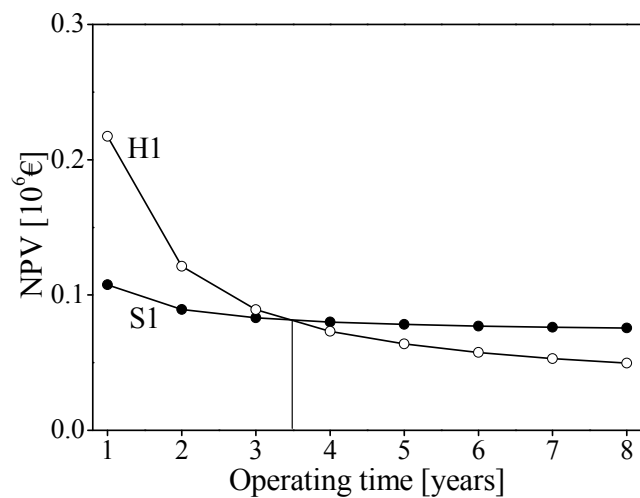


**Figure 6.4** NPV of the low feed, simple S1 (closed symbols) and hybrid H1 (open symbols) systems. The usage of H1 is more beneficial compared to S1 assuming operating times longer than 3.5 years.

## **High feed flow systems**

Here, we discuss the factors that determine the compression costs and we elaborate on the role of the membrane unit.

### **Simple systems S2 – S5**

Based on the variable process parameters and simulation results listed in Table 6.6, and investment and operating costs listed in Table 6.8, the annual costs are plotted. Figure 6.5 compares the annual operating (OPEX) and capital (CAPEX) costs for the systems S2, S3, S4 and S5. Their annual costs are much higher than those of system S1, due to upscaling of the feed stream from 2,000 to 100,000 kg/h.

System S2 has selectivity of 5,000 and an optimized sweep flow of 3,100 kg/h. This system is characterized by low investment costs for membrane unit (not visible on the bars). The low membrane investment costs are due to the high water permeance of 250,000 GPU, and consequently, due to the small membrane surface area required. The annual demand on carbon dioxide, due to its continuous releasing to the atmosphere, is very high (~3 Million €/year).

When shifting from system S2 to S3, the water permeance is reduced from 250,000 to 5,000 GPU, whereas the selectivity and the sweep stream of 5,000 and 3,100 kg/h, respectively, are maintained. The demand for compression and cooling of the refill stream is still the same for both, system S2 and S3. This is caused by equal losses of CO<sub>2</sub> in these two processes. The CO<sub>2</sub> permeance in S2 (50 GPU) is 50 times higher than that in S3 (1 GPU) but the membrane surface area in S2 (64.6 m<sup>2</sup>) is 50 times smaller than that in S3 (3,256 m<sup>2</sup>). Overall, the flow of CO<sub>2</sub> through the membrane remains unchanged for both S2 and S3. Instead, system S3 has significantly increased investment costs for a membrane module, because of the high required membrane surface area.

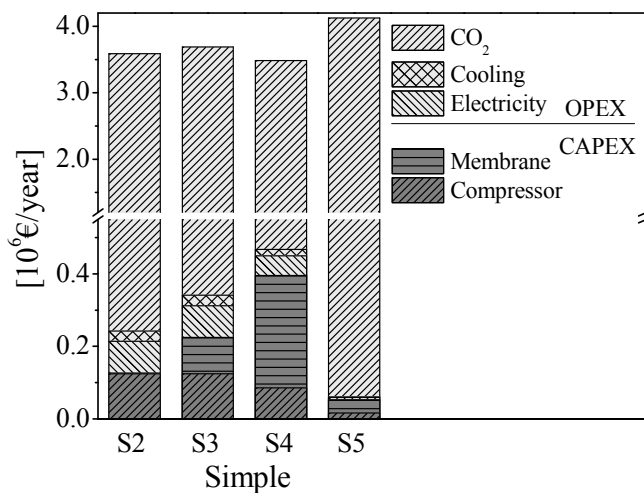


**Figure 6.5** Annual costs for the high feed simple systems.

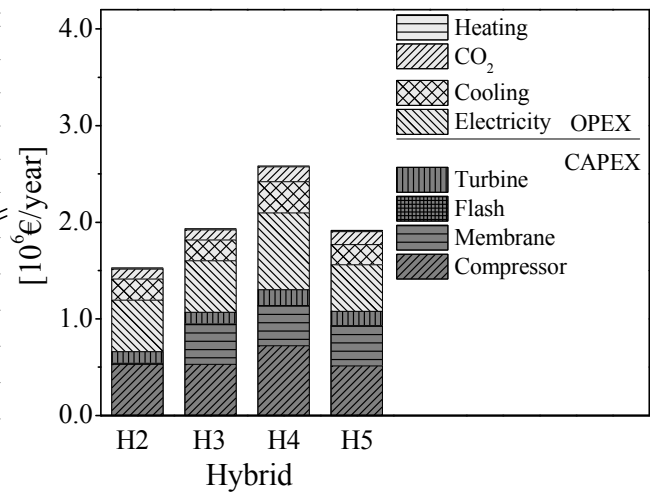


**Figure 6.6** Annual costs for the high feed hybrid systems.

When shifting from system S3 to S4, CO<sub>2</sub> permeance of the membrane is decreased, so that the selectivity increases from 5,000 to 25,000. At the same time, the sweep flow of 3,100 kg/h is maintained, as in the systems S2 and S3. As a consequence, a large membrane surface area is required to perform the dehydration, since the sweep flow is not sufficient. Therefore, system S4, due to the increased selectivity and not adjusted sweep flow, has high membrane investment costs. Simultaneously, the demand for compression and cooling of the refill stream becomes reduced, because of the decreased CO<sub>2</sub> flow over the membrane. These results also show that CO<sub>2</sub> that permeates through the membrane causes “self-sweeping”. Upon selectivity enhancement, the flow rate of the fresh sweep has to be increased. Otherwise, a higher membrane surface area is required. Notably, system S4, with such a large membrane surface area, has lower annual costs than system S2, which has very low costs for the membrane module. This is because the refill stream in S4 (671 kg/h) is smaller as compared to S2 and S3 (1,084 kg/h) (see mass balances in Table 6-S1, Supporting Information) and requires less demand for compression.

When shifting from system S4 to S5, the sweep flow is increased from 3,100 to 5,000 kg/h. This significant increase of the sweep flow results in more effective removal of water from the permeate side, and therefore, in a decrease in the required membrane surface area. Furthermore, the decreased membrane surface area causes a reduction of the CO<sub>2</sub> flow over the membrane, which leads in turn to the reduced refill costs. However, the demand for fresh CO<sub>2</sub> is large.

In summary, the electricity and cooling demand for a compressor, which compresses the refill stream, depends mainly on the feed capacity and the membrane selectivity. Increasing the membrane selectivity reduces the demand for compression. The membrane surface area is on the other hand dependent on the water permeance and on the sweep stream flow. High water permeance and high sweep flow significantly reduce the investment costs for the membrane unit. From all these options the optimum can be taken, and the system can be designed according to the requirements. CO<sub>2</sub> that permeates through the membrane causes “self-sweeping”. When the selectivity significantly increases, thus reducing the CO<sub>2</sub> flow through the membrane, the flow of fresh CO<sub>2</sub> has to be increased such that water can be still effectively removed from the permeate side. If the selectivity increases during operation and the sweep flow is not accordingly adjusted, sufficient dehydration degree will not be reached. On the contrary, if the selectivity decreases during operation, e.g. due to membrane plasticization, the dehydration degree can increase (assuming constant water flow). Using simple systems with a feed flow of 100,000 kg/h, the yearly CO<sub>2</sub> emissions to the atmosphere are 24,800 – 40,000 t/year. Notably, the annual costs can be reduced slightly by using a membrane with high selectivity, so that the refill costs are reduced, as compared to using a membrane with high water permeance. Still, the annual costs are similar for system S2, S3 and S4 (3.48 – 3.68 Million €/year), and 4.12 Million €/year for S5.

### **Hybrid systems HD2 – HD5**

Based on the variable process parameters and simulation results listed in Table 6.7 for the hybrid systems, and investment and operating costs listed in Table 6.8, the annual costs are plotted. Figure 6.6 compares the annual operating (OPEX) and capital (CAPEX) costs for systems H2, H3, H4 and H5. Their annual costs are much higher than those of system H1, due to upscaling of the feed stream from 2,000 to 100,000 kg/h. These are also lower than the annual costs of the simple systems.

In the hybrid systems, the split, the CO<sub>2</sub> flow through the membrane and the flow of the fresh sweep streams determine whether the desired dehydration degree can be reached.

System H2 has a selectivity of 5,000 and the optimal flows of *Sweep* and *Sweep 2* (see the process scheme - Figure 6.2) are 84.5 and 70 kg/h, respectively. The split is set to 0.59 such that the necessary flow rates of *Recycle Sweep* and *Recycle Feed* are ensured. This system is characterized by the high demand for compressors (mainly for Compressor 1 - Table 6.7)

caused by the high feed stream and consequently, by the high *Permeate 1* stream. Due to the high water permeance of 250,000 GPU, smaller membrane surface areas are required. The annual demand on carbon dioxide is lower as compared to simple systems.

When shifting from system H2 to H3, the water permeance is reduced from 250,000 to 5,000 GPU, while the selectivity of 5,000, the flows of *Sweep* and *Sweep 2* of 84.5 and 70 kg/h, and the split of 0.59, are maintained. The demand for compression and cooling of the refill stream is still the same for both system, H2 and H3. This is caused by equal losses of CO<sub>2</sub> in these two processes. CO<sub>2</sub> permeance in H2 (50 GPU) is 50 times higher than that in H3 (1 GPU), but the membrane surface areas in H3 (13,000 and 400 m<sup>2</sup>) are about 50 times higher than those in H2 (260 and 8 m<sup>2</sup>). Overall, the flow of CO<sub>2</sub> through the membrane remains the same for both, H2 and H3. However, system H3 has significantly increased investment costs for the membrane units.

When shifting from system H3 to H4, the selectivity is decreased from 5,000 to 3,300. As a result, more CO<sub>2</sub> permeates through the membrane, causing enhanced “self-sweeping”. This enhanced “self-sweeping” allows decreasing the flow of the fresh sweep streams. In system H4, the flow rates of *Sweep* and *Sweep 2* were decreased from 84.5 to 56.6 kg/h, and from 70 to 46.9 kg/h, respectively, as compared to H3. At the same time, the membrane surface areas were kept the same for H3 and H4, i.e. 13,000 m<sup>2</sup> and 400 m<sup>2</sup> for the *A1* and *A2* membrane units, respectively. However, the sweep flows at reduced membrane selectivity have not been optimized. The sweep flows were too high such that in turn, the obtained dehydration degree of the product stream was 97 %, instead of 95 % (see Supporting Information – mass balances Table 6-S2, water content in *Product* streams). A further consequence is that the demand on compressors increases considerably due to the increased flow of *Permeate 1* (H3 - 10,634 kg/h and H4 - 15,711 kg/h) and of *Stream 3* (H3 – 4,257 kg/h and H4 - 6,320 kg/h). The electricity benefit from the turbine increases due to the increased flow of *Stream 4* (H3 - 6,126 and H4 - 9,095 kg/h) but also the heating demand for this stream is higher (H3 – 289.1 kW and H4 – 418.6 kW).

When shifting from system H4 to H5, the selectivity is increased from 3,300 to 10,000. As a consequence, the CO<sub>2</sub> flow through the membrane decreases, causing reduced “self-sweeping”. The flow rates of *Sweep* and *Sweep 2* in H5 maintain equal as in systems H2 and H3, 84.5 and 70 kg/h, respectively. Therefore, the flow of *Permeate 1* in H5 is reduced as compared to H2 and H3 (H2, H3 – 10,634 kg/h and H5 – 10,299 kg/h). If we keep the split

ratio of 0.59, the flow of *Recycle Sweep* is not sufficient. Since *Recycle Sweep* is needed to sweep water from the first membrane unit *A1*, its insufficient flow results in this simulation in a dehydration degree of only 51 % (see Table 6.7 – H5). An alternative way to increase *Recycle Sweep* flow and to obtain a dehydration degree of 95 % is to increase the split from 0.59 to 0.785. Simultaneously, a higher amount of CO<sub>2</sub> is passed to the turbine; therefore, more electricity is generated in H5 as compared to H2 and H3, but also the heating costs of the stream leaving the turbine increase. Additionally, lower compression costs and cooling demand are required for *Permeate 1* and *Recycle Feed*.

In summary, the performance of the process can be optimized in various ways – selectivity determines the required sweep flow rate and the split factor determines the dehydration degree. When more specific data are available, such as compressor lifetimes and maintenance costs, the price for a membrane module, the operating costs for zeolites, the size of the factory, profits from selling of dried food. etc., the process can be optimized. One can decide if a higher membrane surface area is more beneficial, or the usage of high sweep flows and connected to that compression costs.

Generally, the demand for recirculation lines depends on the feed flow. The main costs are generated by compressors. Furthermore, it is questionable if the process can be facilitated by reaching the membrane permeance of 250,000 GPU, if much lower values are obtained due to concentration polarization. For membranes derived from SPEEK, a promising polymer for dehydration, the ideal selectivity reported by Liu et al. is  $1 \cdot 10^7$  [19]. However, in a highly swollen state caused by the high water activity, the selectivity drastically decreases and values of 3,000 – 5,000 are estimated. Yet our simulations show that a selectivity enhancement from 5,000 to 10,000 does not decrease the annual costs when comparing system H3 and H5. Those costs are 1.93 and 1.92 Million €/year, respectively. This is because the split ratio and the fresh sweep flow can be accordingly adjusted, based on a given selectivity. Using hybrid systems with a feed flow of 100,000 kg/h, the yearly CO<sub>2</sub> emissions to the atmosphere are 828 – 1236 t/year, which is about 32-fold less than in the simple systems.



### NPV for S2-S5 and H2-H5

The net present value (NPV) of the systems indicates which system is superior, depending on the considered operating time. Figure 6.7 shows that for a large scale process, the simple systems are only beneficial assuming operating time of 1 year.

Concerning simple systems, the most expensive is S5, due to the large emission of CO<sub>2</sub> to the atmosphere. S2, S3 and S4 have actually very similar NPV values, indicating that the variations in membrane properties, selectivity (5,000 to 250,000) and water permeance (5,000 to 25,000 GPU), do not impact the annual costs significantly.

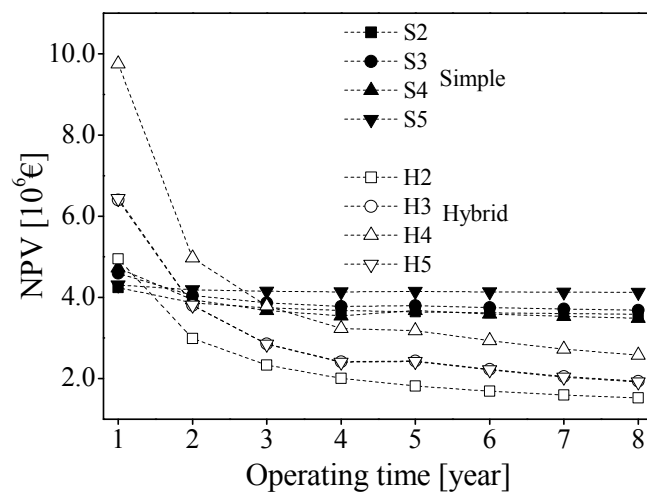


**Figure 6.7** NPV of the high feed, simple (S2-S5) and hybrid (H2-H5) systems. The usage of hybrid systems is more beneficial compared to simple systems, assuming operating times longer than 1 year.

Hybrid systems are already more beneficial when the process is operated for longer than 1 year. System H4 is the most expensive. However, this is because of the higher dehydration degree of 97 %, instead of 95 %, due to not optimized sweep flows. H3 and H5 follow the same NPV, indicating that selectivity variations from 5,000 to 10,000 have no influence on the cost reduction. H2 is the most economical system because of the high water permeance of 250,000 GPU, which however, might not be reachable due to concentration polarization.

## **6.4 Conclusions**

Dehydration of supercritical carbon dioxide (CO<sub>2</sub>) at 100 bar and 50 °C has been simulated in Aspen Plus<sup>®</sup> using a hollow fiber gas permeation model. In this dehydration process, the incorporation of a sweep gas is necessary to effectively remove water from the permeate side. CO<sub>2</sub> was also used as a sweep gas. The advantage of using CO<sub>2</sub> as a sweep is lack of contamination of the feed with other gases and increased selectivity. For a large scale process with a feed capacity of 100,000 kg/h, the usage of a single membrane unit to perform dehydration is not beneficial. This is caused by high emissions of CO<sub>2</sub> to the atmosphere. Hybrid systems with two membrane units and a recirculation line of the permeate streams are a cheaper alternative.

## **Acknowledgements**

This work was performed in the cooperation framework of Wetsus, centre of excellence for sustainable water technology ([www.wetusus.nl](http://www.wetusus.nl)). Wetsus is co-funded by the Dutch Ministry of Economic Affairs and Ministry of Infrastructure and Environment, the European Union Regional Development Fund, the Province of Fryslân, and the Northern Netherlands Provinces. The authors would like to thank the participants of the research theme “Dehydration” for the fruitful discussions and their financial support.

The authors thank Prof. Matthias Wessling from RWTH Aachen University for the fruitful cooperation and the possibility to perform the simulations in his research group.

## References

1. Almeida-Rivera, C.P., S. Khalloufi, and P. Bongers, *Prediction of supercritical carbon dioxide drying of food products in packed beds*. Drying Technology, 2010. **28**(10): p. 1157-1163.
2. Licence, P. and M. Poliakoff, *An Introduction To Supercritical Fluids: From Bench Scale to Commercial Plant*, in *New Methodologies and Techniques for a Sustainable Organic Chemistry*, A. Mordini and F. Faigl, Editors. 2008, Springer Netherlands. p. 171-191.
3. Kemmere, M.F. and T. Meyer, *Supercritical Carbon Dioxide: in Polymer Reaction Engineering*. 2006: Wiley-VCH Verlag GmbH & Co. KGaA. 1-339.
4. Ramsey, E., et al., *Mini-Review: Green sustainable processes using supercritical fluid carbon dioxide*. Journal of Environmental Sciences, 2009. **21**(6): p. 720-726.
5. Nalawade, S.P., F. Picchioni, and L.P.B.M. Janssen, *Supercritical carbon dioxide as a green solvent for processing polymer melts: Processing aspects and applications*. Progress in Polymer Science (Oxford), 2006. **31**(1): p. 19-43.
6. van der Kraan, M., et al., *Equilibrium distribution of water in the two-phase system supercritical carbon dioxide-textile*. Journal of Supercritical Fluids, 2007. **40**(3): p. 336-343.
7. Brunner, G., *Supercritical fluids: Technology and application to food processing*. IV Iberoamerican Congress of Food Engineering (CIBIA IV), 2005. **67**(1-2): p. 21-33.
8. Tan, C.-S., et al., *Separation of supercritical carbon dioxide and caffeine with mesoporous silica and microporous silicalite membranes*. The Journal of Supercritical Fluids, 2003. **26**(1): p. 55-62.
9. Chiu, Y.-W. and C.-S. Tan, *Regeneration of supercritical carbon dioxide by membrane at near critical conditions*. The Journal of Supercritical Fluids, 2001. **21**(1): p. 81-89.
10. Sarmiento, L.A.V., et al., *Performance of reverse osmosis membranes in the separation of supercritical CO<sub>2</sub> and essential oils*. Journal of Membrane Science, 2004. **237**(1-2): p. 71-76.
11. Semenova, S.I., et al., *Separation of supercritical CO<sub>2</sub> and ethanol mixtures with an asymmetric polyimide membrane*. Journal of Membrane Science, 1992. **74**(1-2): p. 131-139.
12. Patil, V.E., et al., *Permeation of supercritical carbon dioxide through polymeric hollow fiber membranes*. Journal of Membrane Science, 2006. **271**(1-2): p. 77-85.
13. Verkerk, A.W., et al., *Permeation of carbon dioxide through a microporous silica membrane at subcritical and supercritical conditions*. Langmuir, 2002. **18**(18): p. 6807-6812.
14. Khalloufi, S., C. Almeida-Rivera, and P. Bongers, *Supercritical-CO<sub>2</sub> drying of foodstuffs in packed beds: Experimental validation of a mathematical model and sensitive analysis*. Journal of Food Engineering, 2010. **96**(1): p. 141-150.
15. Ratti, C., *Hot air and freeze-drying of high-value foods: A review*. Journal of Food Engineering, 2001. **49**(4): p. 311-319.
16. Aguilera, J.M., A. Chiralt, and P. Fito, *Food dehydration and product structure*. Trends in Food Science and Technology, 2003. **14**(10): p. 432-437.
17. Brown, Z.K., et al., *Drying of foods using supercritical carbon dioxide - Investigations with carrot*. Innovative Food Science and Emerging Technologies, 2008. **9**(3): p. 280-289.
18. Thomas, W.J. and B. Crittenden, *I - The development of adsorption technology*, in *Adsorption Technology & Design*, W.J. Thomas and B. Crittenden, Editors. 1998, Butterworth-Heinemann: Oxford. p. 1-7.

19. Nikolaev, V.V., A.N. Vshivtsev, and A.D. Shakhov, *Regeneration of zeolitic adsorbents by organic solvents*. Chemistry and Technology of Fuels and Oils, 1997. **33**(6): p. 344-346.
20. Sijbesma, H., et al., *Flue gas dehydration using polymer membranes*. Journal of Membrane Science, 2008. **313**(1-2): p. 263-276.
21. Liu, S., F. Wang, and T. Chen, *Synthesis of Poly(ether ether ketone)s with High Content of Sodium Sulfonate Groups as Gas Dehumidification Membrane Materials*. Macromolecular Rapid Communications, 2001. **22**(8): p. 579-582.
22. Lohaus, T., et al., *Drying of supercritical carbon dioxide with membrane processes*. The Journal of Supercritical Fluids, 2015. **98**: p. 137-146.
23. Scholz, M., et al., *Modeling gas permeation by linking nonideal effects*. Industrial and Engineering Chemistry Research, 2013. **52**(3): p. 1079-1088.
24. Technology, A., *ASPEN PLUS User Guide: ASPEN PLUS Release 9*. 1994: Aspen Technology.
25. Carlson, E.C., *Don't gamble with physical properties for simulations*. Chemical Engineering Progress, 1996. **92**(10): p. 35-46.
26. Bamberger, A., G. Sieder, and G. Maurer, *High-pressure (vapor + liquid) equilibrium in binary mixtures of (carbon dioxide + water or acetic acid) at temperatures from 313 to 353 K*. Journal of Supercritical Fluids, 2000. **17**(2): p. 97-110.
27. Briones, J.A., et al., *Ternary phase equilibria for acetic acid-water mixtures with supercritical carbon dioxide*. Fluid Phase Equilibria, 1987. **36**(C): p. 235-246.
28. Coan, C.R. and A.D. King Jr, *Solubility of water in compressed carbon dioxide, nitrous oxide, and ethane. Evidence for hydration of carbon dioxide and nitrous oxide in the gas phase*. Journal of the American Chemical Society, 1971. **93**(8): p. 1857-1862.
29. Dohrn, R., et al., *Experimental measurements of phase equilibria for ternary and quaternary systems of glucose, water, CO<sub>2</sub> and ethanol with a novel apparatus*. Fluid Phase Equilibria, 1993. **83**(0): p. 149-158.
30. D'Souza, R., J.R. Patrick, and A.S. Teja, *HIGH PRESSURE PHASE EQUILIBRIA IN THE CARBON DIOXIDE-n-HEXADECANE AND CARBON DIOXIDE-WATER SYSTEMS*. Canadian Journal of Chemical Engineering, 1988. **66**(2): p. 319-323.
31. Hou, S.X., G.C. Maitland, and J.P.M. Trusler, *Measurement and modeling of the phase behavior of the (carbon dioxide + water) mixture at temperatures from 298.15 K to 448.15 K*. Journal of Supercritical Fluids, 2013. **73**: p. 87-96.
32. Freeman, B., Y. Yampolskii, and I. Pinnau, *Materials Science of Membranes for Gas and Vapor Separation*. 2006: Wiley.
33. Metz, S.J., et al., *Transport of water vapor and inert gas mixtures through highly selective and highly permeable polymer membranes*. Journal of Membrane Science, 2005. **251**(1-2): p. 29-41.
34. *Chemical Engineering*. 05/12/2013; Available from: <http://www.che.com/pci/>.
35. *Internal Revenue Service*. 05/27/2013; Available from: <http://www.irs.gov/Individuals/International-Taxpayers/Yearly-Average-Currency-Exchange-Rates>.
36. *Das Statistik-Portal Statista* 05/27/2013; Available from: <http://de.statista.com/statistik/daten/studie/168571/umfrage/strompreis-fuer-die-industrie-in-deutschland-seit-1998/>.
37. Scholz, M., *Membrane Based Biogas Upgrading Processes*. 2013, PhD Thesis Aachen University.
38. *Kältetechnik-Klimatisierung: Zeitschrift für das gesamte Gebiet der Kälteerzeugung, Kälteanwendung und Klimatisierung*. 1972: C.F. Müller.

39. Biegler, L.T., I.E. Grossmann, and A.W. Westerberg, *Systematic methods of chemical process design*. 1997: Prentice Hall PTR.
40. Hirschberg, H.G., *Handbuch der Verfahrenstechnik und Anlagenbau: Chemie, Technik, Wirtschaftlichkeit ; mit 689 Tabellen*. 1999: Springer.
41. Wiebe, R. *The binary system carbon dioxide-water under pressure*. in *Symposium on Reactions and Equilibria in Chemical Systems under High Pressure, Meeting of the American Chemical Society* Detroit, Michigan, September 9-13, 1940.

## Supporting Information

### Mass balances obtained from the simulations

**Table 6-S1** Mass balances for the simple systems.

| S1                        |                  | Feed   | Retentate | Sweep    | Permeate | Refill/Compressed Refill | Product |
|---------------------------|------------------|--------|-----------|----------|----------|--------------------------|---------|
| <b>Mole flow [kmol/h]</b> |                  | 45.56  | 44.88     | 1.41     | 2.09     | 0.50                     | 45.38   |
| <b>Mole fraction</b>      | CO <sub>2</sub>  | 0.9958 | 0.9998    | 0.99999  | 0.9118   | 0.99999                  | 0.9998  |
|                           | H <sub>2</sub> O | 0.0042 | 0.0002    | 0.00001  | 0.0882   | 0.00001                  | 0.0002  |
| <b>Mass flow [kg/h]</b>   |                  | 2,000  | 1,975     | 62       | 87.10    | 21.77                    | 1,997   |
| <b>Mass fraction</b>      | CO <sub>2</sub>  | 0.9983 | 0.9999    | 0.999996 | 0.9620   | 0.999996                 | 0.9999  |
|                           | H <sub>2</sub> O | 0.0017 | 0.0001    | trace    | 0.0380   | trace                    | 0.0001  |

| S2                        |                  | Feed    | Retentate | Sweep    | Permeate | Refill/Compressed Refill | Product |
|---------------------------|------------------|---------|-----------|----------|----------|--------------------------|---------|
| <b>Mole flow [kmol/h]</b> |                  | 2,278   | 2,244     | 70.44    | 104.24   | 24.60                    | 2,269   |
| <b>Mole fraction</b>      | CO <sub>2</sub>  | 0.9958  | 0.9998    | 0.99999  | 0.9117   | 0.99999                  | 0.9998  |
|                           | H <sub>2</sub> O | 0.0042  | 0.0002    | 0.00001  | 0.0883   | 0.00001                  | 0.0002  |
| <b>Mass flow [kg/h]</b>   |                  | 100,000 | 98,751    | 3,100    | 4,349    | 1,083                    | 99,834  |
| <b>Mass fraction</b>      | CO <sub>2</sub>  | 0.9983  | 0.9999    | 0.999996 | 0.9619   | 0.999996                 | 0.9999  |
|                           | H <sub>2</sub> O | 0.0017  | 0.0001    | trace    | 0.0381   | trace                    | 0.0001  |

| S3                        |                  | Feed    | Retentate | Sweep    | Permeate | Refill/Compressed Refill | Product |
|---------------------------|------------------|---------|-----------|----------|----------|--------------------------|---------|
| <b>Mole flow [kmol/h]</b> |                  | 2,278   | 2,244     | 70.44    | 104.27   | 24.63                    | 2,269   |
| <b>Mole fraction</b>      | CO <sub>2</sub>  | 0.9958  | 0.9998    | 0.99999  | 0.9117   | 0.99999                  | 0.9998  |
|                           | H <sub>2</sub> O | 0.0042  | 0.0002    | 0.00001  | 0.0883   | 0.00001                  | 0.0002  |
| <b>Mass flow [kg/h]</b>   |                  | 100,000 | 98,750    | 3,100    | 4,350    | 1,084                    | 99,834  |
| <b>Mass fraction</b>      | CO <sub>2</sub>  | 0.9983  | 0.9999    | 0.999996 | 0.9619   | 0.999996                 | 0.9999  |
|                           | H <sub>2</sub> O | 0.0017  | 0.0001    | trace    | 0.0381   | trace                    | 0.0001  |
| S4                        |                  | Feed    | Retentate | Sweep    | Permeate | Refill/Compressed Refill | Product |
| <b>Mole flow [kmol/h]</b> |                  | 2,278   | 2,253     | 70.4     | 94.90    | 15.26                    | 2,269   |
| <b>Mole fraction</b>      | CO <sub>2</sub>  | 0.9958  | 0.9998    | 1        | 0.9030   | 1                        | 1       |
|                           | H <sub>2</sub> O | 0.0042  | 0.0002    | trace    | 0.0970   | trace                    | trace   |
| <b>Mass flow [kg/h]</b>   |                  | 100,000 | 99,163    | 3,100    | 3,937    | 671.41                   | 99,834  |
| <b>Mass fraction</b>      | CO <sub>2</sub>  | 0.9983  | 0.99999   | 1        | 0.9579   | 1                        | 1       |
|                           | H <sub>2</sub> O | 0.0017  | 0,0001    | trace    | 0.0421   | trace                    | trace   |
| S5                        |                  | Feed    | Retentate | Sweep    | Permeate | Refill/Compressed Refill | Product |
| <b>Mole flow [kmol/h]</b> |                  | 2,278   | 2,267     | 113.61   | 124.59   | 1.79                     | 2,269   |
| <b>Mole fraction</b>      | CO <sub>2</sub>  | 0.9958  | 0.9998    | 0.99999  | 0.9262   | 0.99999                  | 0.9998  |
|                           | H <sub>2</sub> O | 0.0042  | 0.0002    | 0.00001  | 0.0738   | 0.00001                  | 0.0002  |
| <b>Mass flow [kg/h]</b>   |                  | 100,000 | 99,756    | 5,000    | 5,244    | 78.61                    | 99,834  |
| <b>Mass fraction</b>      | CO <sub>2</sub>  | 0.9983  | 0.9999    | 0.999996 | 0.9684   | 0.999996                 | 0.9999  |
|                           | H <sub>2</sub> O | 0.017   | 0.0001    | trace    | 0.0316   | trace                    | 0.0001  |

**Table 6-S2** Mass balances for the hybrid systems.

| H1                        |                  | Feed    | Ret. 1  | Sweep 1 | Perm. 1   | H <sub>2</sub> O 1 | 1      | H <sub>2</sub> O 2 | 2       | Ret. 2  |
|---------------------------|------------------|---------|---------|---------|-----------|--------------------|--------|--------------------|---------|---------|
| <b>Mole flow [kmol/h]</b> |                  | 45.56   | 43.44   | 2.82    | 4.94      | 0.15               | 4.79   | 0.03               | 4.76    | 4.72    |
| <b>Mole fraction</b>      | CO <sub>2</sub>  | 0.9958  | 0.9998  | 0.9991  | 0.9620    | 0.9966             | 0.9924 | 0.0236             | 0.9987  | 0.9991  |
|                           | H <sub>2</sub> O | 0.0042  | 0.0002  | 0.0009  | 0.0380    | 0.0034             | 0.0076 | 0.9764             | 0.0013  | 0.0009  |
| <b>Mass flow [kg/h]</b>   |                  | 2,000   | 1,912   | 124.21  | 212.69    | 2.75               | 209.94 | 0.58               | 209.36  | 207.67  |
| <b>Mass fraction</b>      | CO <sub>2</sub>  | 0.9983  | 0.99999 | 0.9996  | 0.9841    | 0.0084             | 0.9969 | 0.0558             | 0.9995  | 0.9996  |
|                           | H <sub>2</sub> O | 0.0017  | trace   | 0.0004  | 0.0159    | 0.9916             | 0.0031 | 0.9442             | 0.0005  | 0.0004  |
|                           |                  | Sweep 2 | Perm. 2 | 3       | Rec. Feed | 4                  | 5      | Rec. Sweep         | Sweep   | Product |
| <b>Mole flow [kmol/h]</b> |                  | 0.03    | 0.07    | 1.94    | 1.94      | 2.79               | 2.79   | 2.79               | 0.038   | 45.38   |
| <b>Mole fraction</b>      | CO <sub>2</sub>  | 0.99999 | 0.9703  | 0.9991  | 0.9991    | 0.9991             | 0.9991 | 0.9991             | 0.99999 | 0.9998  |
|                           | H <sub>2</sub> O | 0.00001 | 0.0297  | 0.0009  | 0.0009    | 0.0009             | 0.0009 | 0.0009             | 0.00001 | 0.0002  |
| <b>Mass flow [kg/h]</b>   |                  | 1.4     | 3.09    | 85.14   | 85.14     | 122.52             | 122.52 | 122.52             | 1.69    | 1,997   |
| <b>Mass fraction</b>      | CO <sub>2</sub>  | 0.99999 | 0.9876  | 0.9996  | 0.9996    | 0.9996             | 0.9996 | 0.9996             | 0.99999 | 0.9999  |
|                           | H <sub>2</sub> O | trace   | 0.0124  | 0.0004  | 0.0004    | 0.0004             | 0.0004 | 0.0004             | trace   | 0.0001  |

| H2                        |                  | Feed    | Ret. 1  | Sweep 1 | Perm. 1   | H <sub>2</sub> O 1 | 1      | H <sub>2</sub> O 2 | 2      | Ret. 2  |
|---------------------------|------------------|---------|---------|---------|-----------|--------------------|--------|--------------------|--------|---------|
| <b>Mole flow [kmol/h]</b> |                  | 2,278   | 2,172   | 141.19  | 247.18    | 7.60               | 239.59 | 1.55               | 238.04 | 236.05  |
| <b>Mole fraction</b>      | CO <sub>2</sub>  | 0.9958  | 0.9998  | 0.9991  | 0.9620    | 0.0034             | 0.9924 | 0.0236             | 0.9987 | 0.9991  |
|                           | H <sub>2</sub> O | 0.0042  | 0.0002  | 0.0009  | 0.0380    | 0.9966             | 0.0076 | 0.9764             | 0.0013 | 0.0009  |
| <b>Mass flow [kg/h]</b>   |                  | 100,000 | 95,576  | 6,211   | 10,634    | 137.54             | 10,497 | 28.89              | 10,468 | 10,383  |
| <b>Mass fraction</b>      | CO <sub>2</sub>  | 0.9993  | 0.9999  | 0.9996  | 0.9841    | 0.0084             | 0.9969 | 0.0558             | 0.9995 | 0.9996  |
|                           | H <sub>2</sub> O | 0.0017  | 0.1111  | 0.0004  | 0.0159    | 0.9916             | 0.0031 | 0.9442             | 0.0005 | 0.0004  |
|                           |                  | Sweep 2 | Perm. 2 | 3       | Rec. Feed | 4                  | 5      | Rec. Sweep         | Sweep  | Product |
| <b>Mole flow [kmol/h]</b> |                  | 1.59    | 3.57    | 96.78   | 96.78     | 139.27             | 139.27 | 139.27             | 1.92   | 2,269   |
| <b>Mole fraction</b>      | CO <sub>2</sub>  | 1.0000  | 0.9703  | 0.9991  | 0.9991    | 0.9991             | 0.9991 | 0.9991             | 1.0000 | 0.9998  |
|                           | H <sub>2</sub> O | 0.0000  | 0.0297  | 0.0009  | 0.0009    | 0.0009             | 0.0009 | 0.0009             | 0.0000 | 0.0002  |
| <b>Mass flow [kg/h]</b>   |                  | 70.00   | 154.51  | 4,257   | 4,257     | 6,126              | 6,126  | 6,126              | 84.50  | 99,834  |
| <b>Mass fraction</b>      | CO <sub>2</sub>  | 1.0000  | 0.9876  | 0.9996  | 0.9996    | 0.9996             | 0.9996 | 0.9996             | 1.0000 | 0.9999  |
|                           | H <sub>2</sub> O | 0.0000  | 0.0124  | 0.0004  | 0.0004    | 0.0004             | 0.0004 | 0.0004             | 0.0000 | 0.0001  |



| H3                        |                  | Feed    | Ret. 1  | Sweep 1 | Perm. 1   | H <sub>2</sub> O 1 | 1      | H <sub>2</sub> O 2 | 2      | Ret. 2  |
|---------------------------|------------------|---------|---------|---------|-----------|--------------------|--------|--------------------|--------|---------|
| <b>Mole flow [kmol/h]</b> |                  | 2,278   | 2,172   | 141.19  | 247.18    | 7.60               | 239.59 | 1.55               | 238.04 | 236.05  |
| <b>Mole fraction</b>      | CO <sub>2</sub>  | 0.9958  | 0.9998  | 0.9991  | 0.9620    | 0.0034             | 0.9924 | 0.0236             | 0.9987 | 0.9991  |
|                           | H <sub>2</sub> O | 0.0042  | 0.0002  | 0.0009  | 0.0380    | 0.9966             | 0.0076 | 0.9764             | 0.0013 | 0.0009  |
| <b>Mass flow [kg/h]</b>   |                  | 100,000 | 95,576  | 6,211   | 10,634    | 137.54             | 10,497 | 28.89              | 10,468 | 10,383  |
| <b>Mass fraction</b>      | CO <sub>2</sub>  | 0.9983  | 0.9999  | 0.9996  | 0.9841    | 0.0084             | 0.9969 | 0.0558             | 0.9995 | 0.9996  |
|                           | H <sub>2</sub> O | 0.0017  | 0.0001  | 0.0004  | 0.0159    | 0.9916             | 0.0031 | 0.9442             | 0.0005 | 0.0004  |
|                           |                  | Sweep 2 | Perm. 2 | 3       | Rec. Feed | 4                  | 5      | Rec. Sweep         | Sweep  | Product |
| <b>Mole flow [kmol/h]</b> |                  | 1.59    | 3.57    | 96.78   | 96.78     | 139.27             | 139.27 | 139.27             | 1.92   | 2,269   |
| <b>Mole fraction</b>      | CO <sub>2</sub>  | 1.0000  | 0.9703  | 0.9991  | 0.9991    | 0.9991             | 0.9991 | 0.9991             | 1.0000 | 0.9998  |
|                           | H <sub>2</sub> O | 0.0000  | 0.0297  | 0.0009  | 0.0009    | 0.0009             | 0.0009 | 0.0009             | 0.0000 | 0.0002  |
| <b>Mass flow [kg/h]</b>   |                  | 70.00   | 154.51  | 4,257   | 4,257     | 6,126              | 6,126  | 6,126              | 84.50  | 99,834  |
| <b>Mass fraction</b>      | CO <sub>2</sub>  | 1.0000  | 0.9876  | 0.9996  | 0.9996    | 0.9996             | 0.9996 | 0.9996             | 1.0000 | 0.9999  |
|                           | H <sub>2</sub> O | 0.0000  | 0.0124  | 0.0004  | 0.0004    | 0.0004             | 0.0004 | 0.0004             | 0.0000 | 0.0001  |

| H4                 |                  | Feed    | Ret. 1  | Sweep 1 | Perm. 1   | H <sub>2</sub> O 1 | 1      | H <sub>2</sub> O 2 | 2      | Ret. 2  |
|--------------------|------------------|---------|---------|---------|-----------|--------------------|--------|--------------------|--------|---------|
| Mole flow [kmol/h] |                  | 2,278   | 2,123   | 208.06  | 362.71    | 7.02               | 355.70 | 2.30               | 353.39 | 350.46  |
| Mole fraction      | CO <sub>2</sub>  | 0.9958  | 0.9999  | 0.9990  | 0.9733    | 0.0043             | 0.9924 | 0.0236             | 0.9987 | 0.9990  |
|                    | H <sub>2</sub> O | 0.0042  | 0.0001  | 0.0010  | 0.0267    | 0.9957             | 0.0076 | 0.9764             | 0.0013 | 0.0010  |
| Mass flow [kg/h]   |                  | 100,000 | 93,440  | 9,151   | 15,711    | 127.23             | 15,584 | 42.89              | 15,541 | 15,415  |
| Mass fraction      | CO <sub>2</sub>  | 0.9983  | 1.0000  | 0.9996  | 0.9889    | 0.0103             | 0.9969 | 0.0558             | 0.9995 | 0.9996  |
|                    | H <sub>2</sub> O | 0.0017  | 0.0000  | 0.0004  | 0.0111    | 0.9897             | 0.0031 | 0.9442             | 0.0005 | 0.0004  |
|                    |                  | Sweep 2 | Perm. 2 | 3       | Rec. Feed | 4                  | 5      | Rec. Sweep         | Sweep  | Product |
| Mole flow [kmol/h] |                  | 1.07    | 4.00    | 143.69  | 143.69    | 206.77             | 206.77 | 206.77             | 1.29   | 2,267   |
| Mole fraction      | CO <sub>2</sub>  | 1.0000  | 0.9704  | 0.9990  | 0.9990    | 0.9990             | 0.9990 | 0.9990             | 1.0000 | 0.9999  |
|                    | H <sub>2</sub> O | 0.0000  | 0.0296  | 0.0010  | 0.0010    | 0.0010             | 0.0010 | 0.0010             | 0.0000 | 0.0001  |
| Mass flow [kg/h]   |                  | 46.90   | 172.93  | 6,320   | 6,320     | 9,095              | 9,095  | 9,095              | 56.60  | 99,760  |
| Mass fraction      | CO <sub>2</sub>  | 1.0000  | 0.9877  | 0.9996  | 0.9996    | 0.9996             | 0.9996 | 0.9996             | 1.0000 | 0.9999  |
|                    | H <sub>2</sub> O | 0.0000  | 0.0123  | 0.0004  | 0.0004    | 0.0004             | 0.0004 | 0.0004             | 0.0000 | 0.0001  |
| H5                 |                  | Feed    | Ret. 1  | Sweep 1 | Perm. 1   | H <sub>2</sub> O 1 | 1      | H <sub>2</sub> O 2 | 2      | Ret. 2  |
| Mole flow [kmol/h] |                  | 2,278   | 2,220   | 181.98  | 239.59    | 7.70               | 231.9  | 1.50               | 230.39 | 229.38  |
| Mole fraction      | CO <sub>2</sub>  | 0.9958  | 0.9998  | 0.9990  | 0.9606    | 0.0034             | 0.9990 | 0.0236             | 0.9987 | 0.9990  |
|                    | H <sub>2</sub> O | 0.0042  | 0.0002  | 0.0010  | 0.0394    | 0.9966             | 0.0010 | 0.9764             | 0.0013 | 0.0010  |
| Mass flow [kg/h]   |                  | 100,000 | 97,705  | 8,004   | 10,299    | 139.32             | 10,160 | 27.96              | 10,132 | 10,089  |
| Mass fraction      | CO <sub>2</sub>  | 0.9983  | 0.9999  | 0.9996  | 0.9835    | 0.0082             | 0.9996 | 0.0558             | 0.9995 | 0.9996  |
|                    | H <sub>2</sub> O | 0.0017  | 0.0001  | 0.0004  | 0.0165    | 0.9917             | 0.0004 | 0.9442             | 0.0005 | 0.0004  |
|                    |                  | Sweep 2 | Perm. 2 | 3       | Rec. Feed | 4                  | 5      | Rec. Sweep         | Sweep  | Product |
| Mole flow [kmol/h] |                  | 1.59    | 2.61    | 49.32   | 49.32     | 180.06             | 180.06 | 180.06             | 1.92   | 2,270   |
| Mole fraction      | CO <sub>2</sub>  | 1.0000  | 0.9701  | 0.9990  | 0.9990    | 0.9990             | 0.9990 | 0.9990             | 1.0000 | 0.9998  |
|                    | H <sub>2</sub> O | 0.0000  | 0.0299  | 0.0010  | 0.0010    | 0.0010             | 0.0010 | 0.0010             | 0.0000 | 0.0002  |
| Mass flow [kg/h]   |                  | 70.00   | 112.70  | 2,169   | 2,169     | 7,920              | 7,920  | 7,920              | 84.50  | 99,875  |
| Mass fraction      | CO <sub>2</sub>  | 1.0000  | 0.9876  | 0.9996  | 0.9996    | 0.9996             | 0.9996 | 0.9996             | 1.0000 | 0.9999  |
|                    | H <sub>2</sub> O | 0.0000  | 0.0124  | 0.0004  | 0.0004    | 0.0004             | 0.0004 | 0.0004             | 0.0000 | 0.0001  |



# Chapter 7

## Conclusions and Outlook

In the process of dehydration of compressed carbon dioxide, several technical and economic challenges have to be overcome. Within this context, membrane technology is considered a potential commercially competitive alternative for the zeolite adsorbents that are currently used [1]. To assess the potential of membrane technology in dehydration of compressed carbon dioxide, comprehensive research is required that covers a variety of aspects, ranging from membrane material science to process design. This thesis aims to identify and investigate a number of essential aspects of membrane-based dehydration processes. Findings, results, and conclusions are condensed in this last chapter, and suggestions for further research are provided.

## 7.1 Conclusions

### 7.1.1 Intrinsic properties of thin SPEEK films and their implication on swelling behavior in high water activity systems

**Chapter 2** covers intrinsic properties of thin SPEEK films that are relevant for membrane applications. The SPEEK films exhibit optical anisotropy that implies orientations of the polymer chains. Such molecular orientations are associated with internal stresses in a material that will have an impact on the performance of the material in a molecular separation. A variety of experiments have been devoted to the relations between the stresses in the thin SPEEK films and the synthesis method/conditions. The thin films have been prepared via spin-coating and solution deposition. These two methods imply different forces imposed on the polymer chains during film formation. Spin-coating has been done from either methanol or ethanol solutions containing 3, 5 or 7 wt% of SPEEK, and at spin speeds of 1000 – 4000 rpm. In solution deposition technique, the film is formed without spinning, using either the highly volatile methanol or the non-volatile *N*-methylpyrrolidone (NMP).

The SPEEK films are found to be preferentially oriented parallel to the surface of a film, more or less independently of the spin-coating conditions. The optical anisotropy is also not affected by whether methanol or ethanol is used as solvent. Variations in the optical anisotropy are only observed for relatively high concentrations of SPEEK ( $\geq 5$  wt%) combined with low spin speeds (2000 rpm). After one year storage, the spin-coated films still exhibit optical anisotropy. Films formed by solution deposition using methanol as solvent, are also found to exhibit orientations in the in-plane direction, with values of optical anisotropy that are

comparable to the spin-coated films. Bulk SPEEK membranes were found to be preferentially oriented in the in-plane direction elsewhere [2]. These observations substantiate that the molecular orientations in SPEEK films do not originate from hydrodynamic or other forces imposed in the formation procedure. As a consequence, the orientations, and hence internal stresses, are inherent to thin films of this sulfonated polymer and cannot be prevented in a straightforward manner.

The internal stresses in SPEEK films can be released only upon sorption of water and consequently, plasticization of the material. Upon the removal of the water, the internal stresses re-establish. Prior to thermal conditions, NMP-derived SPEEK films are isotropic. Yet the anisotropy of these films returns upon progressive removal of the NMP by heat treatment from 30 to 140 °C. For the alcohol-derived films, a temperature of 140 °C has no impact on film properties as compared to 30 °C.

**Chapter 3** describes the relation between internal stresses present in a film and the swelling behavior of the film in liquid water. Also the effects of the presence of water during film formation on the final molecular assembly in SPEEK is discussed. It is found that distinct molecular arrangements occur in SPEEK films when formed in either a humid or a dry atmosphere.

The water-induced swelling of SPEEK films which are formed in a humid atmosphere shows overshoot swelling dynamics. These dynamics are correlated with the optical anisotropy of the film. Films that exhibit lower anisotropy prior to the exposure to liquid water swell less in water, as compared to films with an equal degree of sulfonation, but with more pronounced initial anisotropy. We ascribe this correlation to two phenomena. Firstly, the optical anisotropy in a film is directly dependent on the ambient relative humidity degree, and therefore, on the water vapor absorbed from the ambient by this film. The higher initial concentration of water vapor in the film prior to swelling causes a pre-saturation of this film with water molecules. Therefore, a subsequent swelling upon contact with liquid water is less apparent for such film. Secondly, the optical anisotropy corresponds to internal stresses in the film that affect the free energy of the film, and hence its potential to swell. In essence, a higher optical anisotropy corresponds to more residual stresses, and thus a higher free energy status, which results in more pronounced swelling. Combined, both effects cause that films with higher initial values of the anisotropy exhibit a higher propensity to swell.

A particular swelling behavior has been observed for films that were deprived of water during formation. This is attributed to a specific internal molecular structure of SPEEK that is generated due to lack of the hydration of the polymer during membrane formation. The dependency of molecular arrangements in SPEEK on humidity/dryness during formation has been described elsewhere [3], and another study explains that the removal of water from SPEEK membranes enables formation of attractive non-covalent interactions between the benzene rings, termed as  $\pi$ - $\pi$  stacking, that fade upon polymer rehydration [4]. Our research shows that in the case when water is removed specifically during formation step, the stacking of aromatic rings in SPEEK films is partially irreversible. SPEEK films formed at relative humidity degree,  $RH=0$  %, swell considerably less than their counterparts, prepared in an identical manner except for humidity conditions ( $RH \geq 20$  %). This finding is of importance since the benzene stacking is associated with a crystalline structure [5] and such structures will affect membrane performances; it is relatively impermeable but in general enhances membrane stability [6].

**Chapter 5** presents a possible method to chemically modify SPEEK membranes. It is apparent from Chapter 3 that native SPEEK films require stabilization. Distinct swelling of those films, in spite of their equal degree of sulfonation, and high internal stresses in a material, which cannot be eliminated, can result in unstable membrane performance (e.g., swelling affects selectivity) and propensity of the films to swell excessively. Chemical modification of inherently stressed polymers is a way to irreversibly affect material properties [7]. Chemical modification of SPEEK was accomplished by adding polyols, ethylene glycol or glycerol, to the casting solutions, and thermal treatment of membranes formed from those solutions. This procedure has been described elsewhere for grafting of polyols on sulfonic acid groups [8]. The modification was systematically studied for both polyols in equal conditions to compare their effectiveness, with the polyol/SPEEK molar ratio between 0.5 – 7 and using anhydrous methanol as a casting solvent.

In glycerol-modified membranes with the glycerol/SPEEK molar ratio  $>1$ , the glass transition temperature was significantly reduced as compared to native membranes, which was measured using DSC on bulk membranes. The modified thin films exhibited significantly reduced optical anisotropy. Those films were also less susceptible to water-induced swelling, and no longer exhibited overshoot swelling dynamics, but positive relaxations. The extent of swelling, expressed by the time dependent swelling factor, is found to be reproducible for

glycerol-derived films, and is found similar for the films with the molar ratio of 2, 3 or 7. The effects on ethylene glycol-derived membranes and films in the same experiments were less apparent.

The results imply that the chemical modification of SPEEK using polyols can stabilize membranes from this material, and the sufficient polyol concentration can be adjusted. The moderate swelling of glycerol-modified films is likely caused by the reduced number of sulfonic acid groups, and hence the reduced affinity for water. The effect cannot be ascribed to the improvement of mechanical properties, because the glass transition temperature of the membranes is actually reduced.

The onset of thermal degradation, for both ethylene glycol- and glycerol-derived membranes, is shifted towards lower temperatures, as compared to native SPEEK. A more detailed characterization of thermal stability of native SPEEK is described in Chapter 4.

### 7.1.2 Thermal stability of SPEEK

**Chapter 4** compares the thermal stability of SPEEK films with two distinct counterions: proton (SPEEK-H) and sodium (SPEEK-Na). Films are exposed to elevated temperatures for shorter and longer periods. Exchanging the proton by a sodium ion significantly enhances the thermal stability of sulfonated polymers.

Short-term heating of bulk SPEEK membranes, performed using TGA-MS, initiated degradation accompanied with the release of SO<sub>2</sub> at ~ 250 °C for the H-form and by 100 °C higher for the Na-form. On the other hand, long term exposure (15 hours) of the proton form to temperatures as low as 160 °C also induced polymer degradation, with more pronounced changes when exceeding 200 °C. The chemical changes occurring in membranes that are exposed to long-term treatment, have been tracked using the <sup>1</sup>H-NMR and ATR-FTIR techniques. Degradation of bulk SPEEK membranes can be inspected visually. SPEEK-H membranes are yellowish and develop some chromophoric groups upon thermally-induced changes; here, the membranes treated at 190 °C turned red. At the same temperature of 190 °C, the colorless SPEEK-Na membranes remained unchanged in term of visible color.

Thin SPEEK films, coated on a silicon wafer, possess a variety of colors due to light interference effect with a substrate. The thermal evolution of thin SPEEK films can be inspected by tracking the UV-Vis absorption spectrum of the material via thermo-ellipsometric



analysis (TEA). The results regarding thermally induced changes in thin films are in line with those of bulk membranes. Long-term exposure of thin films to temperatures as low as 160 °C caused changes in the UV-Vis absorption spectra of SPEEK-H, and no changes in the SPEEK-Na spectrum. At a treatment temperature of 220 °C, the differences between the proton and sodium forms were more pronounced. For H-SPEEK, light absorption increases over nearly the full wavelength range, and strong changes occur around 380 nm. For Na-SPEEK, the changes in the spectrum are limited to minor changes in the absorption in the 300 – 400 nm wavelength range.

Exchanging sodium for proton indicates the prolonged thermal stability of thin films and bulk membranes certainly up to ~ 220 °C, which have a positive implication of membrane post-treatment, for instance, for the removal of high boiling point casting solvents.

### 7.1.3 Process design

**Chapter 6** presents Aspen Plus<sup>®</sup> simulations of dehydration of supercritical carbon dioxide using a membrane unit. Two types of systems have been simulated: (1) Simple - without a recirculation of the permeate stream and consequently, with CO<sub>2</sub> emissions to the atmosphere; (2) Hybrid - with a recirculation of the permeate stream, in which water from the permeate is removed by condensation (due to compression and cooling), and via an additional membrane unit. For both types of systems, the membrane permeance and selectivity have been varied.

It is not straight forward which system type is superior. In this research, the economic viability of the systems is considered based on the duration of the dehydration process and the size of the feed. For hybrid systems, the recirculation and regeneration of the permeate requires high investment and operating costs for compressors. On the other hand, simple systems can be considered environmentally unfriendly and have high operating costs, caused by the high CO<sub>2</sub> emissions. In general, for a pilot plant with low feed stream (2,000 kg/h), the investments in recirculation are not beneficial up to 3.5 years of operation. For the higher feed stream process, (100,000 kg/h), the investments in recirculation is sensible when operating for longer than 1 year.

In hybrid systems, with a currently reported water permeance of 5000 GPU, the membrane costs comprise ~20 % of all costs. Assuming very high water permeance of 250,000

GPU, the membrane costs would be very minor. Still, the rest of the costs comes from the energy demanding compressors. Variation of membrane selectivity in the range 3,000 – 10,000 does not strongly impact the economics of the process, because these variations affect other parameters in the process, ultimately resulting in similar process costs. For the simple systems, a significant reduction of the CO<sub>2</sub> flow through the membrane (at selectivity of 25,000) can significantly reduce process costs, because a lower refill stream to compensate the CO<sub>2</sub> losses from the retentate is in such case required.

## 7.2 Outlook

Here, an outlook is presented with some suggestions for future research. Process design and membrane properties are correlated. In fact, viable process designs will impose requirements with respect to membrane performance. In this context, the outlook starts with a discussion on process design.

### 7.2.1 Membrane development based on process design

#### 1) Recirculation and regeneration of the permeate from Chapter 6

For materials scientists, it could be more interesting to try to improve the selectivity rather than water permeance. We have shown that significant reduction of the CO<sub>2</sub> flow through the membrane reduces the demand for the refill stream. Moreover, concentration polarization effects may limit the actual permeance of water. In this respect, a reduction of the membrane price can be advantageous. If concentration polarization is the limiting factor, other hydrophilic polymeric materials that are cheaper and involve less issues with respect to internal stresses, can be an option.

In addition, the effects of rapid depressurization and phase changes of compressed carbon dioxide on membranes should be addressed, as these can cause membrane foaming and lead to other material defects.

## 2) Removal of water from the permeate by liquid absorption

Absorption dehydration using diethylene glycol or triethylene glycol is used to remove water from the natural gas [9]. Glycols are put in a contact with a wet gas stream to absorb water. Afterwards, the glycols are regenerated by heating such that water, which has much lower boiling temperature than glycols, evaporates. Such approach could be an alternative way to regenerate the permeate in the process of carbon dioxide dehydration, instead of water condensation by compression and cooling, as it has been simulated in Chapter 6.

Alternatively, a hydrophilic absorbing liquid could be pressurized and brought semi-directly into contact with the feed, by implementing a membrane contactor between the two phases. In such configuration, the undesired usage of a sweep gas is avoided and there is no real need for a pressure difference over the membrane, which enhances membrane stability. The membrane properties would need to be adjusted, for instance, to prevent the diffusion of the absorbing liquid to the retentate side. Low solubility of carbon dioxide in an absorbing liquid could facilitate high water/carbon dioxide selectivity.

### 7.2.2 Fundamental research on SPEEK

Further fundamental research on the anisotropy and molecular orientations, especially on benzene stacking in SPEEK or other sulfonated polymers would contribute to better understanding of those phenomena. (Non)crystallinity influences mechanical properties of polymers and internal stresses affect membrane permeance [10]. For scientist starting the research involving SPEEK membranes, it is advised to accurately control humidity and temperature conditions at which membranes are formed and exposed to. Additionally, it is advised to synthesize SPEEK from monomers, rather than from sulfonation of PEEK, such that the degree of sulfonation is homogenous. Treatment of PEEK with sulfuric acid, generates a polymer that is relatively inhomogeneously sulfonated; this can lead to discrepancies in results.

## References

1. Lohaus, T., et al., *Drying of supercritical carbon dioxide with membrane processes*. The Journal of Supercritical Fluids, 2015. **98**: p. 137-146.
2. Reyna-Valencia, A., S. Kaliaguine, and M. Bousmina, *Structural and mechanical characterization of poly(ether ether ketone) (PEEK) and sulfonated PEEK films: Effects of thermal history, sulfonation, and preparation conditions*. Journal of Applied Polymer Science, 2006. **99**(3): p. 756-774.
3. Zhang, Y., et al., *Proton conductivity enhancement by nanostructural control of sulphonated poly(ether ether ketone) membranes*. International Journal of Hydrogen Energy, 2010. **35**(15): p. 8337-8342.
4. Jarumaneeroj, C., K. Tashiro, and S. Chirachanchai, *Shifting from hydrogen bond network to  $\pi$ - $\pi$  Stacking: A key mechanism for reversible thermochromic sulfonated poly(ether ether ketone)*. Macromolecular Rapid Communications, 2014. **35**(16): p. 1397-1401.
5. Dahl, T., *The Nature of Stacking Interactions between Organic Molecules Elucidated by Analysis of Crystal Structures*. Acta Chemica Scandinavica, 1994. **48**: p. 96-106.
6. Freeman, B., Y. Yampolskii, and I. Pinnau, *Materials Science of Membranes for Gas and Vapor Separation*. 2006: Wiley.
7. Zhang, Z., et al., *Novel approach to reducing stress-caused birefringence in polymers*. Journal of Materials Science, 2004. **39**(4): p. 1415-1417.
8. Mikhailenko, S.D., et al., *Properties of PEMs based on cross-linked sulfonated poly(ether ether ketone)*. Journal of Membrane Science, 2006. **285**(1-2): p. 306-316.
9. *Processing Natural Gas*. [cited 2015 23 March]; Available from: <http://naturalgas.org/naturalgas/processing-ng/>.
10. Huang, Y. and D.R. Paul, *Physical aging of thin glassy polymer films monitored by gas permeability*. Polymer, 2004. **45**(25): p. 8377-8393.



# Summary

In this thesis, the properties of thin films from highly sulfonated poly(ether ether ketone) (SPEEK) have been investigated within the context of their application as membranes for the dehydration of compressed carbon dioxide. Spectroscopic ellipsometry has been used as the predominant measurement technique. The relationships between the presence of water during film formation and final film properties have been investigated, as well as the water-induced dynamic swelling and changes in molecular orientations of the final films. Additionally, the feasibility of using composite hollow fibers in the dehydration of compressed carbon dioxide has been evaluated with simulations in Aspen Plus<sup>®</sup>.

**Chapter 1** explains why there is an interest to dehydrate carbon dioxide with membrane technology. Despite the potential of membranes in this process, some difficulties are involved and require research. Although a good performance of membranes in molecular separation is a prerequisite, the membrane stability and integrity in harsh process conditions are decisive for the applicability of the membrane. In the case of strongly hydrophilic polymers, such as SPEEK, a high water activity in compressed carbon dioxide can be detrimental for this material. Additionally, the removal of water from the permeate side to maintain high driving force for water permeation is challenging from the economic point of view.

**Chapter 2** starts with the investigation of optical anisotropy in thin SPEEK films. Optical anisotropy indicates the presence of internal stresses in a material. The experiments conclusively show that SPEEK films are always anisotropic and therefore, have inherent internal stresses. This is independent on formation procedures or solvent used. The stresses can be reversibly relieved via plasticization by sorbents, such as water vapor from the ambient or residual organic solvents. The relief of stresses is manifested by a reduction in value of the optical anisotropy. Upon removal of the plasticizer, the anisotropy is restored.

**Chapter 3** assesses the impact of optical anisotropy in thin SPEEK films on swelling experiments in liquid water. The experiments revealed that swelling, at the particular temperature, of SPEEK films (coated in a humid atmosphere) with an equal degree of sulfonation, can be dissimilar. This divergence was found to be dependent on the anisotropy in the material. Films with higher initial optical anisotropy prior to swelling swell more than films with lower initial anisotropy. A distinct swelling behavior has been observed for SPEEK films that were coated in absolutely dry atmosphere. In those films, a stacking of benzene rings ( $\pi$ - $\pi$  stacking) is induced and results in an irreversible, significantly lower propensity to swelling.

**Chapter 4** focuses on thermal behavior of SPEEK films and thermal stability at relatively high temperatures (160 – 220 °C). Additionally, the thermal stability has been investigated for films, in which the protons in the sulfonic acid groups were exchanged with sodium ions. Results showed that a sodium counter-ions strongly impedes the desulfonation of the material, as protodesulfonation can no longer occur. No thermally-induced changes have been observed for SPEEK-sodium films when these are heated up to 220 °C for 15 hours. In contrast, SPEEK-proton films that are heated up to only 160 °C for 15 hours exhibit significant decomposition.

**Chapter 5** aims at chemical modification of SPEEK films to control and suppress penetrant-induced swelling. Aliphatic polyols, i.e., ethylene glycol and glycerol, were grafted on the sulfonic acid groups via a thermally activated reaction. The effect of reduced and controlled swelling in water (comparing to pure SPEEK films) is more apparent for glycerol-modified films than for ethylene glycol-modified ones. For glycerol-modified films, a depression in the glass transition temperature and in the optical anisotropy has been detected. This implies that the films are internally plasticized and not structurally reinforced. This result is indicative that reduced swelling of SPEEK films can be achieved by chemical modification at the cost of sulfonic acid groups, primarily reducing the tendency of the polymer to take up water.

**Chapter 6** reports Aspen Plus<sup>®</sup> simulations of the dehydration of supercritical carbon dioxide using a hollow fiber membrane module, and an economic evaluation based on these simulations. The choice of a feasible method to remove water from the permeate side is challenging. Here, the usage of a sweep gas (carbon dioxide) has been investigated. The application of a membrane unit itself is considered promising (compared to currently used zeolites adsorbents to dehydrate carbon dioxide). But the release of the sweep to the atmosphere is more or less impossible; it would imply significant losses of this gas and consequently, high operating costs. On the other hand, recirculation of the sweep and its regeneration can be also financially unattractive. Additional equipment, such as compressors and condensers, studied in this chapter to recirculate and recover the sweep gas, are also energy consuming and require high investment costs.

**Chapter 7** presents the conclusions from the experimental chapters and provides derived recommendations. It is advised to focus on SPEEK with reduced predisposition to swell. From a scientific point of view, it is interesting to analyze further the anisotropy-related



thermodynamic of swelling and the stacking of aromatic rings. The latter one has direct implication on membrane properties. Additionally, the impact of fast depressurization and phase changes of compressed carbon dioxide on membranes should be investigated, as well as alternative methods to remove water from the permeate side, in the process of the carbon dioxide dehydration.





# Samenvatting

In deze dissertatie zijn de eigenschappen van dunne films, gemaakt van hoog gesulfoneerd poly(ether ether keton) (SPEEK) onderzocht, binnen de context van hun toepasbaarheid als membraan voor de ontwatering van gecompriëerd CO<sub>2</sub>. Spectroscopische ellipsometrie is gebruikt als voornaamste meetmethode. De relatie tussen de aanwezigheid van water tijdens de filmformatie en de uiteindelijke filmeigenschappen zijn onderzocht, als mede de door water geïnduceerde zwellen en de veranderingen in de moleculaire oriëntatie van de uiteindelijke films. Ook is de toepasbaarheid van het gebruik van composiet holle vezels voor de ontwatering van gecompriëerd CO<sub>2</sub> geëvalueerd met simulaties in Aspen Plus®.

**Hoofdstuk 1** verklaart waarom er een interesse is voor de ontwatering van CO<sub>2</sub> met membraantechnologie. Ondanks de potentie van membranen in dit proces, gaan er nog moeilijkheden mee gepaard die onderzoek vereisen. Hoewel een goede prestatie van de membranen voor het scheidingsproces een vereiste is, zijn de membraanstabieleit en integriteit tijdens extreme procescondities beslissend voor de toepasbaarheid van de membranen. In het geval van zeer hydrofiele polymeren, zoals SPEEK, is een hoge water activiteit schadelijk voor het materiaal. Bovendien is het vanuit een economisch oogpunt uitdagend om het water aan de permeaat zijde te verwijderen, zodat een hoge drijvende kracht behouden kan blijven.

**Hoofdstuk 2** begint met het onderzoek van optische anisotropie in dunne SPEEK films. Optische anisotropie wijst op interne stress in het materiaal. Uit de experimenten kan men concluderen dat SPEEK films altijd anisotropisch zijn en dus inherent interne stress bevatten. Dit is onafhankelijk van de formatieprocedure of het oplosmiddel dat gebruikt is. De stress kan reversibel verminderd worden door plastificering door oplosmiddelen, zoals waterdamp uit de omgeving, of resterende organische oplosmiddelen. De stressverlichting uit zich door een reductie in de optische anisotropie waarde. Wanneer de plastificerende stof weer verwijderd wordt, keert de anisotropie terug naar de originele waarde.

**Hoofdstuk 3** evalueert de impact van optische anisotropie in dunne SPEEK films met zwellingsexperimenten in vloeibaar water. De experimenten tonen aan dat de zwellen van SPEEK films (gecoat in een vochtige omgeving), bij een bepaalde temperatuur en met een gelijke sulfonatiegraad, verschillend kunnen zijn. Deze afwijking was afhankelijk van de anisotropie van het materiaal. Films met een initieel hogere optische anisotropie voor de zwellingsexperimenten zwellen meer dan films met een initieel lagere anisotropie. Een

duidelijk verschil in het zwellingsgedrag is waargenomen bij SPEEK films die gecoat zijn in absoluut droge condities. In deze films vindt een opeenstapeling van benzeenringen plaats ( $\pi$ - $\pi$  stacking), wat resulteert in een onomkeerbare en significant lagere neiging tot zwelling.

**Hoofdstuk 4** focust op het thermisch gedrag van SPEEK films en de thermische stabiliteit bij relatief hoge temperaturen (160 – 220 °C). Ook is de thermische stabiliteit onderzocht van films waarbij de protonen van de sulfonzuurgroep zijn uitgewisseld met natriumionen. De resultaten laten zien dat natriumionen de desulfonering van het materiaal sterk belemmeren, aangezien protondesulfonatie niet langer kan plaatsvinden. Er zijn geen thermisch geïnduceerde veranderingen waargenomen voor SPEEK-natrium films wanneer deze zijn verhit tot 220 °C gedurende 15 uren. Dit in tegenstelling tot SPEEK-proton films die significante decompositie ondergaan wanneer deze verhit worden tot slechts 160 °C gedurende 15 uur.

**Hoofdstuk 5** probeert de chemische modificatie van SPEEK films te controleren en de penetrant geïnduceerde zwelling te onderdrukken. Alifatische polyolen, zoals ethyleenglycol en glycerol zijn gegrift aan de sulfonzuurgroep via een thermische activatiereactie. Het effect van verminderde en gecontroleerde zwelling in water (in vergelijking tot pure SPEEK films) is meer aanwezig voor glycerol gemodificeerde films dan voor de ethyleenglycol gemodificeerde films. Bij de glycerol gemodificeerde film is een verlaging in de glasovergangstemperatuur en in de optische anisotropie waargenomen. Dit impliceert dat de films intern geplastificeerd zijn en niet structureel verstrekt. Dit resultaat toont aan dat een gereduceerde zwelling van SPEEK films bereikt kan worden door chemische modificatie, ten koste van de sulfonzuurgroep, waarbij voornamelijk de neiging van het polymeer om water op te nemen, verminderd wordt.

**Hoofdstuk 6** rapporteert Aspen Plus<sup>®</sup> simulaties van de ontwatering van superkritisch CO<sub>2</sub> in een holle vezel module en de hierop gebaseerde economische evaluatie. De keus van een geschikte methode om water aan de permeaatzijde te verwijderen is uitdagend. Hiervoor is het gebruik van een veeggas (CO<sub>2</sub>) onderzocht. De applicatie van een membraanmodule zelf wordt als veel belovend beschouwd (in vergelijking tot de huidige gebruikte zeoliet absorbeers om CO<sub>2</sub> te ontwateren). Toch is het vrijlaten van het veeggas in de atmosfeer min of meer onmogelijk; Dit zou een significant verlies van dit gas impliceren en daar gaan hoge kosten mee gepaard. Aan de andere kan recirculatie van het veeggas en de regeneratie ook financieel onaantrekkelijk zijn. Additionele apparatuur, zoals compressoren en

condensatoren die bestudeerd zijn in dit hoofdstuk om het veeggas te recirculeren en terug te winnen, kosten ook energie en vereisen hoge investeringskosten.

**Hoofdstuk 7** presenteert de conclusies van de experimentele hoofdstukken en geeft afgeleide aanbevelingen. Het is aangeraden om de focus te leggen op SPEEK met een gereduceerde aanleg tot zwelling. Vanuit een wetenschappelijk oogpunt is het interessant om de anisotropie gerelateerde thermodynamica van zwelling en de opeenstapeling van benzeenringen verder te analyseren. Dit laatste heeft een directe implicatie op de membraaneigenschappen. Ook zou de invloed van een snelle vermindering van de druk en de faseovergang van gecomprimeerd CO<sub>2</sub> op membranen onderzocht moeten worden, evenals een alternatieve methode om water te verwijderen aan de permeaatzijde voor het CO<sub>2</sub> ontwateringsproces.







# Acknowledgements



I really enjoyed my PhD time, both the working and the social part. I have never questioned the decision to join the membrane group of the University of Twente, especially now ☺. Any difficulty just brought me a valuable experience. I would like to start my acknowledgements in more or less chronological order.

I would like to thank Wojciech Ogieglo, from who I found out about my future PhD position in, at that time, MTG group. Wojciech and Joanna Ogieglo strongly encouraged me to apply for this position and gave valuable suggestions. Thank you for that.

My next gratitude goes to Nieck Benes, Antoine Kemperman and Matthias Wessling, who gave me the opportunity to take the PhD project. Straightaway I settled in very comfortably in my new office, thanks to wonderful officemates. Jumeng Zheng, Anne Corine IJzer and Jeroen Ploegmakers, you introduced me to the world of a PhD student, laboratory work, and always helped me whenever I asked. My gratitude also goes to, beloved by everyone, Greet Kamminga, with you all formalities were actually very pleasant. It was also very nice to welcome Audrey Haarnack as Greet's replacement, to who I am very grateful for helping arranging my graduation. I thank my polish transportation mates, Szymon Dutczak and Wojciech, for traveling with me from Steinfurt to Enschede during my first PhD year, and for making me feel comfortable in the group.

Conducting research without the knowledge and experience of Herman Teunis, Erik Rolevink, Erik van de Ven, Wika Wiratha, Marcel Boerrigter, Jan van Nieuwkastele, Ineke Pünt and John Heeks would have been very difficult. Frank Morssinkhof, Cindy Huiskes and Mieke Luiten-Olieman greatly helped me with my work in IM labs. Thanks to all of you for help and patience.

Thank you John for your incredible and warm personality, and for organizing a wonderful Batavierenrace-Party 2012 at your home.

I would like to express my gratitude to people who contributed very frequently to my project, through their knowledge and discussions, Joris de Grooth, Harmen Zwijnenberg and Jeroen. Wojciech, thank you for sharing the knowledge on ellipsometry. I thank Kitty Nijmeijer, Zandrie Borneman and Harro Mengers for sharing the expertise on dehydration topic and SPEEK. I want to thank my master students, Lina Hendrawati Tan and Theresa Lohaus, for their hard work and contribution to my thesis. I appreciate it very much. I also appreciate 3-days long simulations with Theresa at RWTH Aachen University.

I give my great gratitude to my other officemates. Polish-Pakistani Salman Shahid, thank you for all discussions on gas separation and rheology. Pakistani Shazia Ilyas, thank you for advices on writing articles and for gossiping with me about everything. Polish Krzysztof Trzaskus, thanks for all your help, discussions and surviving my talking with the next Polish officemate, Joanna Cookney. Joanna C., the time spent with you was very entertaining. Thank you for your knowledge, support and nice words, and for planting lemon trees in our office.

Throughout 4 years of my PhD, the atmosphere in my office was always nice, which made coming to work very pleasant every day. I thank everyone for filling the office with discussions on a variety of topics, from science to nonsenses.

I am very grateful to Emiel Kappert, Namik Akkilic, Kitty Nijmeijer, Wojciech Ogieglo and Mark Hempenius for a successful collaboration on our articles. Additional gratitude goes to Mark for his knowledge on chemistry, to Emiel for sharing the thesis chapter, and to Namik for fluorescence microscopy. I also thank Wiebe de Vos, Erik Roesink, Antoine Kemperman and Kitty Nijmeijer for constructive criticism and suggestions during/after monday morning presentations.

Many thanks goes to Clemens Padberg and Joost Duvigneau from MTP group, for helping me with SPEEK measurements.

It is my pleasure to acknowledge my Wetsus friends, Sinem Tas, Charu Chawla, Enver Guler, Yusuf Wibisono, Christina Kappel, Andrew Shamu, Terica Sinclair, Janneke Dickhout, David Vermaas and Jordi Moreno.

I thank Salman School-, Batavierenrace-, Pole Dancing- and Party teams: Olga Kattan, Estevao de Oliveira, Yali Zhang, Jie Zhao, Damon Rafieian, Saghar Khadem, Erik Vriezokolk, Izabella Bouhid de Aguiar, Jeroen Polegmakers, Krzysztof and Marzena Trzaskus, Sinem Tas, Ramazan Ünal, Antoine Kemperman, Can Aran, Laura Garcia Alba, Kah-Peng, Enver Guler, Mette Kristensen, Alessio Fuoco, Al-Hadidi, Mayur Dalwani, Tina Thakkar, Wojciech and Joanna Ogieglo, Aura Visan, Barbara Liszka, Bram Zoetebier, Aylin Kertik, Violetta Martin Gil and Sooi Lee.

Thank you Sinem for our common struggle with SPEEK and viscosity measurements. Erik V., it was really fun to have a humehood next to you. My Dutch and bad words vocabulary improved. Thank you Charu for being my roommate during Euromembrane 2012 and for giving me tips about mediation. Thank you Yusuf and Enver for travelling with me to Leeuwarden. Thank you Erik V., Jordi, Damon, Yali and Krzysztof for our last NPS in Utrecht, especially for being my artificial audience during my presentation.

Furthermore, I express my gratitude to other fellow students, post docs and friends for having great fun together during coffee breaks, borrels, conferences, social events and parties, Vic van Dijk, Timon Rijnaarts, Sander Haase, Irdham Kusumaward, Parashuram Kallem, Zeljka Madzarevic, Roberto Floris, Ramato Ashu, Jeff Wood, Sandra Teixeira, Nazely Diban, Marlon Tijink, Henk Huurink, Elif Karatay, Ivonne Escalona, Hammad Qureshi, Khalid Eltayeb, Giri Sripathi, Martin Wolf, Bas ten Donkelaar, Marcel ten Hove, Michiel Raaijmakers, Patrick de Wit, Evelien Maaskant, Emiel Kappert, Kristianne Tempelman, Ana Pinheiro, Cheryl Tanardi, Anne Benneker, Karina Kopeć, Agnieszka Bochyńska, Katarzyna Skrzypek, Imre Qiaink and Maïke van Doorn.

I would like to thank all members of MST, IM and SFI. Everyone contributed in one way or another to my project, personal development and outside-work life. You made my stay in Enschede an incredible experience.

I thank Kitty and MST group for the entertaining events, coffee breaks and group lunches, and that the main language remained, most of the time, English.

I thank my Polish/Lithuanian/Russian community from Steinfurt: Kasia, Grzesiek, Jagoda, Ania, Gosia, Asia Micior (Flügel) and Ogieglo, Wojtek, Danusia, Szymon, Krzysztof Gugula, Arturas, Simas and Marinka, for the time spent together and unforgettable memories.

Olga, thank you for your help when I was ill, for being my paranymph, and for making sure with me that there was no dead body under a broken shower during NYM 2011. Harmen, thank you for being my paranymph and for all discussions, especially about Dutch TV programme's.

I would like to thank my promotion committee, prof. dr. ir. I.F.J. Vankelecom, prof. dr. A.A. van Steenhoven, dr. S. Metz, prof. dr. S.R.A. Kersten, dr. M.A. Hempenius, dr. ir. H. Wormeester, for allowing me to defend my thesis. I acknowledge prof. dr. J.W.M. Hilgenkamp for chairing the defense session. I thank my promoters, prof. dr. ir. D.C. Nijmeijer and prof. dr. ir. N.E. Benes for their knowledge, support, constructive advices and help with the completion of my thesis.

I would like to express my appreciation to the participants of the Wetsus research theme "Dehydration", Daniela Trambitas, Geert Woerlee, Marco Giuseppin, Boris Novakovic, Daniel Bergmair, Simona Strazdaite, Andrew Shamu and Sybrand Metz, for the meetings, productive discussions and your support.

I am deeply grateful to my daily supervisor, Nieck Benes, without your motivation and support, critical evaluation of the thesis content and its improvement, this dissertation might not have been completed. I especially enjoyed my last year, 2014, during which I had a lot of peace, and freedom with working on SPEEK. During the last meeting before my contract terminated, I felt sad that the time ended.

Tea, Harrie, Ria, Dennis, Romy, Leo, Angele, Warner, Iris en Herco, ik wil jullie heel erg graag bedanken voor jullie steun. Meetings met jullie zijn altijd heel gezellig.

Szczególne podziękowania kieruję do mojej mamy Anny i babci Haliny, za wychowanie, stanowienie wzorców do naśladowania, miłość i nieustanne wsparcie. Jak również dziękuję mojej kochanej siostrze Agacie, Tony'emu, Jeanette i siostrzeńcom, Emily i Harrisonowi, oraz pieskom, Astrze i Torresowi, za troskę, pomoc, wsparcie i zawsze cudowne pobyty w Anglii i Polsce.

Finally, my thesis, articles and me would not exist without dr. Jeroen Ploegmakers, dr. Diab. Bel. S., Sul. and Vir. Thank you for our everyday life and of course, for watching all together Michael Scofield!



ISBN: 978-94-6259-806-5

